HIGH-RESOLUTION GEOLOGIC MAPPING OF SEAFLOOR STRUCTURES AND IDENTIFICATION OF STRUCTURAL SYSTEMATICS

DISSERTATION

zur Erlangung des

Doktorgrades der Naturwissenschaften

(Dr. rer. nat.)

am Fachbereich Geowissenschaften

der Universität Bremen

vorgelegt von

Janis Thal

Bremen, Februar 2014

Referent:

Prof. Dr. Wolfgang Bach

Korreferent:

Prof. Dr. Gerhard Bohrmann

Table of Contents

Volcanologic terms

Feeder dike	Dike or conduit that feeds a volcanic eruption.
Volcaniclast	Clast of volcanic origin. No information about the clast formation process is given.
Hyaloclastite	Juvenile, glassy volcaniclast produced by quenching.
Pyroclast	Juvenile, glassy volcaniclast produced by explosion.
Bubble wall fragments	Glass shards produced by bubble burst.
Fluidal clasts (e.g. Pele's tears)	Fluidal shaped pyroclasts produced by explosive ejection of liquid magma into water.
Autobreccia	Juvenile, angular volcaniclast produced by mechanical stress.
Magmatic explosion	Explosive volcanic eruption caused by high partial pressure of magmatic volatiles.
Phreatomagmatic explosion	Explosive volcanic eruption caused by interaction of magma with water in shallow depth.
Dome	Accumulation of high-viscous lava above the feeder dike.
Cryptodome	Intrusive dome emplacement with updoming of the overlying lithology without or only occasional breakthrough of lava.

Abbreviations

ROV	Remotely operated vehicle
AUV	Autonomous underwater vehicle
MOR	Mid ocean ridge
MORB	Mid ocean ridge basalt
BAB	Back-arc basin
mbsl	Meter below sea level
SER	South East Ridges
VMS	Volcanogenic massive sulfide

Abstract

Two comprehensive geologic mapping projects, which were conducted in the eastern Manus Basin, Papua New Guinea, are the core of this dissertation. They provide new perspectives on the local geologic framework and distribution of hydrothermal discharge sites at felsic-hosted hydrothermal systems in an opening back-arc basin. Both mapped areas are interpreted as present-day analogs to volcanogenic massive sulfide (VMS) deposits preserved in the geologic record on land. Our results advance the knowledge of submarine volcanic eruption styles and related eruption products, the interplay of back-arc volcanism with the formation of VMS ore deposits and finally the spatial distribution and influence of hydrothermal activity at the resultant seafloor morphologies.

Of cornerstones importance are high-resolution (1 m) bathymetric maps conducted with the AUV ABE in 2006. These extraordinary detailed terrain models allowed accurately navigated ROV-based visually obtained geologic information to be transferred onto topographic structures. These visual informations were substantiated with rock analyses, temperature measurements and hydrothermal fluid samples. This enabled systematic analyses on the spatial distribution and relationship of various volcanic morphologies, hydrothermal discharge sites and structural systematics.

The first case study was conducted at the PACManus Hydrothermal District which is located on Pual Ridge in 1640 – 1740 mbsl. The volcanic facies at PACManus show a wide range of different lava flow morphologies including pillows, lobate to chaotic jumbled lava flows, massive blocky lava flows and domes. A three-stage chronological sequence for the magmatic accretion could be defined that causes the present day volcanic rocks which make up the seafloor of PACManus. This sequence is based on lava flow morphology, sediment cover and lava SiO_2 concentration:

Stage 1: Slightly to moderately porphyritic lavas (68 - 69.8 wt. % SiO_2) built up domes or cryptodomes.

Stage 2: Aphyric lava (67.2 – 67.9 wt. % SiO_2) formed lobate, jumbled and pillowed lava flows.

Stage 3: Massive blocky lava with 69 - 72.5 wt. % SiO_2 were emplaced on the seafloor.

Comprehensive mapping of these volcanic structures clearly documents that volcanic processes dominate over tectonic processes in the crustal accretion of Pual Ridge

at PACManus. In addition, volcanic structures (i.e. domes, dykes and lava flows) appear to control hydrothermal fluid flow in the shallow subseafloor. Specifically, hydrothermal fields on the seafloor are either based on permeability controlled fluid flow through breccias and hyaloclastites that are associated with domes, or channelized fluid flow along dikes and lava lobes. This is in strong contrast to hydrothermal fields along the MOR where tectonically controlled fractures and faults govern the fluid discharge. Quantitative GIS-based analyses of recognized fluid discharge zones revealed that hydrothermal venting occurs over a total area of 20,279 m^2.

The second mapping project was accomplished at the North Su volcano ~50 km to the West of PACManus. It is the first high resolution geologic mapping project of an active submarine andesite volcano. Again, high-resolution AUV-based bathymetry was merged with ROV-based video observations to identify seafloor structures whose nature was substantiated with rock samples. The volcanic activity occurs in various styles including effusive eruptions of extremely viscous lava that produced spines and blocky outcrops. But also explosive eruptions occur on North Su with variable intensity. North Su hosts two peaks on its summit, North Peak and South Peak. Based on repeated bathymetric surveys and comprehensive geologic mapping in 2006 and 2011, a sequence of four stages depicting the volcanic evolution of North Su could be evaluated:

1) unspecified eruptions forming North Peak

2) South Crater eruption

3) sector collapse of North Peak south slope, perhaps coeval with (2)

4) South Peak eruption

The South Peak eruption occurred between 2006 and 2011 with an estimated volume of $5.8*10^6$ m^3 of volcaniclastics and lava that have been deposited on an area of $2.1*10^5$ m^2. The maximum depth change related to the eruption is +63 m. A group of small (<10 m diameter) and shallow (<3 m depth) craters on South Peak summit indicate localized steam explosions inside the dome. The summit consists of heterolithic clasts (fresh to highly altered clast with abundant crystal fragments lacking pyroclasts) with a dominated grain size of 1-5 mm. High-viscous lava that fails with brittle behavior upon contact with seawater is believed to cause the clast formation. The heterolithic nature is explained by mixing of wall rock fragments and clasts from the slope prior to the eruption, into which South Peak erupted.

On the older North Peak, similar clastic deposits occur, although prolonged hydrothermal discharge has led to a cementation of clasts due to precipitation of hydrothermal minerals in the void space. This increased the slope stability of clastic deposits that are exposed on up to 14 m high cliffs below the North Peak summit. This is contrary to the common assumption that hydrothermal discharge decreases slope stability and subsequently causes sector collapses. This result strongly suggests that hydrothermal activity can also increase the slope stability when hydrothermal fluids are discharged though a pile of volcaniclastics. Key in this process is the sulfuric acid nature of the fluids, which produces copious amounts of alunite and cristobalite precipitate cementing the volcanic clasts. Further, proximal volcanic lithologies on North Su share characteristics (i.e. rounded grain size, heterolithic composition) of deposits that would traditionally be interpreted in facies reconstructions as distal or as redeposited lithologies.

This dissertation illustrates the high potential of video material collected with ROVs while working on the seafloor if high-resolution bathymetry exists.

The maps and data sets I produced during this dissertation set a valuable backdrop for future studies in the PACManus Hydrothermal District and North Su.

Kurzfassung

Den Kern dieser Dissertation bilden geologische Meeresbodenkartierungen von zwei Hydrothermalsystemen in einem jungen, sich öffnenden Backarc-Becken, dem östlichen Manus Becken in Papua Neu-Guinea. Die beiden Kartiergebiete werden von felsischem Vulkanismus dominiert und als rezente Gegenstücke zu fossilen Massivsulfid-Lagerstätten betrachtet. Meine Untersuchungen liefern einen wichtigen Beitrag zum besseren Verständnis von submarinem Vulkanismus in Bezug auf Eruptionsstile und –produkte und die Wechselwirkungen zwischen Backarc-Vulkanismus und der Entstehung von Massivsulfid-Lagerstätten. Darüber hinaus erweitern die Ergebnisse den wissenschaftlichen Kenntnisstand über die kontrollierenden Faktoren in der Anordnung von Hydrothermalquellen und deren Beeinflussung durch vulkanische Aktivität sowie den daraus resultierenden morphologischen Strukturen am Meeresboden.

Hochauflösende bathymetrische Karten sind von essentieller Bedeutung für die Kartierungen. Die Karten haben eine Auflösung von nur einem Meter und wurden mit dem autonomen Unterwasserfahrzeug ABE im Jahr 2006 erstellt. Aufgrund der hohen Detailtreue der Karten konnten Informationen über den Meeresboden, die aus Videoaufnahmen von Tauchrobotern gewonnen wurden, auf Strukturen in den Karten übertragen werden. Gesteins- und Fluidanalysen sowie Temperaturmessungen festigten und ergänzten diese primären Beobachtungen und ermöglichten so eine systematische Untersuchung von Hydrothermalquellen, vulkanischer Fazies und deren räumliche Anordnung.

Die erste Kartierung wurde im Hydrothermalgebiet PACManus durchgeführt, das auf dem Pual Rücken in 1640 – 1740 m Wassertiefe liegt. Die vulkanischen Fazies innerhalb von PACManus reichen von Kissenlaven über lobate bis chaotisch zerbrochene Lavaströme hinzu massiven Blocklavaströmen und Lavadomen. Anhand der Sedimentbedeckung, des Silikatgehalts und der Lavastrommorphologie konnte eine dreistufige Abfolge der vulkanischen Aktivität identifiziert werden:

Stufe 1: Dome und Kryptodome werden durch geringfügig bis mäßig porphyrische Lava mit 68 – 69 gew. % SiO_2 gebildet.

Stufe 2: Aphyrische Lava mit 67.2 – 67.9 gew. % SiO_2 formt Kissenlaven, lobate und zerbrochene Lavaströme.

Stufe 3: Massive Blocklavaströme eruptieren mit 69 – 72.5 gew. % SiO_2.

Die detaillierte Kartierung der vulkanischen Fazies hat gezeigt, dass im Hydrothermalgebiet PACManus vulkanischen Ereignissen eine übergeordnete Rolle zukommt, da keine Hinweise auf tektonische Prozesse auf dem Meeresboden beobachtet wurden. Hinzu kommt, dass die Verteilung der Hydrothermalquellen am Meeresboden offenbar durch vulkanische Strukturen wie Dome, Eruptivgänge und Lavaströme kontrolliert werden. Entweder treten die Hydrothermalfluide kanalisiert entlang von Eruptivgängen und Lavaströmen aus oder die Fluidmigration wird durch die Permeabilität von Brekzien und Hyaloklastiten kontrolliert, die bei der Eruption von Domen und Blocklavaströmen entstehen. Hingegen werden Hydrothermalfelder entlang der Mittelozeanischen Rücken durch tektonische Strukturen, wie Störungen kontrolliert. Mit Hilfe von GIS-basierten Analysen lässt sich die Ausdehnung hydrothermaler Aktivität auf einer Gesamtfläche von 20.279 m² verfolgen.

Das zweite Kartiergebiet, North Su, liegt etwa 50 km westlich von PACManus und ist ein andesitischer Unterwasservulkan mit zwei Gipfeln, North und South Peak. Diese Arbeit ist die erste hoch-auflösende Kartierung eines aktiven Unterwasservulkans mit andesitischer Gesteinszusammensetzung. Auch hier wurden bathymetrische Karten mit dem autonomen Unterwasserfahrzeug ABE erstellt und mit Ergebnissen aus Video-, Gesteins- und Fluidanalysen kombiniert. Effusiver Vulkanismus von North Su produziert hoch-viskose Laven die Lavanadeln und kurze, zerklüftete Lavaströme formen. Verschiedene Krater weisen außerdem auf explosiven Vulkanismus hin.

Mit Hilfe von bathymetrischen Karten von 2002 und 2011 sowie ausführlichen Kartierarbeiten in 2006 und 2011, konnte eine chronologische Abfolge vulkanischer Aktivität bestimmt werden:

1) Unbekannte vulkanische Aktivität formt North Peak
2) South Crater eruptiert
3) Hangrutschung des Südhangs von North Peak, evtl. zeitgleich mit 2)
4) South Peak eruptiert

Die South Peak formende Eruption fand zwischen 2006 und 2011 statt und produzierte $5.8*10^6$ m^3 vorwiegend klastisches vulkanisches Material mit wenigen Lavaströmen, die auf einer Fläche von $2.1*10^5$ m^2abgelagert wurden. Die maximale Mächtigkeit der Ablagerungen beträgt 63 m. Auf dem Gipfel von South Peak deuten eine Gruppe von kleinen (<10 m im Durchmesser) und flachen (<3 m tief) Kratern auf interne Dampfexplosionen hin. Die Gipfelregion von South Peak besteht fast ausschließlich aus

feinen (1-5 mm), heterolithischen Klasten (frisch bis stark alterierte Klasten mit vielen Kristallbruchstücken aber ohne Pyroklastika), deren Entstehung auf das brüchige Verhalten der hochviskosen Lava und auf die Beimengung von Randgestein während der Eruption zurückzuführen ist.

Auf dem älteren North Peak ist eine ähnliche Lithologie aus heterolithischen Klasten zu finden. Diese sind allerdings vielerorts durch hydrothermale Ablagerungen zementiert und tragen somit zu einer erhöhten Hangstabilität bei. Als Folge existieren am Hang von North Peak bis zu 14 m hohe Kliffs aus hydrothermal-zementierten Brekzien. Diese Beobachtung widerspricht jedoch der gemeinhin akzeptierten Annahme, dass hydrothermale Aktivität eine Hanginstabilität fördert und folglich zu Hangrutschungen führt.

Vielmehr scheint die Migration schwefelsaurer Fluide durch klastische Ablagerungen eine massive Kristallisation von Cristobalit und Alunit in Hohlräumen und somit eine umfassende Zementierung von Klasten zu bedingen.

Ablagerungen mit teilweise gerundeten Klasten und heterolithischer Zusammensetzung, wie auf den Gipfeln von North Su, würden bei einer Faziesrekonstruktion fälschlicherweise als distale Ablagerung interpretiert werden.

Die Arbeiten im Rahmen dieser Dissertation zeigen, dass Videomaterial von Tauchrobotern ein hohes Potential für Meeresbodenkartierungen bieten, wenn hoch-auflösende bathymetrische Karten zur Verfügung stehen.

Meine umfangreichen geologischen Karten sind in Kombination mit den ausführlichen Untersuchungen eine hervorragende Basis für weitere Forschungstätigkeiten im Hydrothermalgebiet PACManus und North Su.

1. Introduction

1.1 History of seafloor mapping

The oldest known geologic map is already more than 3,000 years old and depicts, amongst others, the geology of Wadi Hammamat with locations of gold and sandstone quarries in the central Eastern Desert of Egypt. The map was probably authored by the Theban scribe Amennakhte, son of Ipuy, during the reign of Ramses IV (around 1150 B.C.; Harrell et al., 1992). This old map is a magnificent example of the essential need for geologic maps, not only for geologists, but in general to help utilize and exploit the earth for the benefits of mankind.

For earth scientists, mapping of geologic structures is the most fundamental component to develop scientific theories, hypotheses, and models of a specific region. Further, a geologic map enables scientist from other research areas, to place their analyses into the context of geologic information.

During three millennia, after Amennakhte created his map, geologists and cartographers had their focus on mapping subaerial regions as they are relatively easy to access. Therefore, for the majority of subaerial parts of the earth geologic information is available. In contrast, only intermittent geologic information exist about the seafloor, although roughly two third of the earth's surface is covered by sea. At the end of the 19th century oceanographers imagined that "…the sea-bed extends for wide spaces in long undulations and gentle slopes…" (Reclus (1886) in Tyce (1986)). This view did not change dramatically until the first seamounts have been discovered in the 1940s when the US Navy started first mapping projects in the Central Pacific (Hess, 1946). It took another 20 years until the invention of swath mapping echo sounding systems in the 1960s revealed the vast diversity of the seafloor morphology (Tyce, 1986). Today, we know that the world's longest mountain range (mid-ocean ridges) and countless mountains decorate the seafloor, most of which are believed to be of volcanic origin (Smith and Jordan, 1987; Smith and Cann, 1992; Wessel, 2001; Hillier and Watts, 2007).

The technological advances of the last 50 years resulted in remotely operating vehicles (ROV) and autonomous underwater vehicles (AUV) which enable m-scale sensoric and optical mapping of the seafloor and make geologic fieldwork possible in the deep-sea.

For this dissertation data from state-of-the-art technologies were used to produce m-scale geologic maps of the deep sea at two volcanic-hosted hydrothermal systems in the Manus Basin, Papua New Guinea. The aim of this work is to reveal the interplay of volcanic activity and hydrothermal circulation as well as to analyze the eruption and emplacement mechanisms of submarine volcanism in an opening back-arc basin.

1.2 Submarine volcanism

1.2.1 Tectonic settings and magma genesis

One of the most important geologic processes on earth is submarine volcanism. Roughly two-thirds of the earth's surface is covered by oceans, the rocky foundation of which is dense, igneous crust that has formed by submarine volcanism along the world-spanning mid-ocean ridges (MOR). Besides the MOR, two additional geologic settings with active volcanism exist in the sea (Fig. 1.1). In the broadest sense these are oceanic intra-plate volcanism and subduction zone volcanism within intra-oceanic arcs and back-arc basins (BAB), where two oceanic lithospheric plates converge.

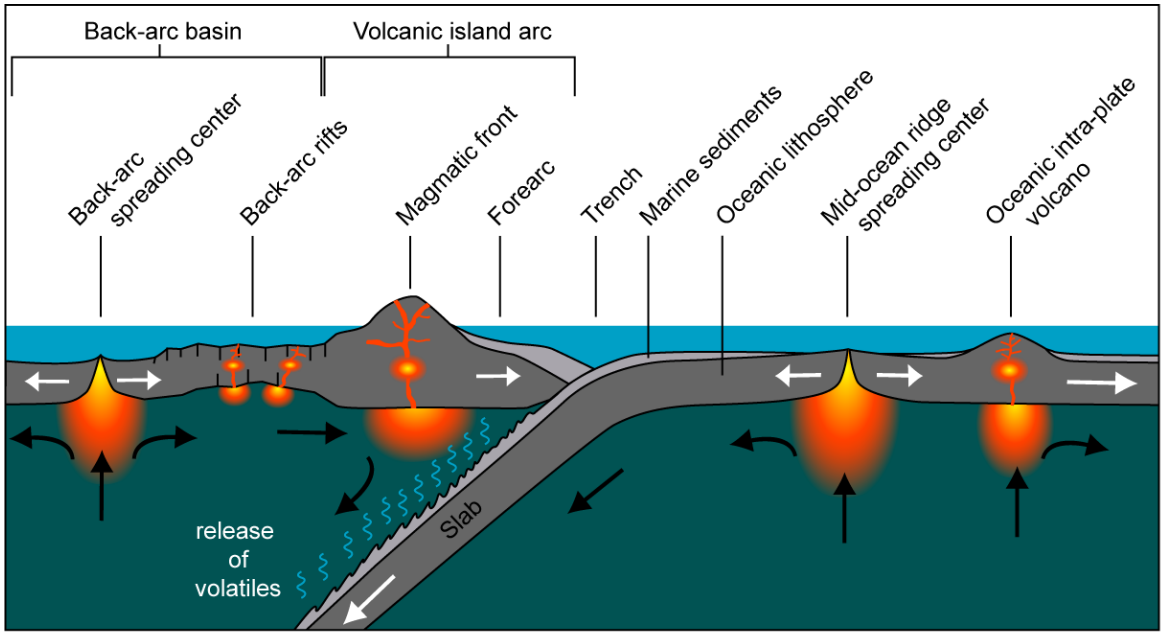

Figure 1.1: Sketch illustrating first-order submarine volcanic settings. White arrows indicate plate motion whereas black arrows show mantle convection.

At seafloor-spreading centers, both MOR and BAB, new oceanic crust is formed. Extension of the lithosphere causes passive mantle upwelling at a rate proportional to the spreading rate. This causes decompression melting of the mantle (Langmuir et al., 1992). The basaltic melts produced by this process are segregated from the solid mantle, ascent and aggregate to form the oceanic crust. Seafloor mapping has shown that fast spreading

MOR form a broad rise with small, if any, central valleys. Slow-spreading ridges, in contrast, are narrower and feature deep central valleys, indicative of pronounced tectonic faulting. These differences are expressions of variable magma production rates, which correlate with spreading rate (Niu and Hékinian, 1997).

Magma of oceanic intra-plate volcanoes is produced by melting of mantle material in mantle plumes, where hot mantle material buoyantly actively rises in an upward convective flow, or by pressure-release in response to extension and thinning of the lithosphere. An example for oceanic intra-plate volcanism above active mantle upwelling is the Emperor-Hawaiian Chain, whereas the Line Islands are produced by lithospheric extension (Davis et al., 2002; Koppers and Watts, 2010; Staudigel and Clague, 2010). Like at MOR, most of the basaltic melts extracted from the mantle in intra-plate settings are tholeiitic, although alkali basalts, indicative of deep melting under a thick lithosphere are also developed.

Subduction zone volcanism can be subclassified into volcanic island arc and back-arc volcanism (Fig. 1.1). Island arcs form when two convergent oceanic lithospheres collide and one lithosphere is subducted underneath the other. During subduction, increasing pressure and temperature cause dehydration of the "wet" slab and metamorphic breakdown of hydrous minerals. As a result, H_2O and other volatiles are released into the overlying mantle wedge, decreasing the solidus of mantle peridotite, and thus causing partial melting (Kushiro et al., 1968; Tatsumi and Eggins, 1995; Schmidt and Poli, 1998). These melts rise buoyantly and form the arc volcanic front(Tamura et al., 2002). Volcanic island arc magma differs from MORB by being, on average, more siliceous and enriched in volatiles (e.g. H_2O, CO_2, H_2S, SO_2).

Back-arc volcanism is influenced by crustal thinning due to lithospheric extension which is generally induced by the slab-pull effect of the subducting oceanic lithosphere (Elsasser, 1971; Moberly, 1972; Scholz and Campos, 1995). In contrast to steady state MOR tectonic settings, BAB evolve in time and therefore are non-steady state settings. On subduction initiation, the overlying oceanic plate experiences extension and initial rifting occurs. Characteristic for the early stage of back-arc opening (back-arc rifts, Fig. 1.1) is bimodal volcanism which is caused by high-temperature, hydrous melts (e.g. boninites; Crawford et al., 1989; R. N. Taylor et al., 1994) and rifting induced partial melting.

With ongoing subduction and continuous rifting, seafloor spreading centers develop in further distance to the volcanic island arc. Similar to MOR, magma production occurs predominantly by pressure-release melting. In relation to the distance to the subduction zone, a trend of different magma genesis and chemistry develops. Volcanic rocks close to the subduction zone are more felsic with a chemical fingerprint of the subducting slab whereas mafic MORB-like magma occurs at back-arc spreading centers (Martinez and Taylor, 2002, 2003; Sinton et al., 2003).

Comprehensive knowledge exists about basaltic volcanism along the mid-ocean ridges but comparably little is known about subduction zone related arc volcanism with exotic magma compositions. This marks a crucial knowledge gap as subduction zones make up roughly 20 % of the earth's plate boundaries (Bird, 2003). Also, back-arc and arc crust which is preserved in the geological record often comprises volcanic-hosted massive sulfide deposits and thus is of economic interest. World-class Cu & Au deposits exist in these arc-settings but the understanding of their formation is predominantly based on facies reconstruction (Barrie and Hannington, 1999; Gibson et al., 1999). Critical for the correct interpretation is a profound knowledge about submarine arc and back-arc volcanism and its controlling mechanisms. The lava flow morphologies and the abundance of variable volcaniclastic deposits are used to reconstruct the environmental conditions (e.g. water depth, arc proximity) in which the deposits were created.

In this dissertation two geologic mapping studies of the eastern Manus Basin are presented in chapter two and three. The Manus Basin is an opening back-arc basin with its eastern part being still in a rifting stage of old island-arc crust without seafloor spreading. This geologic setting generates exotic lava compositions which form a wide range of different eruption products and lava emplacement styles. To integrate chapter two and three into the broader context of submarine volcanism it is essential to discuss the general considerations on submarine volcanism.

1.2.2 General considerations on submarine volcanism

Although, measured by volume, about 80% of Earth's volcanic activity occur beneath the sea (Crisp, 1984), submarine eruption mechanisms are still poorly understood compared to their counterpart on land. Studies of active volcanism in different geologic settings are critical to the understanding of volcanoes but are heavily weighted to subaerial environments (Rubin et al., 2012). This is mainly due to the difficult access to

submarine volcanoes as well as the high costs of marine expeditions which is why continuous observations are rare.

Submarine volcanism differs from subaerial volcanism in many aspects (White et al., 2003a). Most fundamental is the fact that hot lava is injected into water that has different physical properties than air. First of all, water has the ability to vaporize upon contact with magma leading to sudden volume expansion (i.e. steam explosion) which can enable or cause fragmentation down to water depths of ~ 3km, corresponding to the critical pressure of seawater (300 bar; Bischoff and Rosenbauer, 1985). Below this depth, the supercritical phase separation takes place, which involves only negligible volume expansion (McBirney, 1963). On the other hand, the momentum caused by an explosion is easily absorbed by water as it has a higher density and viscosity compared to air. The density of water increases by 1 bar for every 10 m of water depth, leading to very high confining pressures for eruptions in the deep-sea. The high pressure can prevent exsolution of volatiles like CO_2 and H_2O in great depth which lower the solidus and therefore decrease the viscosity of magma which would cause explosive eruptions under atmospheric conditions (de Rosen-Spence et al., 1980; Yamagishi, 1985). The higher density of water compared to air is also reflected by the roughly 10^3 times higher drag forces in water than in air. As a result, eruption columns and ejected pyroclasts will remain, in most cases close (tens of meters) to the vent. In contrast subaerial volcanoes are able to distribute their ejecta several km away from the vent. Additionally, the high heat capacity and high thermal conductivity of water makes it a very efficient coolant which causes very rapid cooling of lava and intense fragmentation.

In addition to the subaqueous environment, several other parameters like the magma temperature, chemical composition, crystal and volatile content as well as the discharge rate, pre-flow topography and volcanic vent architecture influence the nature of submarine volcanism and its products (McBirney, 1963; Stix, 1991; Cas, 1992; Gregg and Fink, 1995; Griffiths and Fink, 1997; Griffiths, 2000; Head and Wilson, 2003; White et al., 2003a).

1.2.3 Clastic eruption products

As a consequence of the different physical properties of water, outlined above, submarine eruptions experience enhanced fragmentation processes when compared to subaerial volcanism. Proposed mechanisms of clast formation and explosivity due to water-magma interaction include several thermo-hydraulic fracturing mechanisms which

account for different clast sizes and shapes (e.g. Sheridan and Wohletz, 1983; Wohletz, 1983; Kokelaar, 1986; Zimanowski et al., 1991; White, 1996; Skilling et al., 2002; Head and Wilson, 2003; Thiéry and Mercury, 2009). Kokelaar (1986), in his landmark paper, defines four major fragmentation mechanisms that can affect low-viscous lava erupting in the submarine environment (Fig. 1.2). Of cornerstone importance in this concept is that fragmentation processes can be self-enhancing and that complex feedbacks may develop between the different mechanisms. Although his considerations are related to basaltic, low-viscosity lava, the principle mechanisms can be transferred to all types of lava and are discussed below.

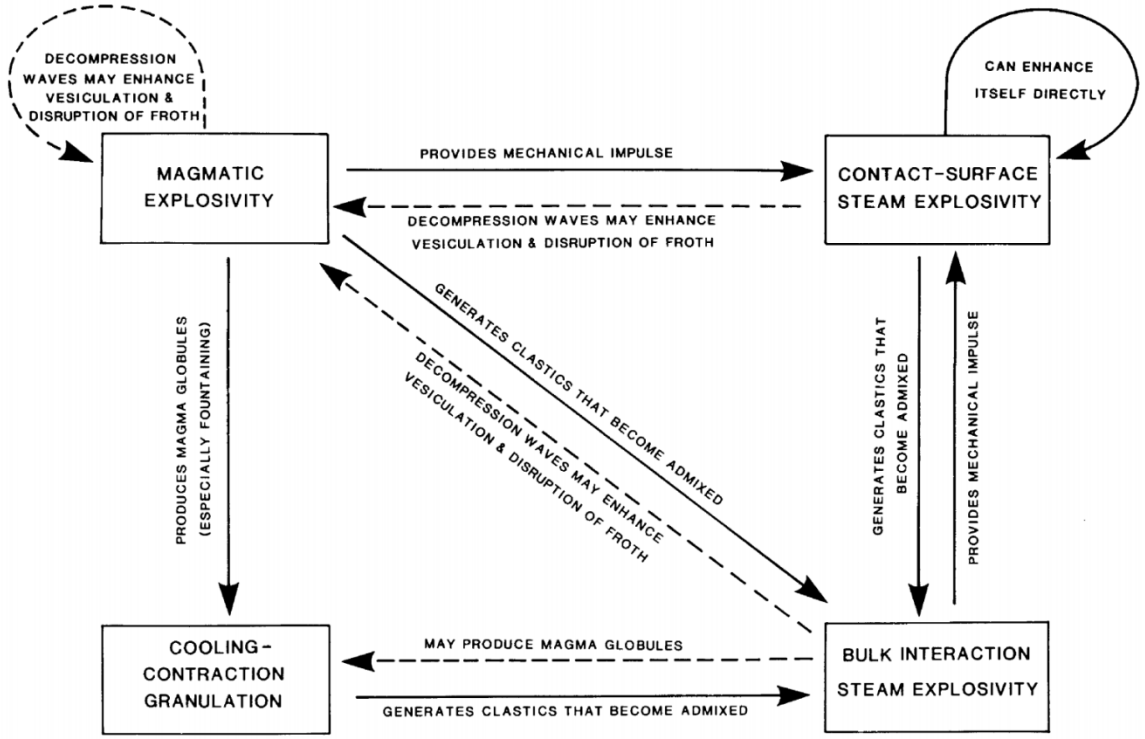

Figure 1.2: Four different clast forming processes with possible enhancement interactions after Kokelaar (1986).

Magmatic explosivity is based on volatile exsolution during ascent of magma or at the water-magma interface. This process is always related to pyroclasts formation and the different scenarios leading to magmatic explosivity will be discussed in more detail in chapter 1.2.5.

The other fragmentation processes are based on cooling, mechanical stress or steam expansion. The clasts produced by these mechanisms are defined in this thesis as hyaloclastites except for the fragmentation products of autobrecciation, which are termed autobreccias. The following processes can occur together or isolated.

Bulk interaction steam explosivity describes the interaction of magmatic heat with water that is either engulfed by magma or trapped close to it. Pressure waves associated with explosions shatter the rigid magma and a tearing apart of the magma occurs (Kokelaar, 1986). This is likely to happen when magma intrudes into wet slurry (e.g. water-saturated sediment) causing local explosions due to steam expansion and disruption of juvenile material and country rock (Zimanowski et al., 1991; Skilling et al., 2002).

Cooling-contraction granulation (e.g. quench fragmentation) is the process of magma fragmentation due to cooling of magma upon contact with cold sea water. The thermal contraction leads to cracking or granulation, producing sand- and granule-sized clasts (Kokelaar, 1986; Head and Wilson, 2003). Cooling-contraction granulation is the only fragmentation process that also acts after the emplacement and continues while the lava cools, even if it cools well below the glass transition temperature (Porreca et al., 2014). Additionally, this process occurs is all water depth.

Contact-surface steam explosivity, also known as fuel-coolant interaction, is characterized by an isolating, stable vapor film at the lava-water interface. When this film collapses, explosive gas expansion disrupts the lava, which results in the formation of fluidal clasts. The disruption can trigger self-enhancement and cause runaway fragmentation that leads to violent explosions (Wohletz, 1983; Kokelaar, 1986). This process is unlikey to occur at the surface of viscous lava flows due to its rugged and autobrecciated nature, which prohibits the growth of a stable vapor film.

Autobrecciation occurs in every water depth and is related to eruptions of lava that either has an increased viscosity and reacts in plastic or brittle behavior upon mechanical stress, or the lava developed a cooled, rigid crust which cracks (Cas, 1992). In both cases, fracturing occurs when the external shear stress exceeds the internal shear strength.

These fragmentation processes can produce a huge variety of different clast sizes and shapes. A dominant aspect governing the shape of clasts is the fluidal state of the erupted magma. If low-viscos magma is erupted, related clasts will have a fluidal to blocky shape and the clast size will be relatively small. In contrast, high-viscous lava will be related to predominantly blocky clasts and due to increased autobrecciation the average clast size will be bigger compared to low-viscous lava related clasts.

A common feature of all types of clasts, despite their genesis, is their predominantly glassy texture with only minor crystals and microlites. This is due to the fact that most magma erupts in a liquid state, above solidus, where only minor crystals have grown. But

in rare cases, a crystal-rich, highly viscous magma erupts which tends to fail with brittle behavior and the resulting clasts will be blocky, exclusively and mimic fractured, non-altered country rock (Sparks et al., 2000).

As the discussion above outlined the related clast production of submarine eruptions, it is essential to define the possible eruption styles and related modes of lava emplacement in the submarine environment. Submarine eruptions are distinguished, similar to the subaerial analogs, by their explosivity. There are explosive eruptions that can be further subclassified (e.g. Hawaiian-style fountain, Vulcanian etc.) and effusive eruptions.

1.2.4 Effusive submarine eruptions

Effusive eruptions producing lava flows are the dominant form of submarine volcanism. At MOR, eruptions occur predominantly through volcanic vents that are aligned along an eruptive fissure, whereas eruptions at intra-plate or arc volcanoes originate from a single or more localized vent. Despite the different vent architectures, modes of lava emplacement are heavily related to the lava viscosity in all geologic settings. Therefore, the products and styles of effusive eruptions can be classified based on a lower or higher viscosity.

Effusive eruption products of low-viscosity lava form a variety of flow structures ranging from pillow to lobate and lineated sheets to jumbled sheets that are well documented for MOR (Ballard and Moore, 1977). For these low-viscosity lavas, laboratory experiments revealed a strong dependency of lava flow morphology on extrusion and cooling rate as well as slope (Table 1; Gregg and Fink, 1995).

Laboratory morphology	Submarine morphology	Cooling rate	Slope	Flow rate
pillows rifts folds levees	pillows lobate lineated sheets ropy sheets jumbled sheets			

Table 1.1: Correlation between laboratory-derived morphology and observed submarine morphology in dependence on cooling rate, slope and flow rate. Modified after (Gregg and Fink, 1995).

These flow morphologies (Table 1.1) are common for lavas with basaltic compositions typical for MOR and intra-plate volcanoes but are also observed in some cases for rhyolitic lavas in arc settings (Bevins and Roach, 1979; de Rosen-Spence et al., 1980; Yamagishi, 1985; Binns and Scott, 1993). A common feature of these low-viscosity lava flows is a glassy outer crust that develops due to rapid cooling upon contact of lava with water. This crust protects the flow-interior from further rapid cooling which allows the lava to flow further. Quenching and shattering of the glassy crust produces hyaloclastites while the lava is emplaced on the seafloor (Pichler, 1965; McPhie et al., 1993).

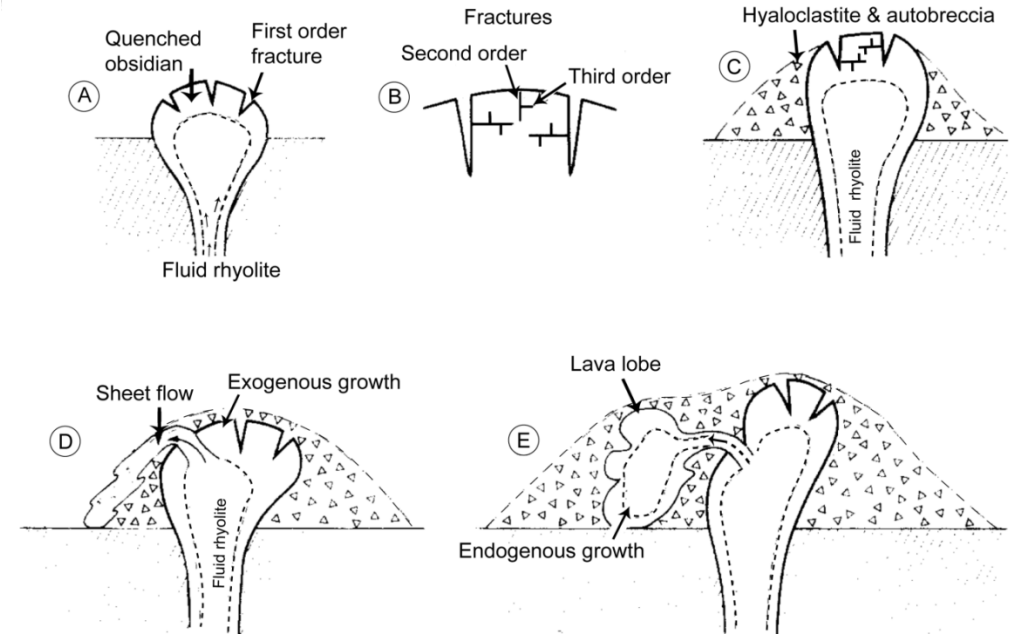

Figure 1.2: Formation of a submarine rhyolite lava dome.

A: The feeder dike reaches the seafloor and upon contact with sea water, intense quench fragmentation of the surface produces hyaloclastites while contraction fractures develop perpendicular to the surface.

B: Second and third order contraction fractures develop.

C: The quenched surface layer undergoes autobrecciation due to mechanical stress. A pile of in-situ and resedimented hyaloclastites and autobreccia encircle the dome.

D: A first-order contraction fracture taps the fluid interior of the feeder dyke and a sheet lava flow extrudes upon the clastic pile illustrating exogenous dome growth. E: The sheet flow develops into a thick lava lobe which itself undergoes fragmentation. The continuous injection of hot magma causes endogenous growth as no extruding lava lobes are produced. Modified after Yamagishi and Dimroth (1985) and Yamagishi (1987).

In contrast to the well-understood basaltic (low-viscosity) lava flow mechanisms, comparably little is known about the eruption and flow characteristics of intermediate to highly viscous lava. The general idea of effusive highly viscous lava emplacement entails the formation of either thick and blocky lava flows (e.g. Kano et al., 1991; Scutter et al.,

1998) or domes (Fig. 1.2; Pichler, 1965; McPhie et al., 1993; Goto and McPhie, 1998; De Rita et al., 2001; Nemeth et al., 2008). In both cases, lava emplacement is related to intense clast production due to the high-viscosity which is caused by several factors.

Commonly, high-viscosity lava is related to high silica content, but as mentioned above, rhyolites can also develop flow morphologies related to low-viscosity lavas. More important for the viscosity is the crystal content, lava temperature, volatile content and confining pressure. Domes are the dominant lava flow morphology formed by high-viscous lava. Figure 1.2 illustrates the primary components of common models for subaqueous dome emplacement, which are based on lava with a poor flow behavior.

The dome growth is related to quench fragmentation, cooling-contraction-granulation and autobrecciation upon direct contact of magma with seawater resulting in a dome with a coherent core that is covered by a carapace of hyaloclastites and autobreccia (Pichler, 1965; Yamagishi and Dimroth, 1985; McPhie et al., 1993; Goto and McPhie, 1998; De Rita et al., 2001; Goto and Tsuchiya, 2004; Nemeth et al., 2008; Allen et al., 2010). This clastic cover can be >100 m thick as observed on an ancient submarine dome complex on Ponza Island, Italy (De Rita et al., 2001). Continuous volcanic activity occurs through injections of hot melt into the still molten dome causing either a dome inflation (endogenous growth, e.g. lava lobe in Fig. 1.2 E; Griffiths and Fink, 1997; Goto and McPhie, 1998) or lava lobes or spines that extrude the dome (exogenous growth, Fig. 1.2 D, E; Yamagishi and Dimroth, 1985; Griffiths and Fink, 1997).

1.2.5 Explosive submarine eruptions

The other submarine eruption style is characterized by explosive behavior which can be triggered by magmatic gas expansion (magmatic explosion) and by steam explosivity (phreatomagmatic explosion; Heiken, 1974; Kokelaar, 1986; Head and Wilson, 2003). Explosive eruptions are driven by volatile exsolution followed by magmatic gas expansion, which predominantly takes place in response to decreasing pressure during ascent of magma. The most prominent characteristic of this type of eruption is the formation of pyroclasts. They form when liquid lava gets disrupted and ejected into the water column where they freeze. Depending on the style of magmatic explosion and different shapes and sizes of pyroclasts are produced. The dominant characteristics controlling general pyroclast formation are the volatile content, degree of oversaturation, crystal content, viscosity, surface tension, temperature, and depth (Verhoogen, 1951). These general parameters are also valid for submarine volcanism, although the eruption

products of submarine magmatic explosions differ from the subaerial analogs due to the different environmental conditions as mentioned in section 1.2.2. Pyroclast formation for the submarine environment is summarized by Head and Wilson (2003). These authors distinguish between three different endmembers of submarine eruption styles that cause pyroclast formation due to magmatic explosivity: Strombolian-activity, Vulcanian explosions and Hawaiian-style fountaining (Fig. 1.3).

Hawaiian-style eruptions (Fig. 1.3: 1 + 4) are determined by a low and narrow fountain that occurs through the ejection of a jet that consists of pyroclasts, disrupted magma and gas. Two scenarios cause this type of eruption, whereas the first occurs with an enhanced activity due to artificial pressure buildup: 1) Magmatic degassing builds up a layer of foam below the roof of a magma chamber. When the partial pressure of the magma chamber exceeds the strength of the country rock, the foam will rise fast and eject into the sea. 2) The other scenario is defined by a low-viscous, volatile rich magma that ascents with a high rise speed. Volatile exsolution during the fast ascent causes magma disruption already inside the conduit. This mixture erupts with a high rise speed into the sea, forming a smaller fountain than in 1). The related landforms of Hawaiian-style eruptions are cones, several to tens of meters in diameter, made up of pyroclastic deposits that surround the pit-like volcanic vent. Proximal pyroclasts tend to be welded and distal deposits are fragmented and partly agglutinated. If effusive extrusion of lava is related to the eruption, sheet flows are likely to occur as Hawaiian-style eruptions are linked to a high effusion rate (Head and Wilson, 2003).

Another eruption style, Strombolian-activity (Fig. 1.3: 2), in contrast is related to a low effusion rate and a higher degree of explosivity. In this case, the magma rise speed is very slow that a runaway bubble coalescence process leads to a buildup of sufficient bubbles that are able to disrupt the lava at the water-lava interface. Bubbles can be up to 2 m and the resulting deposits (bubble wall fragments) are likewise smaller due to bubble bursts. The eruption deposits comprise abundant blocks and bombs in distal areas with an increased amount of finer, partly agglutinated pyroclasts proximal to the vent. Associated landforms are small (< 20m in diameter) cones of pyroclastic deposits surrounding a crater. Effusive lava emplacement would be expressed in the form of short pillows due to the low eruption rate (Head and Wilson, 2003).

The third and most violent explosive eruption style is Vulcanian explosivity (Fig. 1.3: 3), which is characterized by the artificial pressure buildup inside a clogged conduit

due to accumulating volatiles. When the partial pressure of the gas phase exceeds the strength of the country rock, a sudden pressure release will result in a sudden gas expansion, i.e. violent explosion. This explosion will disrupt some lava and particularly, the surrounding and overlying country rock. The related deposits are dominated by fractured, blocky country rocks and only minor pyroclasts. Despite the high explosive energy, clasts will be deposited close to the vent as drag forces in water are 10^3 times higher than within air. Therefore, the resulting landforms comprise an explosion crater surrounded by a cone of predominantly blocky clasts of country rock (Head and Wilson, 2003).

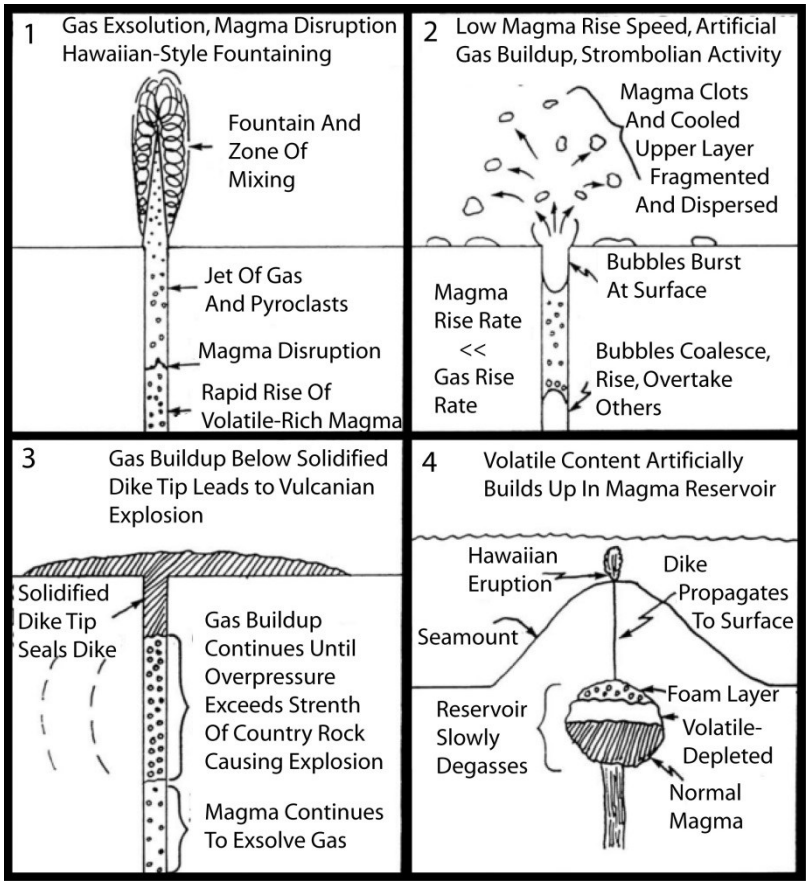

Figure 1.3: Illustration of four major types of submarine magmatic explosions after Head and Wilson (2003).

1) Hawaiin-style fountaining is caused by magma disruption within the conduit. This entails a fast ascending jet of gas and pyroclast which ejects into the water column.
2) Strombolian activity is determined by a relatively faster rising gas phase compared to the magma rise rate. The bubbles exist at the seafloor, they disrupt the lava (bubble burst) and produce bubble wall fragments.
3) A clogged dike causes a gas buildup inside the conduit. When the gas pressure exceeds the strength of the country rock, a Vulcanian explosion occurs.
4) Another scenario leading to a Hawaiian-style where a foam layer builds up inside a degassing magma chamber. If the pressure inside the magma chamber exceeds the strength of the country rock, the foam will thrust along the feeder dike and eject into the water column.

Although, these magmatic explosions occur under water, Head and Wilson (2003) do not consider water-magma interactions to have a major impact on the eruption style. In the magmatic explosions mentioned above, water is only believed to influence the eruption products by its high cooling rate, high density and confining pressure. Therefore, these eruption styles only occur in the deep ocean where the ambient pressure suppresses explosive vaporization of water upon contact with magma.

In contrast, shallow water explosive eruptions (i.e. on shallow seamounts or on the shelf) are dominated by water-magma interaction. The type locality for this eruption style is the Island of Surtsey, Iceland (Kokelaar, 1983). Surtseyan eruptions are explosive by virtue of the hydrostatic pressure in shallow waters being not sufficient to suppress explosive gas expansion. In the course of the eruption, a highly mobile slurry of pyroclasts, hyaloclastites and water cover the volcanic vent (Kokelaar, 1983). New erupting lava intrudes and interacts with this mixture. Explosive steam expansion of incorporated water results in jetting of this slurry into the water column and above the sea level. This fountain is a characteristic of Surtseyan eruptions which occur in water depth less than 200 m for basaltic lava but are believed to occur in much deeper waters for volatile-rich, alkaline magmas (> 700 m; Kokelaar, 1986). Related landforms are steep-sided cones that consist of phreatomagmatic pyroclasts from plume fallout or density-current deposits. If effusive activity occurs, pillow lava will form near the vent.

The eruption styles discussed above represent merely idealized endmembers of submarine volcanism. The different styles can occur as intermediate types or they occur sequentially during an eruption due to changing physical and chemical magma characteristics and variable environmental parameters. Pumice eruptions are such intermediate eruption styles that can be both explosive and effusive and involve abundant pumice formation (see review by Kano, 2003). The most violent endmembers within pumice eruptions are Plinian-type phreatomagmatic eruptions with a high-rising plume consisting of buoyant hot pumice fragments that rise to the sea surface and float until they are water-logged an sink back to the seafloor. The other endmember is magmatic pumice eruptions are related to dome emplacement of highly viscous lava. The thermally and mechanically stressed surface of the dome releases pumice clasts in a non-explosive manner. Kano (2003) points out that phreatomagmatic pumice eruptions do not occur deeper than 300 m and magmatic pumice eruption are not expected to occur deeper than 1000 m. Good examples for the growing knowledge in submarine volcanism are two

recent studies that classified new intermediate pumice related submarine eruption types. Rotella (2013) identified the effusive Tangaroan eruption style at the Macauley seamount which produces abundant buoyant pumice clasts that can drift > 25 km away from the vent. Allen and McPhie (2009) defined the Neptunian eruption style which also produces buoyant pumices but from a magmatic volatile-driven explosion. They assume Neptunian eruptions to occur in depths between 200 and 1300 m.

From these considerations, it follows that water depth has a vital influence on the style and fragmentation mechanism of seafloor eruptions.

1.2.6 Water depth

Water depth is a critical parameter affecting the style of submarine eruptions due to the increasing pressure with increasing depth (+1 bar each 10 m depth). The widely used concept of Kokelaar (1986) indicates the range of depths in which particular styles of eruptions can be expected (Fig. 1.4) and also illustrates some of the uncertainties involved.

One aspect is the effect of confining pressure on the volatile fragmentation depth (Fischer and Schmincke, 1984) that defines the threshold depth, below which the confining pressure is sufficient to suppress volatile exsolution. As a consequence of this effect, a volatile-enriched magma would cause a magmatic explosion in shallow water depths but erupt quietly and effusive in the deep sea. Furthermore, an increased volatile content lowers the magma viscosity and therefore influences its flow morphology (Yamagishi and Dimroth, 1985).

In addition to volatile exsolution, steam expansion is also heavily constrained by the confining pressure, thus violent phreatomagmatic explosions are limited to the upper few hundred meters in the oceans (Kokelaar, 1986; Head and Wilson, 2003; White et al., 2003a). However, this accounts only for mingling of lava with water followed by steam expansion (i.e. Surtseyan eruptions) and *contact surface steam explosivity*. The depth limitations for *bulk-interaction steam explosivity*, e.g. magma intruding into water-saturated sediment, are less clear and commonly believed to be possible down to the depth corresponding to the critical pressure of seawater (i.e. ~ 3 km; Kokelaar, 1986; Head and Wilson, 2003; White et al., 2003a). Some of the existing uncertainties in determining depth limitation for steam explosivity are exemplified by results of an experiment conducted by Wohletz (2003). This author analyzed water-magma interaction above the critical pressure of water and found that the explosive energy increased with

increasing pressure, which is conflicting with the commonly accepted model. But concerns about the validity of the experimental findings exist. The setup used a fixed water-magma ratio, which contrasts the commonly infinite amount of water at the eruption site on the seafloor. Another concern is that the experimental containment vessel may have reflected shock waves (White et al., 2003b).

Recent findings have shown that CO_2-rich magmas can erupt explosively by magmatic volatile exsolution in the deep sea below 4 km depth. These examples comprise pyroclastic deposits on the Gakkel Ridge (Sohn et al., 2008) in 4000 m and in the North Arch Volcanic Field, Hawaii, in 4300 m depth (Clague et al., 2002).

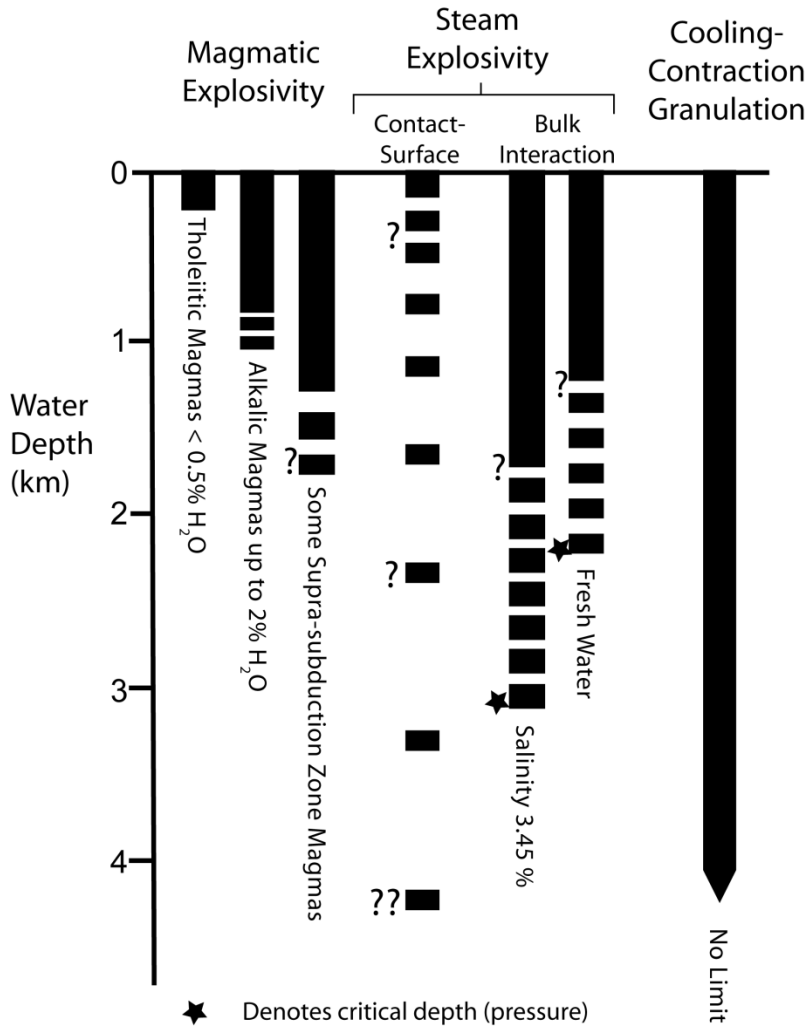

Figure 1.4: Graph of estimated depth ranges for clast forming processes of submarine volcanism by Kokelaar (1986). Note the uncertainties as to the maximum depths of clast-forming processes. Also note that magmatic explosivity is not considered a primary trigger of fragmentation.

In summary, the maximum water depths to which the different explosive mechanisms can occur is still strongly debated (e.g. McBirney, 1963; Sheridan and

Wohletz, 1983; Kokelaar, 1986; Cas, 1992; Zimanowski et al., 1995; Wohletz, 2002; Head and Wilson, 2003; White et al., 2003a; Sohn et al., 2008; Helo et al., 2011). In the upper few hundred meters of water, violent phreatomagmatic explosions can generally produce abundant pyroclastic debris and pumice (e.g. Kokelaar, 1983; Head and Wilson, 2003; White et al., 2003a; Allen and McPhie, 2009; Allen et al., 2010; Rotella et al., 2013). The vigor of steam explosions decreases with increasing water depth due to the heightened confining pressure. Thus, in the deep-sea, below the critical depth of water (~3 km), only magmatic explosivity occurs (Kokelaar, 1986; Zimanowski et al., 1991; White et al., 2003a; Sohn et al., 2008; Clague et al., 2009; Helo et al., 2011).

The heat source of these volcanic settings can produce hydrothermal circulation if a threshold permeability of the basement and the omnipresence of water are given.

1.3 Hydrothermal systems

The discovery of hydrothermal vents on the Galapagos Rift in 1977 (e.g. Corliss et al., 1979) was perhaps one of the most exciting scientific discoveries in the last third of the twentieth century, in particular because of the unique chemosynthetic life forms these vents harbor. But these systems were also recognized for their potential to form massive sulfide deposits, and many researchers believe that submarine vents are modern analogs for volcanogenic massive sulfide deposits on land. In general, submarine hydrothermal processes have an important influence on the global balance of heat and the cycling of elements between the solid earth and the oceans and atmosphere (German and Von Damm, 2003). It is estimated that about 30% of the total heat loss of oceanic crust is controlled by hydrothermal systems (Sclater and Parsons, 1981), which also affect the isotopic and chemical composition of seawater as hydrothermal circulation is a source for Ca, SiO_2, Fe, Mn, Li, Rb and Cs and an important sink for Mg and CO_2 (Edmond et al., 1979; Von Damm et al., 1985).

In general, three major components allow for fluid circulation through oceanic and island-arc crust: (i) a faulted and fissured igneous crust that acts as a permeable medium, (ii) seawater that fills void space in the crust and (iii) the presence of a heat source in form of magma or hot rocks. The size, shape and depth of the heat source, as well as the type of host rock which interacts with the circulating seawater determine the composition of the vent fluids that are discharged in hydrothermally active areas of the seafloor (e.g. Hannington et al., 2005; Tivey, 2007). Alt (1995) distinguished three zones in a

conceptual model of a hydrothermal circulation cell at an MOR (Fig. 1.5), including a "recharge" zone, where first water-rock reactions occur at relatively low temperatures. With increasing depth and temperature, the circulating fluid becomes acidic, anoxic and alkali-rich due to water-rock reactions. Near the heat source, in the "reaction zone", the fluid leaches S and metals (e.g. Cu, Zn, Fe, As, Au, Ag; Ishibashi and Urabe, 1995; Yang and Scott, 2002; Hannington et al., 2005) from the rock and can take up magmatic volatiles (e.g. He, CO_2, CH_4, H_2, SO_2) (e.g. Butterfield et al., 2003). If the seawater-derived fluid is heated above the critical curve, phase separation into a low-salinity vapor phase and a metal-rich brine phase occurs (Von Damm, 1995). In shallow water depths, pressures are subcritical and the fluid will undergo boiling instead of brine condensation. While the hot and buoyant fluid rises rapidly through the "discharge" zone, it further reacts with the host rock. These fluids either discharge directly into the ocean or undergo mixing with seawater entrained into the seafloor near the vents.

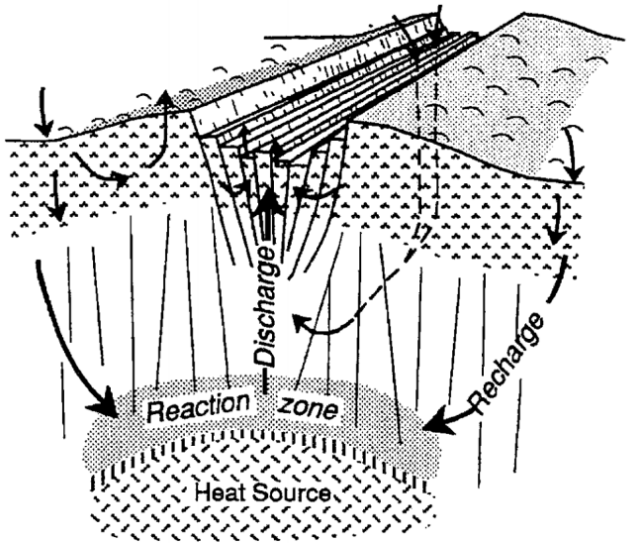

Figure 1.5: Sketch by Alt (1995) illustrating three characteristic zones of a hydrothermal circulation system exemplified for a slow-spreading mid-ocean ridge system. As seawater enters the crust at recharge zones, it reacts at low temperatures with the rocks. At temperatures above 350°C further modifications occur in the reaction zone close to the heat source. The hot and buoyant fluids rise rapidly through the discharge zone to the seafloor. (Alt, 1995)

1.3.1 Hydrothermal vent related fauna

The discovery of hydrothermal vents came along with the discovery of chemosynthetic organisms, which, as we know today, are widespread and occur in many different habitats besides hydrothermal vents (Van Dover et al., 2006; Dubilier et al., 2008). Chemosynthesis stands for the ability of microorganisms to gain energy from the oxidation of reduced inorganic compounds in the vent fluid (e.g. H_2S, S, CH_4) and using this energy to fixing CO_2 in biomass. Using chemosynthesis, the free-living and symbiotic microorganisms form the base of the food web at hydrothermal vents, where a large number of animals have established symbiosis with these microbial endosymbionts.

It is therefore believed that symbiont-associated animals make up the majority of biomass at hydrothermal vents (e.g. Van Dover, 2000; Dubilier et al., 2008). Typical animals hosting endosymbionts are tube worms, mussels, gastropods, clams and shrimps. These animals and perhaps also the endosymbiotic microorganisms tend to occur in distinct biogeographical provinces. For instance, the giant tube work *Riftia* colonizes vents at the East Pacific Rise, while the hydrothermally active sites in the western Pacific arc- and back-arc systems are dominated by the gastropods *Ifremeria* and *Alviniconcha*. Besides these regional characteristic faunas, other parameters like the venting temperature, the fluid composition, the style of venting and mineralogy of deposits also influence the fauna. The geological setting is hence vitally important for the nature and evolution of microbial habitats in seafloor vents.

1.3.2 Back-arc basin hydrothermal systems

A plethora of parameters, including basement composition, intensity of tectonic faulting versus magmatic diking, the style and type of volcanic degassing, the water depths, etc., influences the composition of vent fluids, the type of hydrothermal vents and mineral deposits that evolve on the seafloor. The majority of known hydrothermal vents are located at plate boundaries, with 65 % along MOR, 22 % in back-arc basins, 12 % along volcanic island arcs, while only 1 % is hosted in oceanic intra-plate volcanoes (Baker and German, 2004; Hannington et al., 2005).

Hydrothermal fluid compositions from mature back-arc spreading centers are somewhat similar to compositions from MOR, because both systems are predominantly basalt-hosted (Mottl et al., 2011). Magma compositions at oceanic island arcs and related back-arc rifts (e. g. east Manus Basin) are strongly influenced by fluids originating from the subducted slab, by partial decompression melting and also by fractional crystallization and assimilation of preexisting crust. This complexity is reflected in the rock suite that encompasses MORB-like to high-K calc-alkaline andesites to rhyolites (Binns and Scott, 1993; de Ronde et al., 2001; Sinton et al., 2003; Hannington et al., 2005). Therefore, water-rock reactions cause a wide range of different hydrothermal fluid compositions which can be further influenced by the addition of magmatic volatiles leading to a hydrothermal fluid enriched in metalloids (e.g. As, Sb) and metals such as Cu, Au, Zn, Fe, Ag (Ishibashi and Urabe, 1995; Hannington et al., 2005). Additionally, magmatic SO_2 can be added which disproportionates to form sulfuric acid resulting in very low pH (< 1) fluids (Gamo et al., 1997). The deposits created by these metal-enriched hydrothermal

fluids are of economic interest and thought to represent modern analogs of ancient volcanic massive sulfide (VMS) deposits.

1.3.3 Massive sulfide deposits

Although the majority of hydrothermal vents and associated sulfide deposits are located at MOR, such deposits are only poorly represented in the geological record due to recycling of the oceanic crust at subduction zones. The majority (~80%) of VMS deposits is associated with areas of bimodal volcanism (basalt-rhyolite) and is thought to have formed in extensional geodynamic settings, e.g. arc-related rifts (e.g. Franklin et al., 1981; Mosier et al., 1983; Lentz, 1998; Hannington et al., 2005). Subduction related arc and back-arc volcanism is believed to have generated nearly half of the global VMS tonnage in a relatively short period (340 m. y.), which is persevered along the Paleozoic continental margins of the Appalachians, the North American Cordillera, the Tasman Geosyncline, the Iberian Pyrite Belt, and the Southern Urals (Barrie and Hannington, 1999; Franklin et al., 2005; Hannington et al., 2005).

Studies of present day seafloor hydrothermal systems as they occur in the eastern Manus Basin, which hosts possible modern analogs of Kuroko type deposits (Binns and Scott, 1993), contribute significant information on the genesis and structural control of VMS deposits.

1.4 Regional geology

The Bismarck Sea covers an area about 250,000 km² and is located in the south western Pacific Ocean. The sea extends to northeast of New Guinea (Papua New Guinea mainland) and is bordered to the southeast by the island of New Britain, to northeast by the island of New Ireland and to the north by Manus Island (Fig. 1.6). The islands, as well as Bougainville, belong to the Melanesian island arc.

1.4.1 Evolution of the Bismarck Sea

During the Cenozoic, the rapid and oblique convergence of the Australian and Pacific plate caused a complex tectonic setting in the southwestern Pacific Ocean that comprises, amongst others, microplate formation and rotation, subduction polarity reversal, oceanic island arc formation and lithospheric extension to form back-arc basins and oceanic basins (see reviews by Lee and Ruellan, 2006; Baldwin et al., 2012).

Until the late Miocene, southward subduction of the Pacific-Caroline Plate underneath the Australian Plate occurred along the Manus and North Solomon Trench

and caused the construction of the Melanesian island arcs (Coleman and Packham, 1976). With ongoing subduction, the Ontong Java Plateau collided with the subduction zone in the late Miocene and induced a regional tectonic reorganization leading to a subduction polarity reversal (Coleman and Packham, 1976; Kroenke and Rodda, 1984). As a consequence, northward subduction of the Solomon Plate underneath the Pacific-Caroline Plate occurred at the New Britain and South Solomon Trench, generating a second generation of island arc volcanism on the Melanesian island arc. Thus, the Melanesian island arc consisted of an inner and outer range which is still present at the Solomon Islands. About 3.5 Ma ago, New Guinea collided with parts of the island arc (the Finisterre-Huon Range) which triggered the division of the inner and outer western Melanesian arc (e.g. Manus Island and New Britain). This event was either part of or the initiation of the opening of the Bismarck Sea (Taylor, 1979; Tregoning, 2002; Wallace, 2004; Lee and Ruellan, 2006). The New Guinea Basin is a product of the initial opening as well as the Willaumez Rise which is produced by extensive lava emplacement. At about 0.78 Ma, the Finisterre-Huon Range and New Guinea finally got interlocked. This entailed another change in the tectonic configuration which set up the complex present day plate boundary between the North and South Bismarck Plates (Fig. 1.6). The pinning additionally caused an asymmetric extension of the two plates resulting in an increasing opening speed of the Bismarck Sea towards west (Tregoning et al., 1999; Wallace, 2004; Lee and Ruellan, 2006).

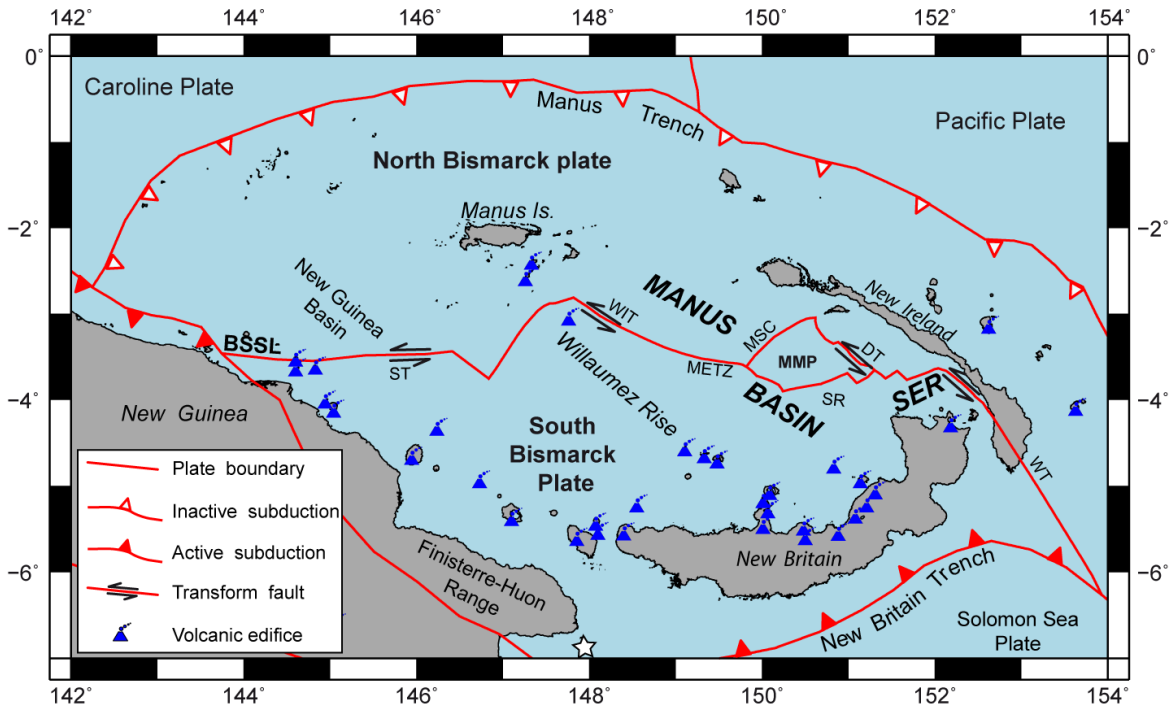

Figure 1.6: Present day tectonic setting of the Bismarck Sea. Plate boundaries from (Bird, 2003). The white star marks the absolute pole of the South Bismarck Plate rotation (Tregoning et al., 1999). Abbreviation: Bismarck Sea Seismic Lineation (BSSL); Schouten Transform (ST); Willaumez Transform (WIT); Manus Spreading Center (MSC); Manus Extensional Transform Zone (METZ); Manus Microplate (MMP); Southern Rifts (SR); Djaul Transform (DT); Weitin Transform (WT).

1.4.2 Present day Bismarck Sea and Manus Basin

Today, the Bismarck Sea hosts two basins: the New Guinea Basin in the West and the Manus Basin in the East. The two basins are separated from each other by the Willaumez Rise, an approximately 400 km long volcanic ridge striking northeast (Fig. 1.6).

The active Bismarck Sea Seismic Lineation (BSSL) divides the North and South Bismarck Plates and defines the plate boundary (Taylor, 1979; B. Taylor et al., 1994; Martinez and Taylor, 1996, 2003). The BSSL is defined from West to East by the Schouten Transform (ST), the Willaumez Transform (WIT), the Manus Extensional Transform Zone (METZ), the Manus Spreading Center (MSC), the Djaul Transform (DT) and the Weitin Transform (WT), which runs southward through New Ireland. Thus, the BSSL comprises two spreading segments (METZ and MSC) and several left-lateral transform faults. These days, major lithospheric extension is limited to the Manus Basin, a young and rapidly opening back-arc basin with an average water depth of 2000 m. Seismic studies revealed the crustal thickness between the Manus Basin (18 km) and New

Britain island arc (35 km) which underlines the presence of back-arc lithospheric extension (Finlayson and Cull, 1973). Rapid clockwise rotation (~ 8° Ma-1) of the South Bismarck Plate about a single pole of rotation at 6.75°S, 147°.98 (white star in Fig. 1.6; Tregoning et al., 1999) results in an asymmetric spreading of the North and South Bismarck Plate, which causes an eastward propagation of the BSSL.

Lithospheric extension in the Eastern Manus Basin is distributed between the MSC, METZ, Southern Rift (SR) and the South East Ridges (SER; Fig. 1.6). New oceanic crust is formed at the METZ and MSC with MORB-like lava compositions and the least contribution of subduction-related components of all Manus Basin lavas (Sinton et al., 2003). Spreading at the MSC occurs in a highly oblique matter, creating a wedge of positively magnetized crust which is 72 km wide at the eastern end and zero at the western tip (Martinez and Taylor, 1996).

The Manus Microplate (MMP) experiences counterclockwise rotation probably induced by the left-lateral motion between the North and South Bismarck Plates. The Southern Rifts occur south of the MMP and host a series of graben structures that are partially floored by lava flows (Martinez and Taylor, 1996).

At back-arc rifts (SER) in the easternmost part of the Manus Basin, rifting of mid-Cenozoic island arc crust occurs (Coleman and Packham, 1976; Falvey and Pritchard, 1982; Kroenke and Rodda, 1984; Binns and Scott, 1993; Martinez and Taylor, 1996; Sinton et al., 2003). The SER are located at the easternmost tip of the BSSL and thus, due to the asymmetric spreading, exhibit the highest spreading rates in the Manus basin (up to 137.5 mm*a-1; Tregoning, 2002; Tregoning et al., 1999). The NE-SW oriented ~70km long neovolcanic zone is bordered by two left-lateral transform faults (Weitin and Djaul Transform; Fig. 1.6, 1.7) and accommodate solitary volcanoes and a series of en echelon volcanic ridges. The ridges are 20 to 30 km long, <5 km wide, and 500 to 700 m high and developed a sigmoidal shape in response to the shearing force of the two transform faults. Magma genesis at the SER is influenced, due to its proximity to the New Britain Arc, by the mantle wedge, subducting slab and remnant island arc crust. This results in bimodal lava composition which include the complete series of basalt to rhyolite with a strong geochemical similarity to lavas of the New Britian island arc (Binns and Scott, 1993; Kamenetsky et al., 2001; Sinton et al., 2003; Lee and Ruellan, 2006). The influence of slab-derived fluids and melt generation from the New Britain Trench decreases with

increasing distance as lavas at the MSC show only traces of subduction (Sinton et al., 2003; Pearce and Stern, 2006).

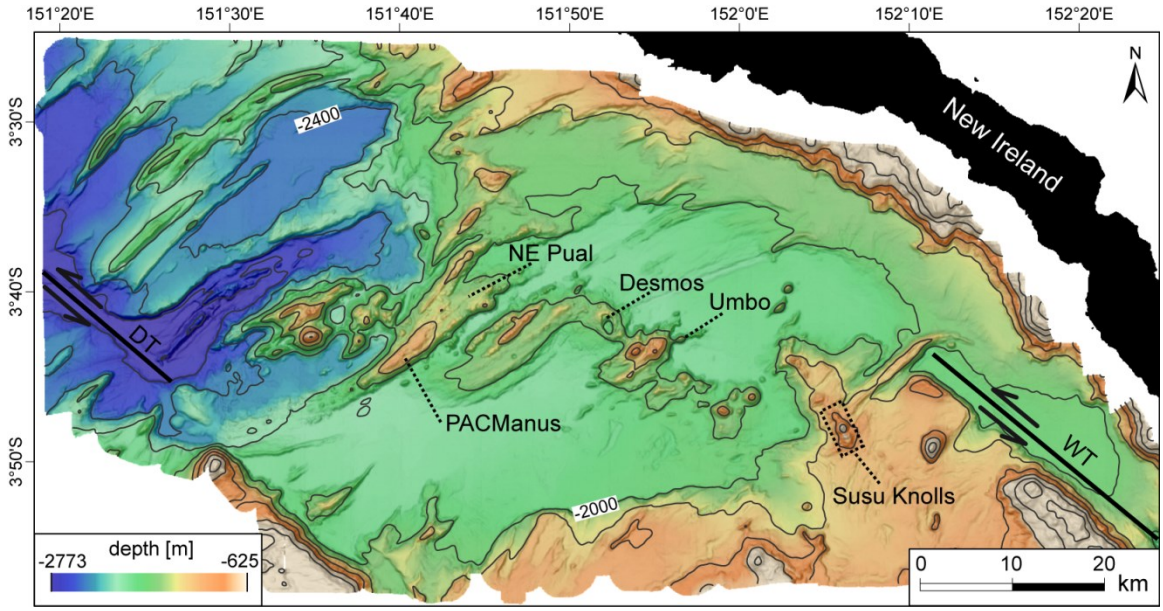

Figure 1.7: Bathymetric map of the South East Ridges (SER) in the eastern Manus Basin with 200 m contours and primary hydrothermal active areas. Positions of the left-lateral Djaul (DT) and Weitin Transform (WT) are estimated based on topographic structures. Bathymetric data was collected at research cruise BAMBUS SO-216 with R/V Sonne in June/July 2011.

1.4.3 Hydrothermal activity at the South East Ridges

Several hydrothermal vent areas, such as PACManus, North Pual, Desmos and SuSu Knolls have been discovered at the SER (Fig. 1.7). Their fluid chemistry shows a large variability and reflects the complex tectonic and magmatic diversity (Binns and Scott, 1993; Auzende et al., 1996a, 2000; Gamo et al., 1997; Hashimoto and Ohta, 1999; Tivey et al., 2006; Bach et al., 2011; Reeves et al., 2011). The accumulation of polymetallic sulfides in these areas has been considered a modern analog of ancient Volcanic Massive Sulfide (VMS) deposits mined on land (e.g. Binns and Scott, 1993; Petersen et al., 2003; Yeats et al., 2008).

1.4.4 Study area #1 - PACManus

The PACManus Hydrothermal District (Papua – Australia – Canada – Manus) is located in the SER in 1640 – 1740 m water depth on the central crest of Pual Ridge, which is ~20 km long, 1 - 1.5 km wide and rises 500 – 600 m above the surrounding seafloor (Fig. 1.7). The hydrothermal district, based on present day knowledge, comprises following hydrothermal vent sites: Tsukushi, Snowcap, Fenway, Solwara 8, Mimosa site, Satanic Mills, Roman Ruins, Rogers Ruins and Solwara 6 and 7. Although the vent sites

are within hundreds of meters of each other, their fluids have different temperatures (max. 358°C, i.e. at boiling point), varying chemical compositions (Reeves et al., 2011) and plume particle colors ranging from clear to grey to black. In areas of persistent fluid discharge, biological communities are well-developed, including bacterial mats, molluscs, tube worms, crabs, anemones, holothurians, and a range of crustaceans and fish (Hashimoto et al., 1999).

PACManus was first discovered and sampled in 1991 by Binns and Scott (1993) via dredge and photo-sled surveys. Volcanic rocks on the seafloor are predominantly aphyric and have a composition that ranges from dacites to rhyolites. AUV bathymetry delineates several volcanic edifices 200-300 m in diameter with steep-sided flow units exhibiting a crenulated worm-like texture. Lava emplacement occurs in form of domes and different styles of effusive volcanism creating pillows, lobate, jumbled and block lava flows. In some cases intense autobrecciation or pumice production accompanies eruptions. On Leg 193 of the Ocean Drilling Programm (ODP), several boreholes penetrated the seafloor at the PACManus area down to a maximum depth of 387 mbsf (Binns et al., 2007). The drilling campaign revealed that Pual Ridge is constructed by multiple lava flows and domes which are accompanied by syn-eruptive clast production (Paulick et al., 2004; Binns et al., 2007). Rock compositions from the interior of Pual Ridge range from andesites to rhyodacites. Subseafloor hydrothermal circulation resulted in a wide range rock alteration, different hydrothermal deposits as anhydrite-cemented breccias and sulfide-impregnated volcaniclastic (Paulick et al., 2004; Binns et al., 2007). Sulfides deposited on the seafloor are enriched in Au, Ag, Pb, As, Sb, and Ba (Binns and Scott, 1993; Moss and Scott, 2001).

1.4.5 Study area #2 - North Su

The second study area, North Su, is located ~50 km to the West of the PACManus Hydrothermal District. North Su is the central volcanic edifice of the SuSu Knolls Hydrothermal District, which comprises three volcanic edifices (South Su, North Su and Suzette) in the easternmost part of the SER (Fig. 1.7). The Susu Knolls are located at the intersection of a NE-trending extensional rift structure (Bugave Ridge) with the NNW striking Tumai Ridge (Moss and Scott, 2001). Analyses of sulfide deposits revealed that the SuSu Knolls Hydrothermal District represents a submarine analogue to terrestrial high sulfidation Cu-Au mineralization(Yeats et al., 2008).

North Su is an active, conically shaped volcano with a double peak and rises from 1600 m to 1154 m water depth with a mean slope between 25° to 30°. Hydrothermal activity was first discovered in 1996 during the PACMANUS III expedition (Binns et al., 1997) when first rock samples have been dredged from the seafloor and visual observation were made via photo sled surveys. Rock samples from North Su are porphyritic andesites with a dacitic to rhyolitic glass composition. Volcanic activity is reflected by a wide range of eruption products which include craters, abundant sand-sized clastic material, stubby lava flows and spines.

The hydrothermal fluids and associated deposits on the seafloor are extremely varied. Acidic white smoker activity with a strong magmatic input (Seewald et al., 2014) discharge in less than 100 m lateral distance to black smoker vents. Besides these two extreme fluid compositions, diffuse fluid discharge of clear fluids exists as well. Volcanic rocks are highly altered in areas of acidic fluid discharge. Also, abundant native sulfur is deposited on the seafloor and discharge of liquid sulfur together with emissions of liquid CO_2 was present in 2011.

1.5 Motivation and outline

This project was conducted in order to give a better understanding of submarine back-arc volcanism and its interplay with related high-temperature hydrothermal systems and their potential to form VMS deposits. A knowledge gap still exists in the field of submarine volcanism in regard to eruption styles and products of intermediate to high-silica lava compositions. The Manus Basin host a wide range of lava compositions and volcanic ranges and thus is a predestine region to study the variety of submarine eruption styles, lava flow morphologies and eruption products.

Besides scientific questions, this project had the ambition to demonstrate the potential of standard ROV video material that is usually recorded as a by-product of scientific work on the seafloor without the explicit aim of mapping. When this video material is combined with AUV based micro-bathymetry, rock and fluid samples, and temperature measurements, a comprehensive data set exists that can be implemented into a GIS to run further quantitative analyses. This method was used to investigate the structural relationship of volcanic facies and hydrothermal activity, and in which way hydrothermal and volcanic activity interact and influence the seafloor morphology.

The research for this dissertation was conducted within the Department of Geosciences of the University of Bremen and funded through the MARUM "Center for Marine Environmental Sciences" as part of the research area GB4 "Geosphere-Biosphere Interaction - From element and energy fluxes to vent ecosystems". Additional funding was received through the DFG Research Center / Excellence Cluster – "The Ocean in the Earth System". This project was carried out from March 2011 until February 2014.

The data used in this work was collected during research cruise "Magellan-06" in 2006 on R/V Melville with ROV Jason-2 and AUV ABE under the direction of Maurice Tivey, and during research cruise "BAMBUS – So216" in 2011 on R/V Sonne with ROV MARUM Quest 4000m under the direction of Wolfgang Bach. Additional bathymetric data was analyzed that was collected during research cruise R/V Sonne 166 in 2002.

The following chapters present two case studies at the eastern Manus Basin where high-resolution geologic mapping studies were conducted to investigated the volcanic facies, hydrothermal systems and their interaction. The thesis is completed by a conclusion and outlook.

Chapter 2: "Geologic Setting of PACManus Hydrothermal Vent Fields – High resolution mapping and in situ observations"

Authors: Janis Thal, Maurice Tivey, Dana Yoerger, Niels Jöns, Wolfgang Bach. (Marine Geology, accepted manuscript)

This high-resolution geological mapping project of the felsic–hosted "PACManus Hydrothermal District" resulted in a comprehensive documentation and analyses of seafloor structures. The aim of this research was the identification of volcanic facies based on lava flow morphologies and rock samples, and to analyze the spatial distribution of hydrothermal vent fields. A shallow subseafloor fluid pathway model was developed that illustrates the influence of volcanic facies on hydrothermal discharge. Additionally, a three-stage chronological sequence for the magmatic accretion was defined.

Chapter 3: "Volcanic and hydrothermal activity of the North Su volcano: New insights from repeated bathymetric surveys and ROV observations"

Authors: Janis Thal, Maurice Tivey, Dana Yoerger, Niels Jöns, Dominik Niedermeyer, Wolfgang Bach. (Journal of Volcanology and Geothermal Research, to be submitted)

The second high-resolution geological mapping project was conducted on the active solitary volcano, North Su. This research focused on an extensive documentation of the hydrothermal discharge sites, volcanic facies and the recent volcanic evolution. Various volcanic eruption styles and eruption products could be characterized which allowed defining a multi-stage chronological sequence of the recent volcanic activity. Further, the influence of acidic hydrothermal fluids on the slope stability was investigated. It is the first documentation of an active submarine volcano erupting porphyritic high-viscous andesite lava.

Chapter 4: "Synthesis and outlook"

This dissertation closes with a conclusion and outlook to emphasize the importance of geologic seafloor mapping and the use of ROV video recordings with suggestions how to increase the usability of ROV video data. The importance of research on submarine arc-related volcanism is outlined with the influence on ore-forming mechanisms. Finally, concepts for further investigations in the Manus Basin are presented.

1.6 Scientific contributions

In the framework of this dissertation, comprehensive research activity resulted in two first-author manuscripts that are presented in chapter two and three, and six co-authorships.

Prior to the dissertation project, I took part at the MENEZKART – R/V Poseidon cruise 402 to the Menez Gwen hydrothermal field as marine geologist and being responsible for geologic mapping. During the dissertation, I contributed chapters to the cruise report (1) and acted as a consultant for geologic questions. This geologic background data of Menez Gwen and further geologic consultancy contributed to the scientific paper of Marcon et al. 2013 (2).

During research cruise BAMBUS – R/V Sonne 216 in the Manus Basin, I was responsible for geologic mapping, data management and ROV dive preparation. Part of this work resulted in contributions to the cruise report (3) and a report published at InterRidge News (4). Further, I could provide geologic background information to a manuscript by Müller et al. (5).

On research cruise Marie S. Merian 20/5 to North Pond, I was responsible for bathymetric mapping and data management, and contributed to the cruise report (6).

(1) Borowski, C., Meinecke, G., Meyer, V., Nowald, N., Renken, J., Ruhland, G., Wendt, J., Wintersteller, P., **Thal, J.**, **2010**. MENEZKART - RV Poseidon Cruise No. 402.

(2) Marcon, Y., Sahling, H., Borowski, C., dos Santos Ferreira, C., **Thal, J.**, Bohrmann, G., **2013**. Megafaunal distribution and assessment of total methane and sulfide consumption by mussel beds at Menez Gwen hydrothermal vent, based on geo-referenced photomosaics. Deep Sea Res. Part I Oceanogr. Res. Pap. 75, 93–109.

(3) Bach, W., Jöns, N., **Thal, J.**, Breuer, C., Shu, L., Dubilier, N., Borowski, C., Meyerdierks, A., Pjevac, P., Brunner, B., Müller, I., Petersen, S., Hourdez, S., Schaen, A., Koloa, K., Jonda, L., Team, M.Q. 4000m, **2011**. Report and preliminary results of RV SONNE Cruise SO-216, Townsville (Australia) - Makassar (Indonesia), June 14 – July 23, 2011. BAMBUS, Back-Arc Manus Basin Underwater Solfataras. Berichte, Fachbereich Geowissenschaften, Univ. Bremen 280, 87.

(4) Bach, W., Jöns, N., **Thal, J**., Breuer, C., Shu, L., Dubilier, N., Borowski, C., Meyerdierks, A., Pjevac, P., Brunner, B., Müller, I., Petersen, S., Hourdez, S., Schaen, A., Koloa, K., Jonda, L., Team, M.Q. 4000m, **2012**. Interactions between fluids, minerals, and organisms in sulfur-dominated hydrothermal vents in the eastern Manus Basin, Papua New Guinea – A report from RV Sonne Cruise 216. InterRidge News 21, 31–34.

(5) Müller, A.I., Brunner, B., Max, T., Breuer, C., Reeves, E., **Thal, J.**, Bernasconi, M.S., Bach, W., (**to be submitted**). The sulfur and oxygen isotope signature of magmatic SO_2 disproportionation: Implications from laboratory experiments and a hydrothermally active site in the Manus Basin, Papua New Guinea. Earth Planet. Sci. Lett.

(6) Bach, W., Edwards, K.J., Girguis, P., Glazer, B., Hulme, S., Jaekel, U., Lin, H., Orcutt, B., **Thal, J**., Villinger, H., Wheat, G., Collasius, A., Hansen, S., Hutchinson, B., Kevis-stirling, A., 2012. Borehole microbial observatory science

in basaltic ocean crust: The North Pond area on the western Mid-Atlantic Ridge flank at 23°N. DFG Senat. für Ozeanogr. MSM20/5, 60pp.

1.7 References

Allen, S.R., Fiske, R.S., Tamura, Y., 2010. Effects of water depth on pumice formation in submarine domes at Sumisu, Izu-Bonin arc, western Pacific. Geology 38, 391–394.

Allen, S.R., McPhie, J., 2009. Products of neptunian eruptions. Geology 37, 639–642.

Alt, J., 1995. Subseafloor processes in mid-ocean ridge hydrothennal systems, in: Humphris, S.E., Zierenberg, R.A., Mullineaux, L.S., Thomson, R.E. (Eds.), Seafloor Hydrothermal Systems: Physical, Chemical, Biological, and Geological Interactions. American Geophysical Union, Washington, D. C., pp. 85–114.

Auzende, J.-M., Ishibashi, J.-I., Beaudoin, Y.C., Charlou, J.-L., Delteil, J., Donval, J.-P., Fouquet, Y., Ildefonse, B., Kimura, H., Nishio, Y., Radford-Knoery, J., Ruøllan, E., 2000. Extensive magmatic and hydrothermal activity documented in Manus Basin. Eos, Trans. Am. Geophys. Union 81, 449–453.

Auzende, J.-M., Urabe, T., Party, S., 1996a. Cruise explores hydrothermal vents of the Manus Basin. Eos (Transactions, Am. Geophys. Union) 77, 244.

Auzende, J.-M., Urabe, T., Ruellan, E., Chabroux, D., Charlou, J.-L., Gena, K., Gamo, T., Henry, K., Matsubayashi, O., Matsumoto, T., Naka, J., Nagaya, Y., Okamura, K., 1996b. “Shinkai 6500” Dives in the Manus Basin : New STARMER Japanese-French Program. JAMSTEC J. Deep Sea Res. 12, 323–334.

Bach, W., Jöns, N., Thal, J., Breuer, C., Shu, L., Dubilier, N., Borowski, C., Meyerdierks, A., Pjevac, P., Brunner, B., Müller, I., Petersen, S., Hourdez, S., Schaen, A., Koloa, K., Jonda, L., Team, M.Q. 4000m, 2011. Report and preliminary results of RV SONNE Cruise SO-216, Townsville (Australia) - Makassar (Indonesia), June 14 – July 23, 2011. BAMBUS, Back-Arc Manus Basin Underwater Solfataras. Berichte, Fachbereich Geowissenschaften, Univ. Bremen 280, 87.

Bach, W., Jöns, N., Thal, J., Breuer, C., Shu, L., Dubilier, N., Borowski, C., Meyerdierks, A., Pjevac, P., Brunner, B., Müller, I., Petersen, S., Hourdez, S., Schaen, A., Koloa, K., Jonda, L., Team, M.Q. 4000m, 2012. Interactions between fluids, minerals, and organisms in sulfur-dominated hydrothermal vents in the eastern Manus Basin, Papua New Guinea – A report from RV Sonne Cruise 216. InterRidge News 21, 31–34.

Baker, E.T., German, C.R., 2004. On the global distribution of mid-ocean ridge hydrothermal vent-fields, in: German, C.R., Lin, J., Parson, L.M. (Eds.), Mid-Ocean Ridges: Hydrothermal Interactions between the Lithosphere and Oceans. American Geophysical Union, Washington, D. C., pp. 245–266.

Baldwin, S.L., Fitzgerald, P.G., Webb, L.E., 2012. Tectonics of the New Guinea Region. Annu. Rev. Earth Planet. Sci. 40, 495–520.

Ballard, R.D., Moore, J.G., 1977. Photographic Atlas of the Mid-Atlantic Ridge Rift Valley. Springer New York, New York, NY.

Barash, M.S., Kuptsov, V.M., 1997. Late Quaternary palaeoceanography of the western Woodlark Basin (Solomon Sea) and Manus Basin (Bismarck Sea), Papua New Guinea, from planktic foraminifera and radiocarbon dating. Mar. Geol. 142, 171–187.

Barrie, C.T., Hannington, M.D., 1999. Classification of volcanic-associated massive sulfide deposits based on host-rock composition. Rev. Econ. Geol. 8, 1–11.

Barriga, F.J.A.S., Binns, R.A., Baldauf, J., Miller, D.J., 2000. Anatomy of an Active, Felsic-Hosted Hydrothermal System, Eastern Manus Basin. ODP Leg 193 Sci. Prospect.

Bartetzko, A., Paulick, H., Iturrino, G., Arnold, J., 2003. Facies reconstruction of a hydrothermally altered dacite extrusive sequence: Evidence from geophysical downhole logging data (ODP Leg 193). Geochemistry Geophys. Geosystems 4, 1087.

Bevins, R.E., Roach, R.A., 1979. Pillow lava and isolated-pillow breccia of rhyodacitic composition from the Fishguard Volcanic Group, Lower Ordovician, SW Wales, United Kingdom. J. Geol. 87, 193–201.

Binns, R.A., 2004. Data report: spinifex-textured basalt xenoliths at PACMANUS, Papua New Guinea, in: Barriga, F.J.A.S., Binns, R.A., Miller, D.J., Herzig, P.M. (Eds.), Proceedings of the Ocean Drilling Program, Scientific Results. College Station, TX (Ocean Drilling Program), pp. 1–19.

Binns, R.A., Barriga, F.J.A.S., Miller, D.J., 2007. Leg 193 synthesis: Anatomy of an active felsic-hosted hydrothermal system, eastern Manus Basin, Papua New Guinea, in: Barriga, F.J.A.S., Binns, R.A., Miller, D.J., Herzig, P.M. (Eds.), Proceedings of the Ocean Drilling Program, Scientific Results. College Station, TX (Ocean Drilling Program), pp. 1–71.

Binns, R.A., Scott, S., 1993. Actively forming polymetallic sulfide deposits associated with felsic volcanic rocks in the eastern Manus back-arc basin, Papua New Guinea. Econ. Geol. 88, 2226–2236.

Binns, R.A., Scott, S.D., Gemmell, J.B., Crook, K.A.W., Party, S., 1997. The SuSu Knolls Hydrothermal Field, Eastern Manus Basin, Papua New Guinea. Eos Trans. AGU Fall Meet. Suppl. 78, #V22E–02 (abstr.).

Bird, P., 2003. An updated digital model of plate boundaries. Geochemistry, Geophys. Geosystems 4, 1–52.

Bischoff, J.L., Rosenbauer, R.J., 1985. An empirical equation of state for hydrothermal seawater (3.2 percent NaCl). Am. J. Sci. 285, 725–763.

Bonatti, E., Harrison, C.G. a., 1988. Eruption styles of basalt in oceanic spreading ridges and seamounts: Effect of magma temperature and viscosity. J. Geophys. Res. 93, 2967.

Butterfield, D.A., Fouquet, Y., Halbach, M., Halbach, P.E., Humphris, S.E., Lüders, V., Petersen, S., Seyfried, W.R.J., Shimizu, M., Tivey, M.K., 2003. Group Report: How can we describe fluid-mineral processes and the related energy and material fluxes?, in: Halbach, P.E., Tunnicliffe, V., Hein, J.R. (Eds.), Energy and Mass Transfer in Marine Hydrothermal Systems. Dahlem University Press, Berlin, pp. 183–209.

Butterfield, D.A., Nakamura, K. -i., Takano, B., Lilley, M.D., Lupton, J.E., Resing, J. a., Roe, K.K., 2011. High SO2 flux, sulfur accumulation, and gas fractionation at an erupting submarine volcano. Geology 39, 803–806.

Cas, R.A.F., 1992. Submarine volcanism; eruption styles, products, and relevance to understanding the host-rock successions to volcanic-hosted massive sulfide deposits. Econ. Geol. 87, 511–541.

Clague, D.A., Rubin, K., Keller, N., 2009. Products of submarine fountains and bubble-burst eruptive activity at 1200 m on West Mata Volcano, Lau Basin. AGU Fall Meet. Suppl. 90, Abstract V43I – 02.

Clague, D.A., Uto, K., Satake, K., Davis, A.S., 2002. Eruption style and flow emplacement in the submarine North Arch Volcanic Field, Hawaii, in: Takahashi, E., Lipman, P.W., Garcia, M.O., Naka, J., Aramaki, S. (Eds.), Hawaiian Volcanoes: Deep Underwater Perspectives. American Geophysical Union, Washington, D. C., pp. 65–84.

Coleman, P.J., Packham, G.H., 1976. The Melanesian Borderlands and India — Pacific plates' boundary. Earth-Science Rev. 12, 197–233.

Corliss, J.B., Dymond, J., Gordon, L.I., Edmond, J.M., von Herzen, R.P., Ballard, R.D., Green, K., Williams, D., Bainbridge, A., Crane, K., van Andel, T.H., 1979. Submarine thermal sprirngs on the galapagos rift. Science (80-.). 203, 1073–83.

Craddock, P.R., Bach, W., 2010. Insights to magmatic–hydrothermal processes in the Manus back-arc basin as recorded by anhydrite. Geochim. Cosmochim. Acta 74, 5514–5536.

Crawford, A.J., Falloon, T.J., Green, D.H., 1989. Classification, petrogenesis and tectonic setting of boninites, in: Crawford, A.J. (Ed.), Boninites and Related Rocks. Unwin Hyman, New York, pp. 1–49.

Crisp, J.A., 1984. Rates of magma emplacement and volcanic output. J. Volcanol. Geotherm. Res. 20, 177–211.

Davis, A.S., Gray, L.B., Clague, D.A., Hein, J.R., 2002. The Line Islands revisited: New 40 Ar/ 39 Ar geochronologic evidence for episodes of volcanism due to lithospheric extension. Geochemistry, Geophys. Geosystems 3, 1–28.

De Rita, D., Giordano, G., Cecili, A., 2001. A model for submarine rhyolite dome growth: Ponza Island (central Italy). J. Volcanol. Geotherm. Res. 107, 221–239.

De Ronde, C.E.J., Baker, E.T., Massoth, G.J., Lupton, J.E., Wright, I.C., Feely, R. a., Greene, R.R., de Ronde, C.E.J., 2001. Intra-oceanic subduction-related hydrothermal venting, Kermadec volcanic arc, New Zealand. Earth Planet. Sci. Lett. 193, 359–369.

De Rosen-Spence, A.F., Provost, G., Dimroth, E., Gochnauer, K., Owen, V., 1980. Archean subaqueous felsic flows, Rouyn-Noranda, Quebec, Canada, and their Quarternary equivalents. Precambrian Res. 12, 43–77.

Dinel, E., Saumur, B.M., Fowler, A.D., 2008. Spherulitic Aphyric Pillow-Lobe Metatholeiitic Dacite Lava of the Timmins Area, Ontario, Canada: A New Archean Facies Formed from Superheated Melts. Econ. Geol. 103, 1365–1378.

Dubilier, N., Bergin, C., Lott, C., 2008. Symbiotic diversity in marine animals: the art of harnessing chemosynthesis. Nat. Rev. Microbiol. 6, 725–40.

Edmond, J.M., Measures, C., McDuff, R.E., Chan, L.H., Collier, R., Grant, B., Gordon, L.I., Corliss, J.B., 1979. Ridge crest hydrothermal activity and the balances of the major and minor elements in the ocean: The Galapagos data. Earth Planet. Sci. Lett. 46, 1–18.

Elsasser, W.M., 1971. Sea-floor spreading as thermal convection. J. Geophys. Res. 76, 1101–1112.

Falvey, D.A., Pritchard, T., 1982. Preliminary Paleomagnetic Results from Northern Papua New Guinea : Evidence for Large Microplate Rotations, in: Watson, S.T. (Ed.), Transactions of the Third Circum-Pacific Energy and Mineral Resources Conference. American Association of Petrolium Geologists, Tulsa, Oklahoma, pp. 593–600.

Finlayson, D.M., Cull, J.P., 1973. Structural profiles in the New Britain / New Ireland region. J. Geol. Soc. Aust. 20, 37–47.

Fischer, R. V., Schmincke, H.-U., 1984. Pyroclastic rocks. Springer Verlag, Berlin.

Franklin, J., Gibson, H.L., Jonasson, I., Galley, A., 2005. Volcanogenic massive sulphide deposits. Econ. Geol. 100th anni, 523–560.

Franklin, J., Lydon, J., Sangster, D.F., 1981. Volcanic-associated massive sulfide deposits. Econ. Geol. 75th anniv, 485–627.

Gamo, T., Okamura, K., Charlou, J., Urabe, T., Auzende, J., Ishibashi, J., Shitashima, K., Chiba, H., Shipboard Scientific Party of the ManusFlux Cruise, 1997. Acidic and

sulfate-rich hydrothermal fluids from the Manus back-arc basin, Papua New Guinea. Geology 25, 139–142.

Gena, K., Mizuta, T., Ishiyama, D., Urabe, T., 2001. Acid-sulphate Type Alteration and Mineralization in the Desmos Caldera, Manus Back-arc Basin, Papua New Guinea. Resour. Geol. 51, 31–44.

German, C.R., Lin, J., Parson, L.M., 2004. Mid-Ocean Ridges: Hydrothermal Interactions Between the Lithosphere and Oceans. American Geophysical Union, Washington, D. C.

German, C.R., Von Damm, K.L., 2003. Hydrothermal Processes, in: Turekian, K.K., Holland, H.D. (Eds.), Treatise on Geochemistry. Elsevier, Amsterdam, pp. 181–222.

Gibson, H.L., Morton, R.L., Hudak, G.J., 1999. Submarine volcanic processes, deposits, and environments favourable for the location of volcanic-associated massive sulfide deposits, in: Barrie, C.T., Hannington, M.D. (Eds.), Volcanic-Associated Massive Sulfide Deposits: Processes and Examples in Modern and Ancient Settings. Reviews in Economic Geology, pp. 13–51.

Goto, Y., McPhie, J., 1998. Endogenous growth of a Miocene submarine dacite cryptodome, Rebun Island, Hokkaido, Japan. J. Volcanol. Geotherm. Res. 84, 273–286.

Goto, Y., Tsuchiya, N., 2004. Morphology and growth style of a Miocene submarine dacite lava dome at Atsumi, northeast Japan. J. Volcanol. Geotherm. Res. 134, 255–275.

Gregg, T.K.P., Fink, J.H., 1995. Quantification of submarine lava-flow morphology through analog experiments 23–27.

Griffiths, R., 2000. The dynamics of lava flows. Annu. Rev. Fluid Mech. 32, 477–518.

Griffiths, R.W., Fink, J.H., 1992. Solidification and morphology of submarine lavas: a dependence on extrusion rate. J. Geophys. Res. 97, 19,729–19,737.

Griffiths, R.W., Fink, J.H., 1997. Solidifying Bingham extrusions: a model for the growth of silicic lava domes. J. Fluid Mech. 347, 13–36.

Hannington, M.D., de Ronde, C.E.J., Petersen, S., 2005. Sea-Floor Tectonics and Submarine Hydrothermal Systems. Econ. Geol. 100th Anni, 111–141.

Hannington, M.D., Jamieson, J., Monecke, T., Petersen, S., Beaulieu, S., 2011. The abundance of seafloor massive sulfide deposits. Geology 39, 1155–1158.

Harrell, J.A., Brown, V.M., The, S., Jan, N., 1992. The World's Oldest Surviving Geological Map: The 1150 B.C. Turin Papyrus from Egypt. J. Geol. 100, 3–18.

Hashimoto, J., Ohta, S., 1999. Hydrothermal vent fields and vent-associated biological communities in the Manus Basin, SOPAC Cruise Report 148.

Hashimoto, J., Ohta, S., Fiala-Médioni, A., Auzende, J., 1999. Hydrothermal vent communities in the Manus Basin, Papua New Guinea: Results of the BIOACCESS cruises' 96 and'98. InterRidge News 8 (2), 12–18.

Head, J.W., Wilson, L., 2003. Deep submarine pyroclastic eruptions: theory and predicted landforms and deposits. J. Volcanol. Geotherm. Res. 121, 155–193.

Heiken, G., 1974. An Atlas of Volcanic Ash. Smithson. Contrib. to Earth Sci. 101.

Helo, C., Longpré, M.-A., Shimizu, N., Clague, D.A., Stix, J., 2011. Explosive eruptions at mid-ocean ridges driven by CO2-rich magmas. Nat. Geosci. 4, 260–263.

Herzig, P.M., 1999. Economic potential of sea-floor massive sulphide deposits: ancient and modern. Philos. Trans. R. Soc. A Math. Phys. Eng. Sci. 357, 861–875.

Hess, H.H., 1946. Drowned ancient islands of the Pacific Basin. Am. J. Sci. 244, 772–791.

Hillier, J.K., Watts, A.B., 2007. Global distribution of seamounts from ship-track bathymetry data. Geophys. Res. Lett. 34, L13304.

Hrischeva, E., Scott, S.D., Weston, R., 2007. Metalliferous sediments associated with presently forming volcanogenic massive sulfides: the SuSu Knolls hydrothermal field, eastern Manus Basin, Papua New. Econ. Geol. 102, 55–73.

Iizasa, K., 1999. Potential Marine Mineral Resources by Hydrothermal Activity. Chem. Ind. 50, 379–384.

Ishibashi, J.-I., Urabe, T., 1995. Hydrothermal activity related to arc-backarc magmatism in the western Pacific, in: Taylor, B. (Ed.), Backarc Basins: Tectonics and Magmatism. Plenum Press, New York, pp. 451–495.

Kamenetsky, V.S., Binns, R.A., Gemmell, J.B., Crawford, A.J., Mernagh, T.P., Mass, R., Steele, D., 2001. Parental basaltic melts and fluids in eastern Manus backarc Basin: implications for hydrothermal mineralisation. Earth Planet. … 184, 685–702.

Kano, K., 2003. Subaqueous Pumice Eruptions and Their Products : A Review, in: White, J.D.L., Smellie, J.L., Clague, D.A. (Eds.), Explosive Subaqueous Volcanism. American Geophysical Union, Washington, D. C., pp. 213–229.

Kano, K., Takeuchi, K., Yamamoto, T., Hoshizumi, H., 1991. Subaqueous rhyolite block lavas in the Miocene Ushikiri formation, Shimane Peninsula, SW Japan. J. Volcanol. Geotherm. Res. 46, 241–253.

Kokelaar, B.P., 1983. The mechanism of Surtseyan volcanism. J. Geol. Soc. London. 140, 939–944.

Kokelaar, P., 1986. Magma-water interactions in subaqueous and emergent basaltic. Bull. Volcanol. 48, 275–289.

Koppers, A., Watts, A., 2010. Intraplate seamounts as a window into deep Earth processes. Oceanography 23, 42–57.

Kroenke, L., Rodda, P., 1984. Cenozoic tectonic development of the Southwest Pacific. U.N. ESCAP, CCOP/SOPAC Tech. Bull. 6.

Kushiro, I., Syono, Y., Akimoto, S., 1968. Melting of a peridotite nodule at high pressures and high water pressures. J. Geophys. Res. 73, 6023–6029.

Langmuir, H., Klein, E.M., Plank, T., 1992. Petrological Systematics of Mid-Ocean Ridge Basalts : Constraints on Melt Generation Beneath Ocean Ridges, in: Phipps Morgan, J., Blackman, D.K., Sinton, J.M. (Eds.), Mantle Flow and Melt Generation at Mid-Ocean Ridges. American Geophysical Union, Washington, D. C., pp. 183–280.

Lee, S., Ruellan, E., 2006. Tectonic and magmatic evolution of the Bismarck Sea, Papua New Guinea: Review and new synthesis, in: Christie, D.M., Fisher, C.R., Lee, S.-M., Givens, S. (Eds.), Back-Arc Spreading Systems: Geological, Biological, Chemical, and Physical Interactions. American Geophysical Union, Washington, D. C., pp. 263–286.

Lentz, D., 1998. Petrogenetic evolution of felsic volcanic sequences associated with Phanerozoic volcanic-hosted massive sulphide systems: the role of extensional geodynamics. Ore Geol. Rev. 12, 289–327.

Martinez, F., Taylor, B., 1996. Backarc spreading, rifting, and microplate rotation, between transform faults in the Manus Basin. Mar. Geophys. Res. 18, 203–224.

Martinez, F., Taylor, B., 2002. Mantle wedge control on back-arc crustal accretion. Nature 416, 417–420.

Martinez, F., Taylor, B., 2003. Controls on back-arc crustal accretion: insights from the Lau, Manus and Mariana basins. Geol. Soc. London, Spec. Publ. 219, 19–54.

McBirney, A., 1963. Factors governing the nature of submarine volcanism. Bull. Volcanol. 26, 455–469.

McPhie, J., Doyle, M.G., Allen, S.R., 1993. Volcanic textures: a guide to the interpretation of textures in volcanic rocks. Centre for Ore Deposit and Exploration Studies - University of Tasmania.

Moberly, R., 1972. Origin of lithosphere behind island arcs, with reference to the western Pacific. Geol. Soc. Am. Mem 132, 35–55.

Mosier, D.L., Berger, V.I., Singer, D.A., 2009. Volcanogenic massive sulfide deposits of the world; database and grade and tonnage models, U.S. Geological Survey Open-File Report.

Mosier, D.L., Singer, D.A., Salem, B.B., 1983. Geologic and grade-tonnage information on volcanic-hosted copper-zinc-lead massive sulfide deposits. United States Geol. Surv. Open File Rep. 83-89, 77.

Moss, R., Scott, S.D., 2001. Geochemistry and Mineralogy of Gold-Rich Hydrothermal Precipitates From the Eastern Manus Basin, Papua New Guinea. Can. Mineral. 39, 957–978.

Mottl, M.J., Seewald, J.S., Wheat, C.G., Tivey, M.K., Michael, P.J., Proskurowski, G., McCollom, T.M., Reeves, E., Sharkey, J., You, C.-F., Chan, L.-H., Pichler, T., 2011. Chemistry of hot springs along the Eastern Lau Spreading Center. Geochim. Cosmochim. Acta 75, 1013–1038.

Nemeth, K., Pecskay, Z., Martin, U., Gmeling, K., Molnar, F., Cronin, S.J., 2008. Hyaloclastites, peperites and soft-sediment deformation textures of a shallow subaqueous Miocene rhyolitic dome-cryptodome complex, Palhaza, Hungary. Geol. Soc. London, Spec. Publ. 302, 63–86.

Niu, Y., Hékinian, R., 1997. Spreading-rate dependence of the extent of mantle melting beneath ocean ridges. Nature 385, 326–329.

Park, S.-H., Lee, S.-M., Kamenov, G.D., Kwon, S.-T., Lee, K.-Y., 2009. Tracing the origin of subduction components beneath the South East rift in the Manus Basin, Papua New Guinea. Chem. Geol. 269, 339–349.

Paulick, H., Bach, W., 2006. Phyllosilicate alteration mineral assemblages in the active subsea-floor Pacmanus hydrothermal system, Papua New Guinea, ODP Leg 193. Econ. Geol. 101, 633–650.

Paulick, H., Vanko, D.., Yeats, C.., 2004. Drill core-based facies reconstruction of a deep-marine felsic volcano hosting an active hydrothermal system (Pual Ridge, Papau New Guinea, ODP Leg 193). J. Volcanol. Geotherm. Res. 130, 31–50.

Pearce, J.A., Stern, R.J., 2006. Origin of Back-Arc Basin Magmas: Trace Element and Isotope Perspectives, in: Christie, D.M., Fisher, C.R., Lee, S.-M., Givens, S. (Eds.), Back-Arc Spreading Systems: Geological, Biological, Chemical, and Physical Interactions. American Geophysical Union, Washington, D. C., pp. 63–86.

Petersen, S., Herzig, P., Hannington, M.D., Gemmell, J.B., 2003. Gold-rich massive sulfides from the interior of the felsic-hosted PACMANUS massive sulfide deposit, Eastern Manus Basin (PNG), in: Eliopoulos et al. (Ed.), Mineral Exploration and Sustainable Development. Millpress, Rotterdam, pp. 171–174.

Pichler, H., 1965. Acid hyaloclastites. Bull. Volcanol. 28, 293–310.

Porreca, M., Cifelli, F., Soriano, C., Giordano, G., Romano, C., Conticelli, S., Mattei, M., 2014. Hyaloclastite fragmentation below the glass transition: An example from El Barronal submarine volcanic complex (Spain). Geology 42, 87–90.

Reclus, E., 1886. A new physical geography, vol. 2, Air and Ocean. G.G. Virtue and Co., London.

Reeves, E., Seewald, J.S., Saccocia, P., Bach, W., Craddock, P.R., Shanks, W.C., Sylva, S.P., Walsh, E., Pichler, T., Rosner, M., 2011. Geochemistry of hydrothermal fluids from the PACMANUS, Northeast Pual and Vienna Woods hydrothermal fields, Manus Basin, Papua New Guinea. Geochim. Cosmochim. Acta 75, 1088–1123.

Rotella, M.D., Wilson, C.J.N., Barker, S.J., Wright, I.C., 2013. Highly vesicular pumice generated by buoyant detachment of magma in subaqueous volcanism. Nat. Geosci. 6, 129–132.

Rubin, K.H., Soule, S.A., Chadwick Jr., W.W., Fornari, D.. J., Clague, D.A., Embley, R.W., Baker, E.T., Perfit, M.R., Caress, D.W., Dziak, R.P., 2012. Volcanic eruptions in the deep sea. Oceanography 25, 142–157.

Sangster, D.F., 1980. Quantitative characteristics of volcanogenic massive sulphide deposits. Bull. Can. Inst. Min. Metall. 73, 74–81.

Schmidt, M.W., Poli, S., 1998. Experimentally based water budgets for dehydrating slabs and consequences for arc magma generation. Earth Planet. Sci. Lett. 163, 361–379.

Scholz, C.H., Campos, J., 1995. On the mechanism of seismic decoupling and back arc spreading at subduction zones. J. Geophys. Res. 100, 22103–22115.

Sclater, J.G., Parsons, B., 1981. Oceans and continents: similarities and differences in the mechanisms of heat loss. J. Geophys. Res. 86, 11535–11552.

Scutter, C., Cas, R.A.F., Moore, C., De Rita, D., 1998. Facies architecture and origin of a submarine rhyolitic lava flow-dome complex, Ponza, Italy. J. Geophys. … 103, 27,551–27,566.

Seewald, J., Reeves, E.P, Bach, W., Saccocia, P.J., Craddock, P.R., Shanks III, W.C., Sylva, S.P., Pichler, T., Rosner, M., Walsh, E., 2014. Submarine Venting of Magmatic Volatiles in the Eastern Manus Basin, Papua New Guinea. Geochim. Cosmochim. Acta XX.

Sheridan, M.F., Wohletz, K.H., 1983. Hydrovolcanism: Basic considerations and review. J. Volcanol. Geotherm. Res. 17, 1–29.

Shipboard Scientific Party, 2002a. Leg 193 summary, in: Barriga, F.J.A.S., Binns, R.A., Miller, D.J., Herzig, P.M. (Eds.), Proceedings of the Ocean Drilling Program, Initial Reports. College Station, TX (Ocean Drilling Program), pp. 1–84.

Shipboard Scientific Party, 2002b. Site 1188, in: Binns, R.A., Barriga, F.J.A.S., Miller, D.J., Al., E. (Eds.), Proceedings of the Ocean Drilling Program, Initial Reports. College Station, TX (Ocean Drilling Program), pp. 1–305.

Shipboard Scientific Party, 2002c. Site 1189, in: Binns, R.A., Barriga, F.J.A.S., Miller, D.J., Al., E. (Eds.), Proceedings of the Ocean Drilling Program, Initial Reports. College Station, TX (Ocean Drilling Program), pp. 1–259.

Sinton, J.M., Ford, L.L., Chapell, B., McCulloch, M.T., 2003. Magma genesis and mantle heterogeneity in the Manus back-arc basin, Papua New Guinea. J. Petrol. 44, 159–195.

Skilling, I.P., White, J.D.L., McPhie, J., 2002. Peperite: a review of magma–sediment mingling. J. Volcanol. Geotherm. Res. 114, 1–17.

Smith, D.K., Cann, J.R., 1992. The role of seamount volcanism in crustal construction at the Mid-Atlantic Ridge (24°–30°N). J. Geophys. Res. 97, 1645–1658.

Smith, D.K., Jordan, T.H., 1987. The size distribution of Pacific Seamounts. Geophys. Res. Lett. 14, 1119–1122.

Sohn, R. a, Willis, C., Humphris, S.E., Shank, T.M., Singh, H., Edmonds, H.N., Kunz, C., Hedman, U., Helmke, E., Jakuba, M., Liljebladh, B., Linder, J., Murphy, C., Nakamura, K.-I., Sato, T., Schlindwein, V., Stranne, C., Tausenfreund, M., Upchurch, L., Winsor, P., Jakobsson, M., Soule, A., 2008. Explosive volcanism on the ultraslow-spreading Gakkel ridge, Arctic Ocean. Nature 453, 1236–8.

Sparks, R.S.J., Murphy, M.D., Lejeune, A.M., Watts, R.B., Barclay, J., Young, S.R., 2000. Control on the emplacement of the andesite lava dome of the Soufriere Hills volcano, Montserrat by degassing-induced crystallization. Terra Nov. 12, 14–20.

Staudigel, H., Clague, D., 2010. The geological history of deep-sea volcanoes. Oceanography 23, 58–71.

Stix, J., 1991. Subaqueous, intermediate to silicic-composition explosive volcanism: a review. Earth-Science Rev. 31, 21–53.

Stoffers, P., Worthington, T.J., Schwarz-Schampera, U., Hannington, M.D., Massoth, G.J., Hekinian, R., Schmidt, M., Lundsten, L.J., Evans, L.J., Vaiomo'unga, R., Kerby, T., 2006. Submarine volcanoes and high-temperature hydrothermal venting on the Tonga arc, southwest Pacific. Geology 34, 453–456.

Tamura, Y., Tatsumi, Y., Zhao, D., Kido, Y., Shukuno, H., 2002. Hot fingers in the mantle wedge: new insights into magma genesis in subduction zones. Earth Planet. Sci. Lett. 197, 105–116.

Tatsumi, Y., Eggins, S., 1995. Subduction Zone Magmatism, 1st ed. Blackwell Science, Cambridge, Massachusetts.

Taylor, B., 1979. Bismarck Sea: Evolution of a back-arc basin. Geology 7, 171–174.

Taylor, B., Crook, K., Sinton, J., 1994. Extensional transform zones and oblique spreading centers. J. Geophys. Res. 99, 19,707–19,718.

Taylor, R.N., Nesbitt, R.W., Vidal, P., Harmon, R.S., Auvray, B., Croudace, I.W., 1994. Mineralogy, Chemistry, and Genesis of the Boninite Series Volcanics, Chichijima, Bonin Islands, Japan. J. Petrol. 35, 577–617.

Thiéry, R., Mercury, L., 2009. Explosive properties of water in volcanic and hydrothermal systems. J. Geophys. Res. 114, B05205.

Tivey, M.A., Bach, W., Seewald, J., Tivey, M.K., Vanko, D.A., Party, S.S., 2006. Cruise Report for R/V Melville Cruise MGLN06MV—Hydrothermal Systems in the Eastern Manus Basin: Fluid Chemistry and Magnetic Structure as Guides to Subseafloor Processes.

Tivey, M.K., 2007. Generation of seafloor hydrothermal vent fluids and associated mineral deposits. Oceanography 20, 50–65.

Tregoning, P., 2002. Plate kinematics in the western Pacific derived from geodetic observations. J. Geophys. Res. 107, 1–8.

Tregoning, P., Jackson, R.J., Mcqueen, H., Larnbeck, K., Stevens, C., Little, R.P., Curley, R., Rosa, R., 1999. Motion of the South Bismarck Plate, Papua New Guinea. Geophys. … 26, 3517–3520.

Tyce, R.C., 1986. Deep seafloor mapping systems-A review. Mar. Technol. Soc. J. 20, 4–16.

Van Dover, C.L., 2000. The ecology of deep-sea hydrothermal vents. Princeton University Press, New Jersey.

Van Dover, C.L., Biscotto, M., Gebruk, A., Hashimoto, J., Tunnicliffe, V., Tyler, P., Desbruyeres, D., 2006. Milestones in the discovery of hydrothermal-vent faunas, in: Desbruyeres, D., Segonzac, M., Bright, M. (Eds.), Handbook of Deep-Sea Hydrothermal Vent Fauna. Denisia, pp. 13–25.

Verhoogen, J., 1951. Mechanics of ash formation. Am. J. Sci. 249, 729–739.

Von Damm, K.., Edmond, J.., Grant, B., Measures, C.., Walden, B., Weiss, R.., 1985. Chemistry of submarine hydrothermal solutions at 21 °N, East Pacific Rise. Geochim. Cosmochim. Acta 49, 2197–2220.

Von Damm, K.L., 1995. Controls on the chemistry and temporal variability of seafloor hydrothermal fluids, in: Humphris, S.E., Zierenberg, R.A., Mullineaux, L.S., Thomson, R.E. (Eds.), Seafloor Hydrothermal Systems: Physical, Chemical, Biological, and Geological Interactions. American Geophysical Union, Washington, D. C., pp. 222–247.

Wallace, L.M., 2004. GPS and seismological constraints on active tectonics and arc-continent collision in Papua New Guinea: Implications for mechanics of microplate rotations in a plate boundary zone. J. Geophys. Res. 109, 1–16.

Wessel, P., 2001. Global distribution of seamounts inferred from gridded Geosat/ERS-1 altimetry. J. Geophys. Res. 106, 19,431–19,441.

White, J.D.L., 1996. Impure coolants and interaction dynamics of phreatomagmatic eruptions. J. Volcanol. Geotherm. Res. 74, 155–170.

White, J.D.L., Smellie, J.L., Clague, D.A., 2003a. Explosive subaqueous volcanism, Geophysica. ed. American Geophysical Union.

White, J.D.L., Smellie, J.L., Clague, D.A., 2003b. Introduction : A Deductive Outline and Topical Overview of Subaqueous Explosive Volcanism, in: White, J.D.L., Smellie, J.L., Clague, D.A. (Eds.), Explosive Subaqueous Volcanism. American Geophysical Union, Washington, D. C., pp. 1–23.

Wohletz, K.H., 1983. Mechanisms of hydrovolcanic pyroclast formation: Grain-size, scanning electron microscopy, and experimental studies. J. Volcanol. Geotherm. Res. 17, 31–63.

Wohletz, K.H., 2002. Water/magma interaction: some theory and experiments on peperite formation. J. Volcanol. Geotherm. Res. 114, 19–35.

Yamagishi, H., 1985. Growth of pillow lobes—Evidence from pillow lavas of Hokkaido, Japan, and North Island, New Zealand. Geology 13, 499–502.

Yamagishi, H., 1987. Studies on the Neogene subaqueous lavas and hyaloclastites in southwest Hokkaido. Rep. Geol. Surv. Hokkaido 59, 55–117.

Yamagishi, H., Dimroth, E., 1985. A comparison of Miocene and Archean rhyolite hyaloclastites: evidence for a hot and fluid rhyolite lava. J. Volcanol. Geotherm. Res. 23, 337–355.

Yang, K., Scott, S., 2002. Magmatic degassing of volatiles and ore metals into a hydrothermal system on the modern sea floor of the eastern Manus back-arc basin, western Pacific. Econ. Geol. 97, 1079–1100.

Yeats, C.J., Binns, R.A., Parr, J., 2008. The SuSu Knolls hydrothermal field, Eastern Manus Basin, Papua New Guinea: An actively forming submarine high sulfidation copper-gold system, in: International Geological Congress. Oslo, p. MRD–03.

Zimanowski, B., Fröhlich, G., Lorenz, V., 1991. Quantitative experiments on phreatomagmatic explosions. J. Volcanol. Geotherm. Res. 48, 341–358.

Zimanowski, B., Fröhlich, G., Lorenz, V., 1995. Experiments on steam explosion by interaction of water with silicate melts. Nucl. Eng. Des. 155, 335–343.

2. Geologic Setting of PACManus Hydrothermal Vent Fields – High-resolution mapping and in situ observations.

Janis Thal[1*], Maurice Tivey[2], Dana Yoerger[2], Niels Jöns[1], Wolfgang Bach[1]

[1]*MARUM, University of Bremen, 28359 Bremen, Germany*

[2]*Woods Hole Oceanographic Institution, Woods Hole, MA02543, USA*

**corresponding author:*

email: ja_th@uni-bremen.de,

phone: (+49) 421-218-46405

***Marine Geology**, accepted manuscript*

2.1 Abstract

This study presents a systematic analysis and interpretation of autonomous underwater vehicle-based micro-bathymetry combined with remotely operated vehicle (ROV) video recordings, rock analyses and temperature measurements within the PACManus Hydrothermal District located on Pual Ridge in the Bismarck Sea of eastern Manus Basin. The data obtained during research cruise Magellan-06 and SO-216 provides a framework for understanding the relationship between the volcanic host units, tectonic framework and hydrothermal activity. The PACManus Hydrothermal District is a felsic-hosted system that hosts multiple vent fields located within several hundred meters of one another but with different fluid chemistries, vent temperatures and morphologies. The total area of hydrothermal activity is estimated to be 20,279 m^2. The micro-bathymetric maps combined with the ROV video observations allows for high resolution mapping on the areal extents of the hydrothermal activity compared with earlier estimates. In contrast to the dominantly tectonic controlled discharge pathways of hydrothermal vent fluids at fast and slow spreading mid-ocean ridges, the hydrothermal systems in PACManus are primarily controlled by volcanic features that include lava domes, thick and massive blocky lava flows, hyaloclastite deposits and feeder dykes. Variations in the local volcanic facies permeability appear to control the distribution of venting within a field.

We define a three-stage chronological sequence for the magmatism of the PACManus Hydrothermal District based on flow morphology, sediment cover and lava SiO_2 concentration. In stage-1, sparsely to moderately porphyritic dacite lavas (68 - 69.8 wt. % SiO_2) built up domes or cryptodomes. In stage-2, aphyric lava with slightly lower SiO_2 concentrations (67.2 – 67.9 wt. % SiO_2) formed lobate, jumbled and pillowed lava flows. In the most recent phase, stage-3, massive blocky lavas with 69 to 72.5 wt. % SiO_2 were emplaced on the seafloor constructing a volcanic ridge identified as the neovolcanic zone of the PACManus Hydrothermal District. The transition between the stages may be gradual and related to progressive heating of a silicic magma following a recharge event of hot, mantle-derived melts.

Keywords: PACManus; submarine volcanism, Manus Basin, hydrothermal vent, ROV, black smoker

2.2 Introduction

Submarine hydrothermal processes are an important influence on the balance of global heat flux and the cycling of mass and chemical elements between the solid interior of the earth and the oceans and atmosphere. It is estimated that about 30% of the total heat loss of oceanic crust is controlled by hydrothermal systems (Sclater and Parsons, 1981). Hydrothermal activity can occur throughout the ocean basins, but it is particularly well-developed at mid-ocean ridge spreading axes, faulted ridge flanks, transform zones, seamounts and in back-arc areas above and behind subduction zones (Hannington et al., 2005). The mass transfer between seawater and the oceanic crust also has significant impact on the chemical and isotopic composition of the oceans and oceanic crust (Edmond et al., 1979). The temperature and chemical composition of the hydrothermal fluids as well as the sulphide deposits provides the energy and substrate for diverse and unique biological communities to exist and thrive in the extreme environments of deep sea hydrothermal springs (e.g. Van Dover et al., 2006).

Compared to the well-studied hydrothermal systems at the basalt-hosted mid-ocean ridge (MOR) spreading centers (e.g. German et al., 2004) much less is known about hydrothermal systems at ridges dominated by felsic volcanism. Felsic volcanic systems in the marine environment are potentially important analogs for many ore-deposits found on land today and indeed the felsic-rich host rock combined with the volatile dominated magmatic systems help to enrich economically important metals such as copper, gold and zinc (e.g. Sangster, 1980; Herzig, 1999; Iizasa, 1999; Hannington et al., 2005, 2011; Mosier et al., 2009). The PACManus (Papua-Australia-Canada-Manus) hydrothermal district on the crest of the Pual Ridge in the eastern Manus Basin of the Bismarck Sea (Fig. 2.1) is a good example of a hydrothermal system at a felsic-dominated spreading center. This hydrothermally active region was first discovered on the PACManus-1 expedition in 1991 (Binns and Scott, 1993) and was followed by several other expeditions to the region to study various aspects of the hydrothermal systems including the fluid chemistry, the geologic structure of Pual Ridge, the biology, the hydrothermal deposits and the bathymetry (e.g. Binns and Scott, 1993; Auzende et al., 1996b; Gamo et al., 1997; Hashimoto et al., 1999; Shipboard Scientific Party, 2002a; Tivey et al., 2006; Craddock and Bach, 2010; Reeves et al., 2011). This area is also of economic interest to a commercial mining company, Nautilus Minerals Inc., who currently holds exploration licenses for this area.

Several of the PACManus hydrothermal sites on Pual Ridge were drilled in 2000 during the Ocean Drilling Program (ODP) Leg 193, but major questions on the distribution of fluid flow remained following the completion of the drilling campaign (Binns et al., 2007). In 2006, to provide a more quantitative geologic context for the drill hole results and to investigate the role of hydrothermal processes at PACManus, the Woods Hole Oceanographic Institution (WHOI) collaborated with the, then, newly formed commercial mining company, Nautilus Minerals Inc. to undertake the Magellan-06 research expedition using the remotely-operated vehicle (ROV) Jason-2 and autonomous underwater vehicle (AUV) ABE. High-resolution bathymetry and magnetic data were recorded by ABE, supplemented by detailed rock and fluid sampling by ROV Jason-2. In addition, ship-based multibeam bathymetric mapping and CTD casts were conducted over PACManus and several other vent areas in the eastern Manus basin region including Manus Ridge (Vienna Woods) and the Suzette (Solwara-1) and North and South Su vent areas.

Data collected before the Magellan-06 expedition were restricted to low resolution photo sled surveys and a few Shinkai submersible dives (Binns and Scott, 1993; Auzende et al., 1996; Gamo et al., 1997). The high-resolution ABE bathymetry from Magellan-06 combined with the video recordings from 10 ROV Jason-2 dives allows us to document the first detailed, georeferenced mapping of the volcanic and hydrothermal structures at the PACManus hydrothermal sites. Another 10 ROV dives using the ROV MARUM Quest were completed in 2011 on the SO-216 BAMBUS-cruise, allowing us to confirm the previous mapping and document potential temporal changes in activity. During the 2011 SO-216 cruise, we were able to confirm the meter-scale reliability of the ABE maps generated during the Magellan-06 expedition. Nautilus Minerals have also conducted their own surveys and we have added in their reported discoveries where appropriate.

This study presents a systematic analysis using a Geographical Information Systems (GIS) database of AUV-based micro-bathymetry combined with video recordings, rock analyses and temperature measurements of individual vent locations for the hydrothermal fields of the PACManus Hydrothermal District in the SE Manus Basin. High-resolution micro-bathymetry maps with meter-scale precision obtained by ABE were combined with ROV video observations from two cruises to identify landmarks in the pronounced morphology of the PACManus Hydrothermal District and correct navigation offsets in seafloor features from previous expeditions to compile an internally consistent framework

of observations. Our analysis of the data has resulted in a set of comprehensive maps of the geological structures of the PACManus Hydrothermal District.

2.2.1 Geological setting

The Bismarck Sea is situated in the western Pacific Ocean northeast of the Papua New Guinea mainland and covers an area about 250,000 km² (Fig. 2.1). The sea is bordered to the southeast by the island of New Britain, to the west by mainland of New Guinea, to northeast by the island of New Ireland and to the north by Manus Island. The Bismarck Sea hosts two basins: the New Guinea Basin in the northwest and the Manus Basin in the east. The two basins are separated from each other by the Willaumez Rise, an approximately 400 km long ridge striking northeast (Fig. 2.1).

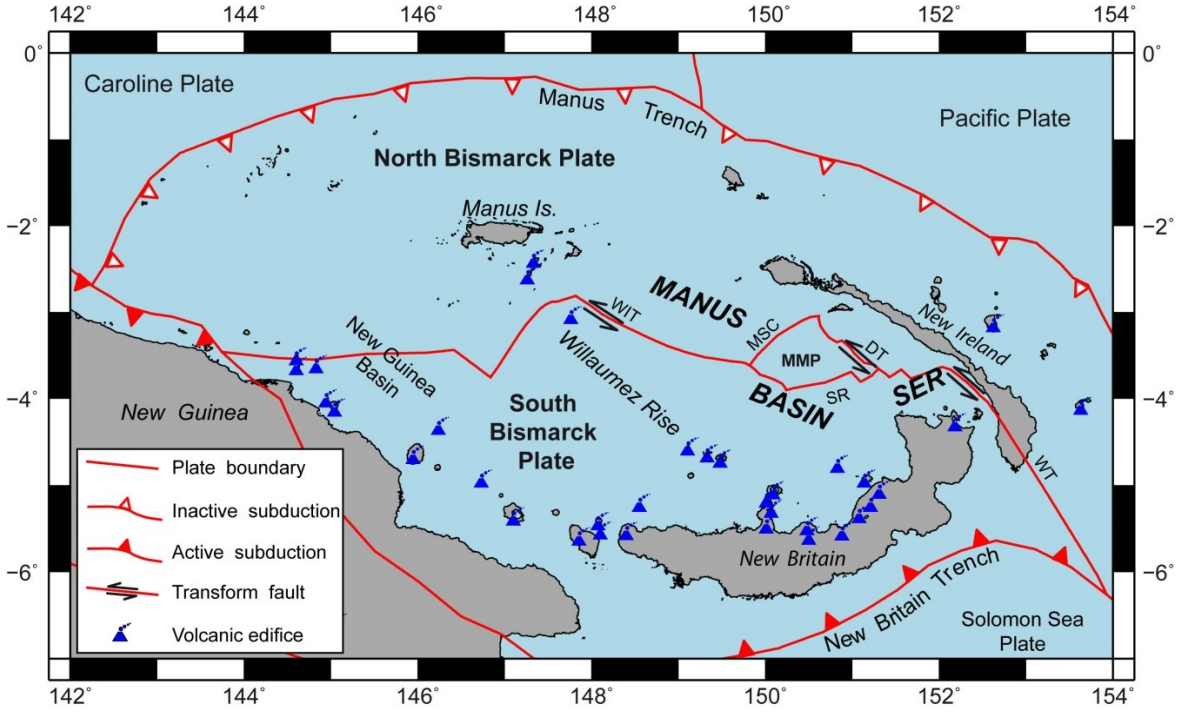

Figure 2.1: Tectonics at the Manus Basin. Abbreviations: WT = Weitin Transform; DT = Djaul Transform; WIT = Willaumez Transform; MMP = Manus Microplate; SR= Southern Rifts; SER = South East Ridges; MSC = Manus Spreading Centre. Plate boundaries from Bird (2003).

The Manus Basin, with an average water depth of 2000 m, is a back-arc basin with a complex history of spreading associated with the South Bismarck plate and conjugate North Bismarck plate and Manus microplate (Fig. 2.1). The slab-pull effect by the active subduction zone at the nearby New Britain Trench, where the Solomon Plate is being subducted underneath the South Bismarck Plate, leads to the opening of the Manus Basin with a spreading rate of 115 to 145 mm a^{-1} at the Manus Spreading Centre (MSC) (Taylor, 1979; Martinez and Taylor, 1996; Lee and Ruellan, 2006). Crustal spreading in

the Eastern Manus Basin is distributed between the MSC, the Manus Extensional Transform Zone (METZ), the Southern Rifts (SR) and the South East Ridges (SER, Fig. 2.1; Martinez and Taylor, 1996).

Volcanic ridges at SER show a sigmoidal shape due to the strike-slip movement generated by the two bordering left lateral transform faults; the Weitin Transform (WT) and the Djaul Transform (DT) (B. Taylor et al., 1994) (Figs. 2.1, 2.2). Bimodal, basaltic to rhyolitic volcanism in the SER region (Binns and Scott, 1993) is typical of the initial opening phase of a back-arc-basin. The PACManus Hydrothermal District lies on the central crest of Pual Ridge, which is part of the SER. The ridge is ~20 km long, 1 - 1.5 km wide and rises 500 – 600 m above the surrounding seafloor (Fig. 2.2). The ABE micro-bathymetry map of the PACManus Hydrothermal District on the central portion of Pual Ridge provides sub-meter scale resolution and delineates several volcanic edifices 200-300 m across with steep-sided flow units exhibiting a crenulated worm-like texture (Figs. 2.3 and 2.4). The summit of Pual Ridge is capped by a 200 m by 800 m long central neovolcanic eruptive edifice.

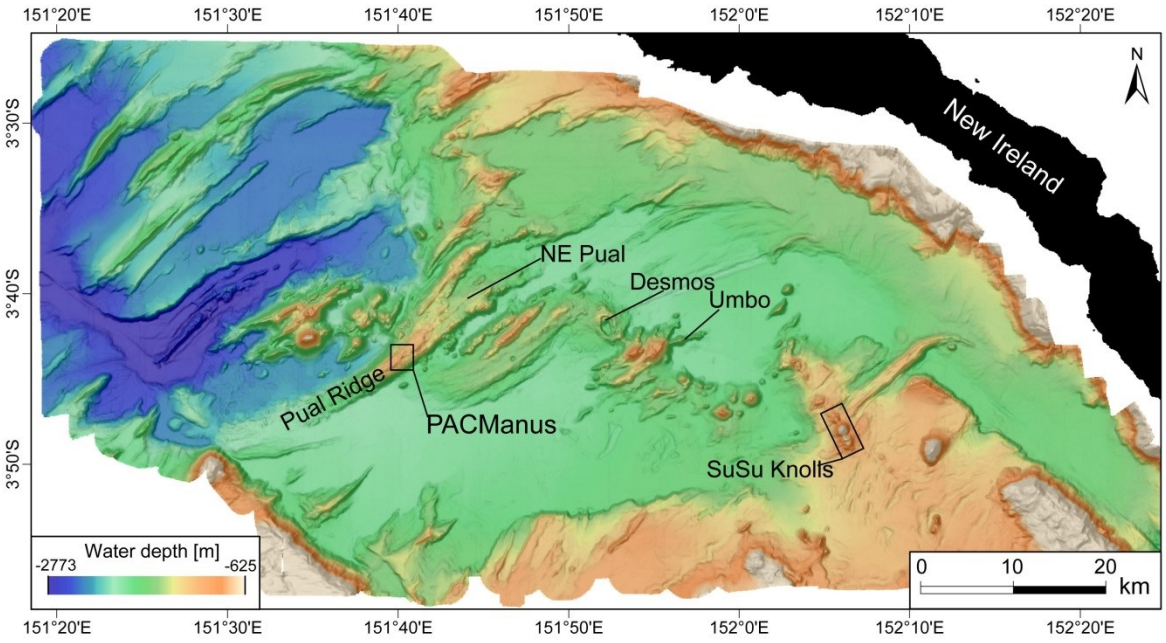

Figure 2.2: Multibeam bathymetry map of South Eastern Ridges (SER) region of the Eastern Manus Basin with vent regions. Data recorded on BAMBUS – RV Sonne 216 cruise.

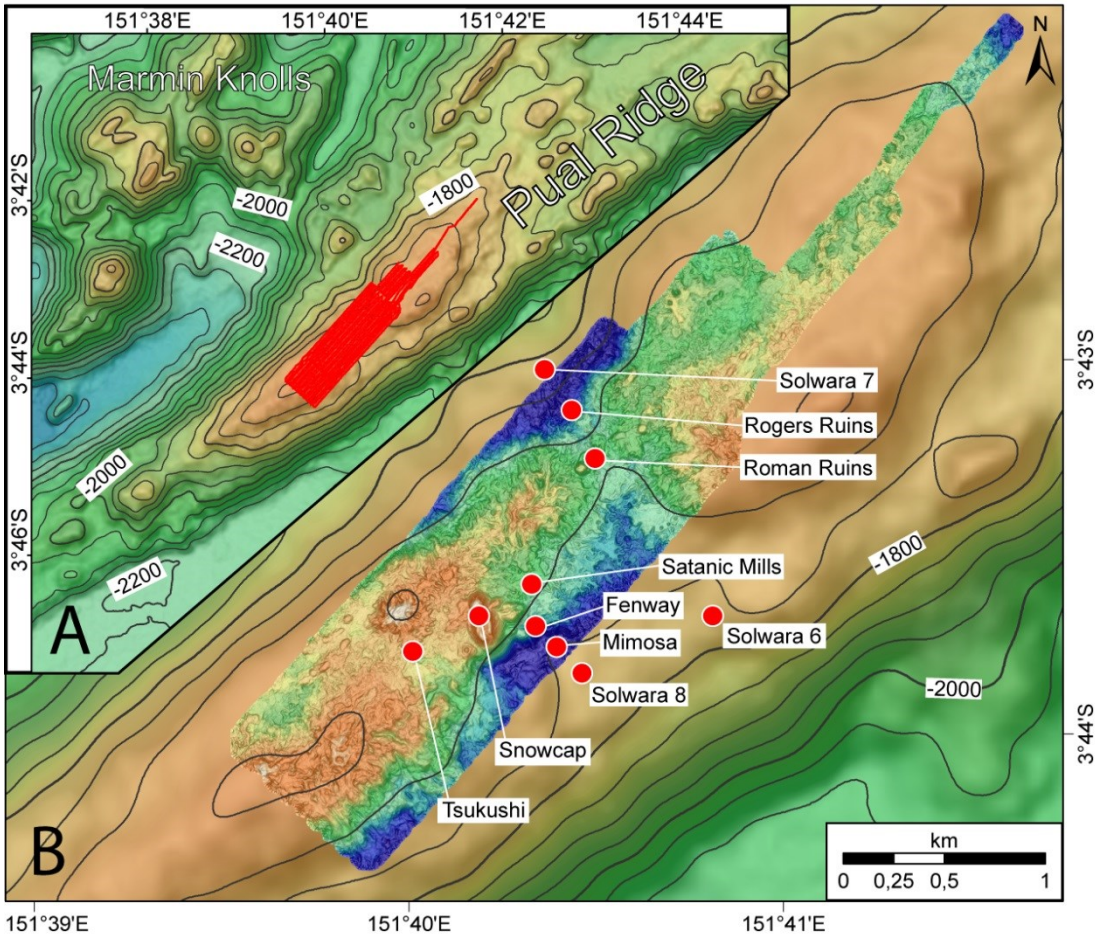

Figure 2.3 a+b: Red lines in Fig.2.3a indicate trackline coverage of AUV ABE high resolution multibeam mapping surveys. Figure 2.3b shows detailed AUV ABE multibeam bathymetry map of Pual Ridge with the primary PACManus vent regions. Background bathymetry from BAMBUS - RV Sonne 216 cruise.

2.2.2 PACManus Hydrothermal District (3°43.5' S - 151°40.5' E)

The PACManus Hydrothermal District (Papua – Australia – Canada – Manus) on the crest of Pual Ridge, at a water depth around 1640 – 1740 m, was discovered in 1991 (Binns and Scott, 1993) and is the most active known hydrothermal area of the SER. PACManus Hydrothermal District hosts several hydrothermal discharge sites, each up to 100 – 200 m in diameter. From south to north the vents sites are identified as follows: Tsukushi, Snowcap, Fenway (and adjacent Solwara-8), Satanic Mills, Roman Ruins, Rogers Ruins (and adjacent Solwara-6 and Solwara-7) (Fig. 2.4). Nautilus Minerals groups the PACManus vent sites with the exception of Solwara-6, 7 and 8 as the Solwara-4 prospect. Although the vent sites are within hundreds of meters of each other, their fluids have different temperatures (max. 358°C), varying chemical compositions (Reeves et al., 2011) and plume particle colours ranging from clear to grey to black. In areas of chronic fluid discharge, biological communities are well-developed, including bacterial

mats, molluscs, tube worms, crabs, anemones, holothurians, and a range of crustaceans and fish (Hashimoto et al., 1999).

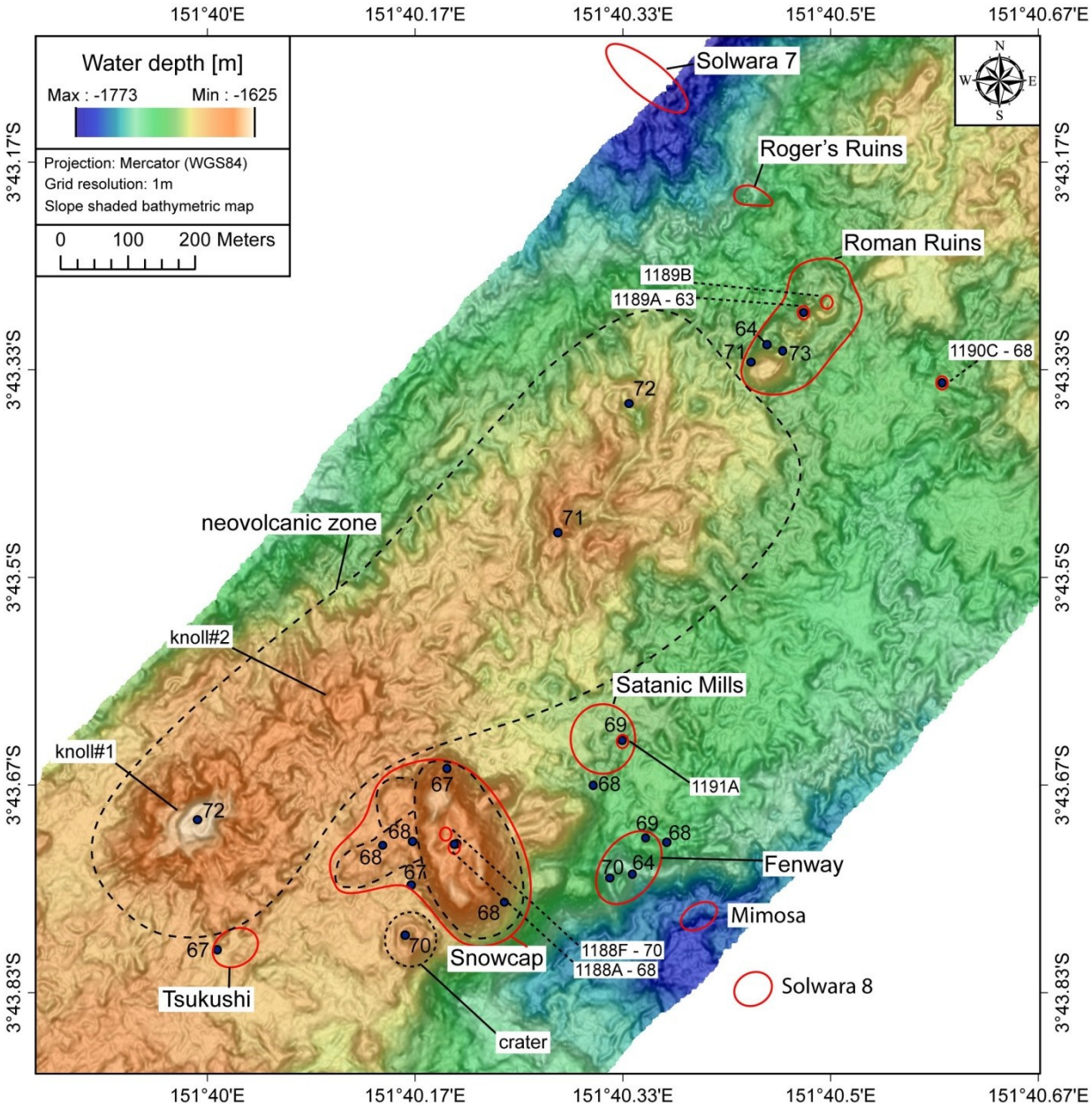

Figure 2.4: Overview of PACManus with all hydrothermal discharge sites (except Solwara 6), ODP boreholes, major morphological features and rock sample locations with SiO_2 concentration (wt. %).

2.3 Methods

Ship-based multibeam bathymetry was complemented by high-resolution AUV bathymetry and magnetic data on 18 ABE dives along with 30 ROV Jason-2 dives that collected rock as well as fluid samples during RV Melville cruise Magellan-06. This cruise was carried out by Woods Hole Oceanographic Institution in July/August of 2006 and was funded by the US National Science Foundation and with partial funding by

Nautilus Minerals Inc. The first part of the Magellan-06 cruise focused on the Manus Spreading Centre (6 ABE dives 182-187 and 8 Jason-2 dives 200-207), while the remainder of the program focused on the SER ridges. A total of 3 ABE dives (188, 190, 191) and 10 ROV-Jason-2 dives (208-216, 222) focused on the PACManus summit area of Pual Ridge. A follow-up cruise with RV Sonne (SO-216) used the ROV MARUM Quest in June/July of 2011 to record additional seafloor video images and collect fluids and biota. For this study, we analysed video data from 20 ROV dives and coregistered the information with the micro-bathymetry map recorded by AUV ABE. We have also included the results of analyses of rock compositions, fluid sample chemistry (Reeves et al., 2011), sulphide chimney compositions (Craddock et al., 2010) as well as fluid temperatures in our interpretations.

The high-resolution bathymetry basemap used in this analysis (Fig. 2.4) was generated from near-bottom multibeam data collected by the AUV ABE. ABE carried a 200 kHz Simrad multibeam sonar along with a 3-axis fluxgate magnetometer, an Eh sensor (provided by Koichi Nakamura of AIST, Japan), an optical backscatter sensor and a CTD for plume sensing. ABE typically operated at an altitude of 50 m with a line spacing of 50 m providing 100% sonar coverage. The vehicle operated within a long baseline (LBL) transponder network and produced navigation tracks with <10 m resolution. The raw sonar pings were corrected for the attitude of the vehicle (pitch, roll, and heading), and merged with the navigation and interpolated onto a 1-meter grid cell map. ROV Jason-2 also operated within the LBL transponder network and supplemented these ABE data with a high-data rate (1 Hz) Doppler Velocity Log (DVL) estimate of position. Again, the accuracy of the ROV position is <10 m. During cruise SO-216, the Ultra Short-Baseline Posidonia positioning system with accuracy of < 10 m was used to navigate the ROV MARUM Quest.

Typically, the ROV Jason-2 carries three video cameras; one fixed brow camera and two pan and tilt cameras; a pilot camera and a science camera. ROV MARUM Quest carried a similar configuration, but with an HD science camera. In generating geological maps, footage from these three cameras was used to provide different perspectives of seafloor structures. The HD-camera on ROV MARUM Quest markedly improved the mapping abilities with the video data. The size of recorded objects was determined by using a laser scale device mounted on the ROV, which allowed for dimensional measurement of seafloor features. Rock sample compositions reported in this paper

(Table 2.A1) were analysed with a JXA 8900 R Electron Probe Microanalyser at the Christian-Albrechts-Universität zu Kiel.

As part of our analysis, we employed a Geographical Information System (GIS) to correlate and coregister the available map and video data and to superimpose different volcanic facies, hydrothermal deposit observations, and sediment cover identified from the videos onto the micro-bathymetry basemap.

2.3.1 Seafloor structures

We use the terminology for volcanic morphology based on definitions from McPhie et al. (1993). In general, the direction of lava movement was determined from flow structures on the surface of lava flows observed in the video data. The sediment thickness in areas without hydrothermal activity was used as a crude proxy for the relative age of volcanic events. For regions with a very thick sediment cover, the unit "single outcrops" was used, because an identification of the underlying lava structure was not possible. Based on visual criteria, the volcanic seafloor was mapped as blocky lava (for irregular, angular and blocky structures), lobate lava (for flat and smooth lava), pillow lava, and volcaniclastic deposits. Some volcanic flow units have surface structures intermediate between those of pillow and blocky lava, including slabby, cloddy and jumbled lava. They are mapped as "mixed lava" that often also comprises various lava types, such as blocky lava with pillowed or lobate subdomains. An example is the large lava field between two of the vent sites (Tsukushi and Snowcap) in the southern part of the PACManus Hydrothermal District. See Figure 2.5 for photographic examples of these different volcanic morphologies. Sulphide chimney clusters were mapped as "active" when they showed focused fluid discharge through orifices in chimneys. In the absence of discrete venting, the smokers were mapped as "inactive". Shimmering water and the occurrence of vent-related fauna was used to identify diffuse discharge. There is no focus on mapping biological communities in this study, though we note briefly our observations of recognized macro fauna to complement the description of each vent site without assigning organisms to a taxonomic level.

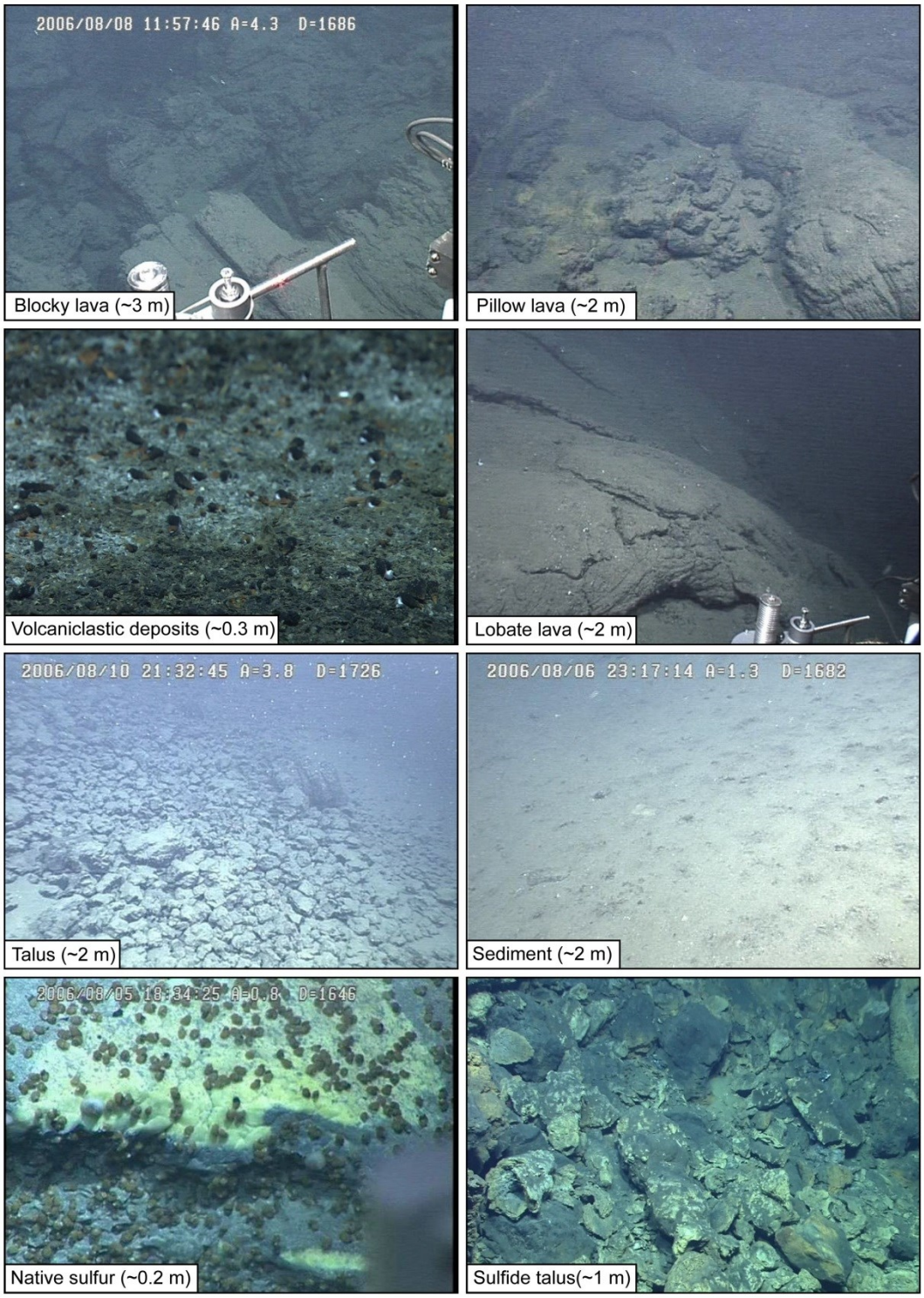

Figure 2.5: Examples of the major mapping units with estimated picture width

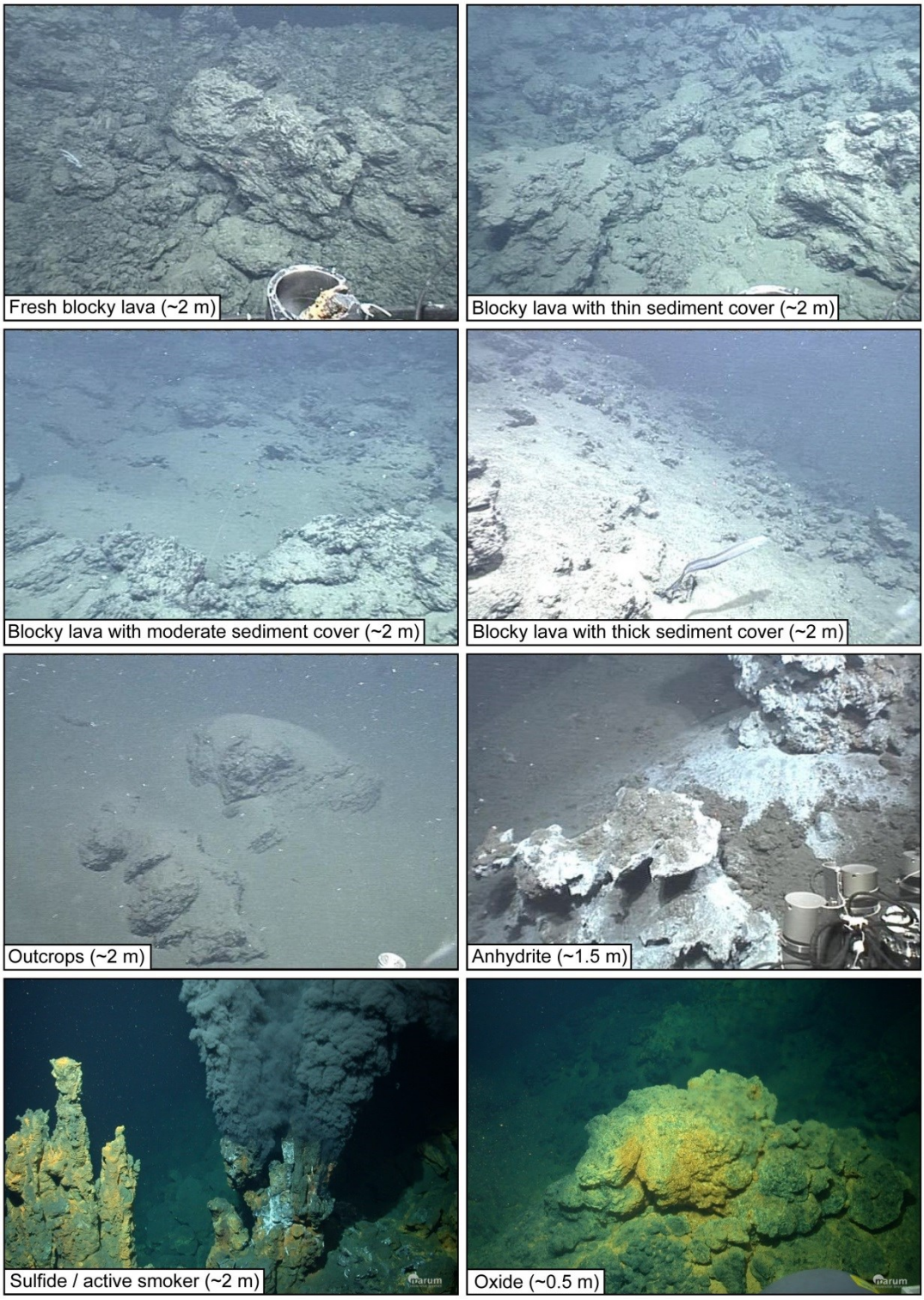

Figure 2.5 (continued): Examples of the major mapping units with estimated picture width.

Other types of deposits at discharge sites, such as elemental sulphur or oxides, were also identified and mapped. At Fenway hydrothermal field, irregularly-shaped anhydrite deposits are abundant and we mapped these as separate units. Lava flow fronts are only depicted where a sudden and obvious change in the lithology was encountered. In-situ brecciated lava in front of a thick lava flow was mapped as talus when the lateral extent

exceeded ~10 m. Figure 5 shows examples of the main lithologic units distinguished in the maps.

2.4 Results

Using the methods described above, detailed geological mapping was conducted in the five main hydrothermal areas of the PACManus Hydrothermal District of central Pual Ridge. Following the strike of Pual Ridge from southeast to northwest, these areas are Tsukushi, Snowcap, Fenway, Satanic Mills, and Roman/Roger's Ruins (Fig. 2.4) and we describe each of them in the following sections.

2.4.1 Tsukushi

Tsukushi (Jap. for cat-tail) is also known as Field G (Binns and Scott, 1993; Hashimoto et al., 1999) is located at the southwestern end of the PACManus Hydrothermal District. It is situated at a water depth around 1660 m on the crest of Pual Ridge and extends about 40 m in east-west direction (Fig. 2.6). Tsukushi is bordered to the north by a thick blocky lava flow that emanates from the summit crater of Pual Ridge neovolcanic zone ~150 m to the north and terminates in a well-defined flow front a few meters from the Tsukushi vent field, as marked in Fig. 2.6. Tsukushi is separated into two parts: the western side has active and diffuse fluid discharge and oxide deposits, while the eastern side has inactive sulphide chimneys. Two chimney clusters with diameters <10 m dominate the smoker site with columnar chimneys up to 13 m high with snow-white, cone-shaped tops. A Shinkai 6500 submersible dive in 1996 (Gamo et al., 1997) found active black and gray smoker activity, but in 2006 this activity had waned and ROV Jason-2 found only diffuse flow. No active venting was observed in 2011. The western part of Tsukushi has diffuse discharge of warm fluids (max. 62°C in 2006 and max. 53°C in 2011) through cracks in the lava with small (meter-sized) patches of knobby oxide mounds (e.g. see panel "Oxides" in Fig. 2.5). The size of the chimney field is roughly 35 x 35 m (1225 m²) and the elongated area covered with oxide crust has max. length of 56 m and a max. width of 32 m (1792 m²).

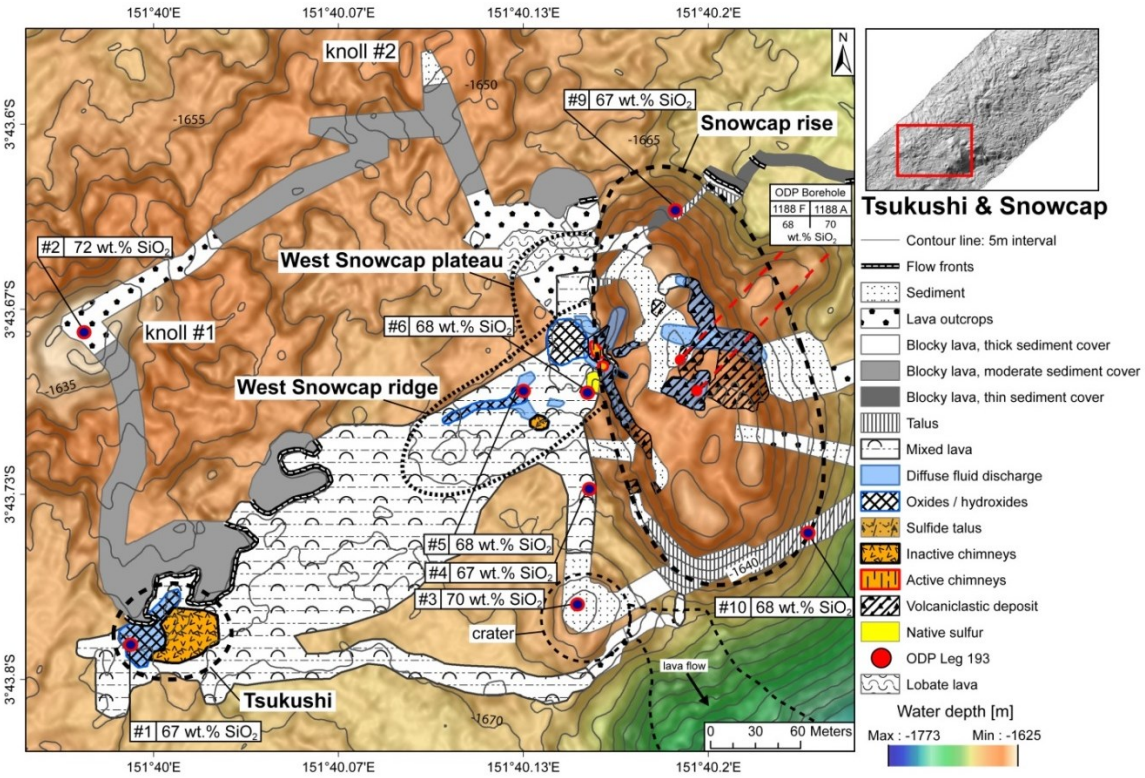

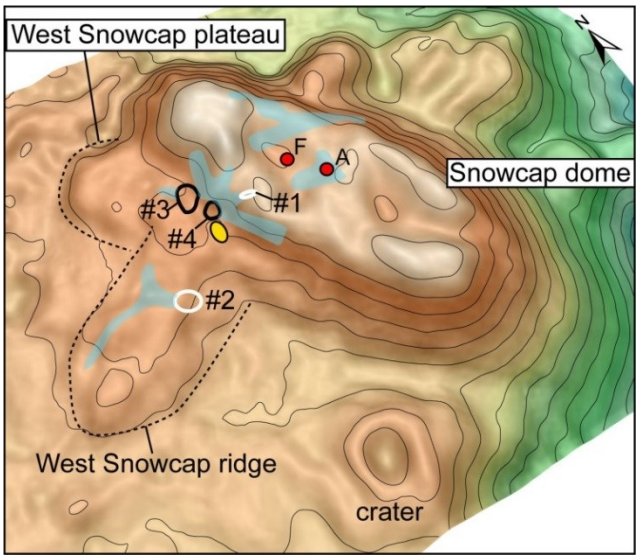

Figure 2.6 a + b:

2.6 a (above): Geological map of the southwest PACManus area. Shown are all mapped seafloor structures on the AUV bathymetry (1 m grid size) with contour lines at in interval of 5 m.

2.6 b (left): Oblique projection of the Snowcap area with prominent structures. Blue areas - diffuse venting; red dots – ODP drill sites 1188; yellow – native sulphur plates; black circles – active chimney cluster; white circles – inactive chimney cluster.

Using the ROV, we also explored the central Pual Ridge neovolcanic zone to the north of Tsukushi and west of the Snowcap area (Fig. 2.6). This edifice is comprised of two volcanic knolls (knoll #1 & #2, Fig. 2.4 + 2.6) that rise 20 - 30 m high above the surrounding seafloor. Their slopes consist of blocky lava with moderate pelagic sediment cover. The eastern knoll (#2) is characterised by several meter-deep trenches with heavily sediment-covered pillow lava on their floors. Both knolls have flat tops with a thick sediment cover and occasional outcrops of lava that is often brecciated. Some areas show

whitish-yellowish staining, which may be due to bacterial activity. Patches of volcaniclastic deposits occur, but due to their small lateral extent they were not mapped.

2.4.2 Snowcap

Snowcap hydrothermal field is also known as Mont Blanc/Kai Kai site and Field D (Binns and Scott, 1993; Hashimoto et al., 1999). The Snowcap area (Fig. 2.6) is characterised by a prominent dome rising to about 1635 mbsl on the flank of the Pual Ridge in the PACManus Hydrothermal District with a largely sediment-covered summit. Moderately sedimented and apparently younger volcanic flows stick out of the sediment in a few places, especially in the northern part. Eponymous for Snowcap is a laterally extensive area with a pronounced white coating on the seafloor, which was visible during the early photo sled surveys (Binns and Scott, 1993) and in ROV Jason-2 video recordings from 2006. It was uncertain whether the nature of the white coating was mineral staining or bacterial mats. The HD video recordings of 2011 revealed that these "white patches" are areas of diffuse venting through volcaniclastic deposits that are densely colonised by microbial filaments along with tiny crustaceans, sea anemones, and gastropods. These communities reflect the ROV lights causing the white colour imaged in the earlier ROV, Shinkai and photo sled surveys (Binns and Scott, 1993; Auzende et al., 1996b).

Two small craters, 1-2 m deep and 3-4 m in diameter were mapped in 2006 on top of Snowcap dome. The surrounding slopes are steeply dipping (30±5°) and predominantly covered by pelagic sediment with occasional talus fields or lava outcrops. The West Snowcap ridge extends in a southwesterly direction from the foot of the Snowcap dome 150 m towards Tsukushi and is about 40 m wide (Fig. 2.6). A narrow, sediment-covered gully marks the intersection of the ridge with the dome. The West Snowcap ridge was apparently built by several eruption events differing in age as indicated by the variable sediment thickness and lava morphology ranging from heavily sedimented lobate lava and moderately sedimented slabby, jumbled lava to lightly sedimented chaotic jumbled lava with occasional pillow tubes. The lightly sedimented centre of the elongate ridge hosts a diffuse venting field (~700 m²) with an inactive chimney cluster and a small crater like depression (10 m across, 4 m deep).

North of the ridge and adjacent to Snowcap dome is the West Snowcap plateau (Fig. 2.6), which shows two different lithologies: (i) the top is heavily sedimented towards the north and west where the slope shows lobate lava flow structures, (ii) to the

south, the seafloor is covered by cloddy, slabby and jumbled lava and sedimented mounds with oxide slabs, which extends to the gully separating it from the Snowcap vent field.

The entire Snowcap area hosts four chimney clusters. One group of small (<1 m) inactive chimneys is situated on the western slope of Snowcap dome on top of a small (~2 m wide) lava flow (Fig. 2.6, #1 in Fig. 2.6b). Another cluster – featuring numerous solitary, inactive, knotted, 3 - 4 m high chimneys – is located on the southern slope of the central West Snowcap ridge (Fig. 2.6, #2 in Fig. 2.6b). This chimney cluster only discharges diffuse fluids through its base (T_{max} 63°C in 2006). Two other chimney complexes combine to form the Snowcap vent field that is found inside the gully between the Snowcap dome and the West Snowcap ridge and is bordered to the east by a steep ~3 m high escarpment. The northern Snowcap vent field chimney complex (#3 in Fig. 2.6b) consists of several inactive chimneys with one cluster of branched 6 - 7 m high chimneys with diffuse and rare focused fluid discharge (T_{max}. in 2006: 179°C; T_{max} in 2011: 224°C). Paralvinella inhabit this environment along with gastropods and crabs. The southern Snowcap vent field smoker complex (#4 in Fig. 2.6b) comprises only one chimney cluster with a diameter of 2 – 3 m and discharges mostly clear fluid (T_{max}. 34°C in 2011).

Inside the gully, southwest of the Snowcap vent field, is a small (2 - 3 m high, ~ 13 m long) mound with sediment and decimetre thick slabs of native sulphur (Fig. 2.6a,b and panel Fig. 2.5 - sulphur). These slabs are colonised by many small gastropods, which – like the native sulphur – were not observed elsewhere in the PACManus Hydrothermal District. In the area west of the sulphur slabs and smokers, there is a mound with abundant oxide crusts that is sedimented, but with knobby lava prominent in outcrop. The mapped area of diffuse fluid discharge at the foot of, and on top of, Snowcap dome is estimated to be ~2970 m². In contrast, the area with active venting chimneys covers only about 76 m².

The area between Tsukushi and Snowcap is generally flat with moderate sediment cover and is characterised by several different lava types, which often build up small (< 10 m high) mounds of jumbled lava morphology. Pillows and mega pillows seem to be developed mainly at the foot of the mounds, whereas the lobate lava, that is occasionally fractured, covers greater areas. Southeast of this area, a circular volcanic cone rises above the seafloor and is covered by pelagic sediment ("crater" in Fig. 2.6a + b). The cone is 30 to 35 m in diameter and features a prominent crater 8 meters deep, which drains a blocky lava flow downslope to southeast (Fig. 2.6a).

The two ODP boreholes (1188A and 1188F) drilled into the centre of Snowcap dome to depths of 190 and 360 mbsl respectively (Shipboard Scientific Party, 2002a). While core recovery was poor (6.8-18.3%), recovered rocks indicated moderately porphyritic dacite lavas and hydrothermally altered aphyric lavas (Paulick et al., 2004) that were relatively thick and coherent based on downhole logging results (Bartetzko et al., 2003). Both holes have steel re-entry cones through which no fluid discharge has been observed. Despite the high temperature (313°C) measured near the bottom of Hole 1188F (Shipboard Scientific Party, 2002b), the hole appears to be recharging, even 11 years after drilling in 2000.

2.4.3 Fenway

The Fenway hydrothermal field is situated east of Snowcap on the southeast flank of the Pual Ridge in a depression surrounded by steep (30°) slopes to the W, NW and N (Fig. 2.4, Fig. 2.7). The vent field was discovered during the Magellan-06 cruise and sits halfway between the Satanic Mills and Snowcap vent fields and apparently was not detected by any of the previous cruises (Binns and Scott, 1993; Auzende et al., 1996b). Fenway consists of three clusters of hydrothermal vents and a central black smoker complex (Big Papi) at a water depth of ~1715 m. The total area with diffuse fluid discharge inside the Fenway field amounts to ~4450 m². Active sulphide chimneys are present in a smaller area of ~300 m². Two terraces mark the slope west of Big Papi (Fig. 2.7 a+b). On the upper terrace at 1680 mbsl, lava flows are mostly covered by thick sediment. In contrast, on the lower terrace (elevation change is 15 m lower) the sediment thickness is variable and the central part shows overlapping small lava lobes (< 50 cm). Sediment cover increases considerably from the centre towards the edge of the lower terrace. Only on the lower reaches of the west slope are blocky lavas clearly identifiable, with sediment thickness increasing from north to south. Approximately 10 m west of Big Papi, at the foot of the slope, vent fluids discharge diffusely through a talus field that is colonized by typical hydrothermal vent fauna (gastropods, fish, shrimps, mussels, tube worms and crabs).

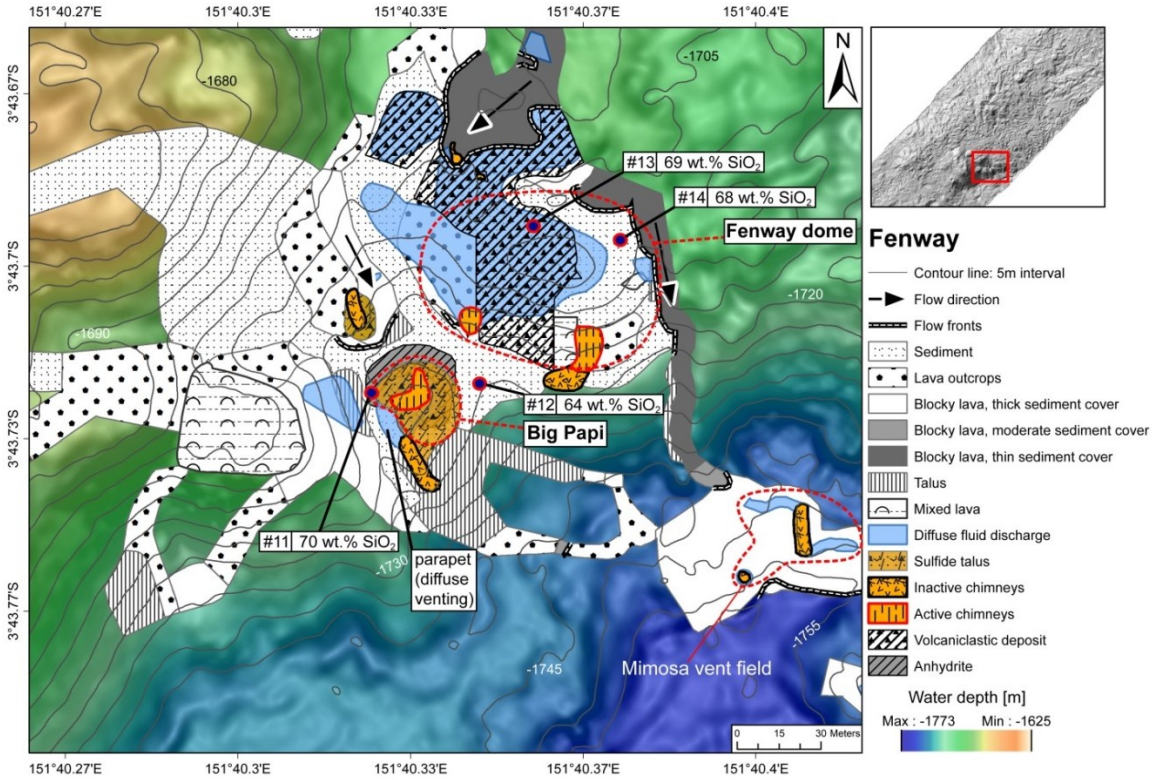

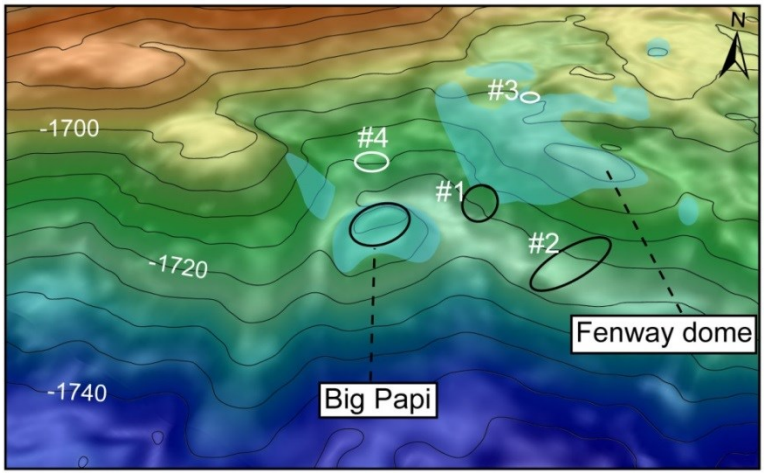

Figure 2.7 a + b:

2.7 a: Geologic map of the Fenway hydrothermal vent site. Shown are all mapped seafloor structures on the AUV bathymetry (1 m grid size) with contour lines at in interval of 2 m.

2.7 b: Oblique projection of the Fenway hydrothermal area with 5 m contours. Blue areas - diffuse venting; black circles – active chimney cluster; white circles – inactive chimney cluster.

The northwestern slope of Fenway features virtually continuous sediment cover, except for one area of blocky lava, which is also heavily sedimented. The flow front of that blocky lava flow is located just 5 m north of Big Papi and hosts an inactive smoker field with several meters high columnar chimneys (cluster #4, Fig. 2.7 b). At the base of the flow front, lava rock fragments form a small talus field. A ~10-m wide entirely sedimented corridor separates the blocky lava flow from a large area of diffuse fluid discharge on the northeastern slope of the Fenway field, where a dome-like mound is present (Fenway dome). In this ~80 m wide section (main field), diffuse hydrothermal activity is abundant with wide-spread patches of mussels, gastropods, tube worms, anemones, and crabs. At the foot of the Fenway dome lava outcrops become increasingly

covered by sediment and pyroclastic deposits. A partly active smoker field (cluster #1, Fig. 2.7b) is found ~15 m northeast of Big Papi on top of a flow front and has small, solitary chimneys with a max. vent temperature of 330°C. The fauna is similar to that in the diffuse vent area, but also includes abundant shrimp.

The area on top of Fenway dome is dominated by hyaloclastites that are cemented in place. This cementation is clearly visible on the edge of a plateau where, in a few places, decimetre-thick flanges of hyaloclastite outcrop. A temperature of 11°C was measured several centimeters deep in the sediment at this location in 2006. A thinly sedimented blocky lava flow with 3-5 m high flow fronts is emplaced on top of the hyaloclastites on the north and east sides of Fenway dome. Near the westernmost tip of that flow, a small cluster (cluster #3, Fig. 2.7b) of inactive sulphide chimneys is developed directly at the contact zone between the flow front and the underlying hyaloclastite deposits. The sharp boundary of the blocky lava flow (3 – 5 m high) is remarkably well-defined and can be traced for about 180 m downslope (Fig. 2.7). Just ~10 m south of this pronounced flow front and in the southeastern corner of the "Fenway" area we found another small hydrothermal field, which we named "Mimosa". This field is composed of two small sites with extinct chimneys with diffuse venting through trunks and underneath flanges. Eponymous for the Mimosa field is a flange that is densely colonized by tube worms which retract their red plumes into the tube to avoid danger bringing the Mimosa plant to mind. No further investigation has been done at Mimosa hydrothermal field. The Solwara 8 vent field features clusters of ~12 m high chimneys, but is outside of the ABE micro-bathymetry basemap, about 150 m southeast of the Mimosa field (Fig. 2.4).

Big Papi is a prominent mound in the centre of the Fenway hydrothermal field (Fig. 2.7) and consists of active chimneys (T_{max} 2011: 304°C), sulphide chimney talus, massive anhydrite-sulphide blocks, as well as anhydrite and sulphide sand. To the west and south, it is bordered by a 2 - 3 m high sedimented parapet, littered with indurated slabs of sediment, and settled by Paralvinella, gastropods, worms and other vent fauna. Vigorous diffuse venting of about 90°C hot fluids was observed throughout the area of the parapet. A small ridge extends to the southeast from the parapet and consists of rust-red coloured massive sulphides with volcanic and sulphidic rock fragments on its flanks. At ~1725 m, the ridge terminates in a cliff with clasts of volcanic and sulphide rocks. Remnants of chimney bases with a diameter of several tens of centimeters can be seen in the talus pile.

The slope south and southeast of Big Papi consists of an apparently young volcanic and sulphidic talus deposit, which shows little or no sediment dusting. To the north, a narrow trench with dark sediment and occasional talus separates Big Papi from a blocky lava flow front described previously. Prominent outcrops of massive anhydrite mark the northern border of Big Papi. These anhydrite deposits show clear signs of dissolution and emerge from dark sediment, on top of which cm-sized, worm-like creatures are scattered. The most vigorous fluid discharge is observed from cracks and crevices on the summit of the Big Papi mound. Scattered multiple branched chimneys also occur on the northern slope of the structure.

Diffuse venting is prominent in the immediate vicinity of Big Papi manifested by shimmering water streaming up from the surrounding anhydrite sand and sediment. It is noticeable that, in spite of the range in venting styles, only shrimp live on Big Papi while other members of the typical hydrothermal vent fauna are absent. In some places strings of filigree chimneys that are only a few cm in diameter decorate fissures in the mound. The base of the Big Papi mound is covered exclusively with white or dark-grey sediment that is distinct from the light-grey, presumed pelagic sediment at greater distances from the structure.

2.4.4 Satanic Mills

Satanic Mills is also known as Field E, Black Smoker Site and the Juvenile Site (Binns and Scott, 1993; Hashimoto et al., 1999). It is an active hydrothermal field with numerous isolated hydrothermal vents northeast of the Snowcap field at 1695-1675 m (Figs. 7 and 8). Apart from a few areas, Satanic Mills is dominated by three blocky lava flow units, which can be mapped based on their 3 - 6 m high steep flow fronts, which are apparent in the ABE micro-bathymetric map (Fig. 2.8). They are labelled flows #1, #2, and #3 (Fig. 2.8) based on their emplacement order with flow #1 overlying flow #2 and flow #3 overlying flow #2. The majority of the hydrothermal vent sites are located near the front of flow #2.

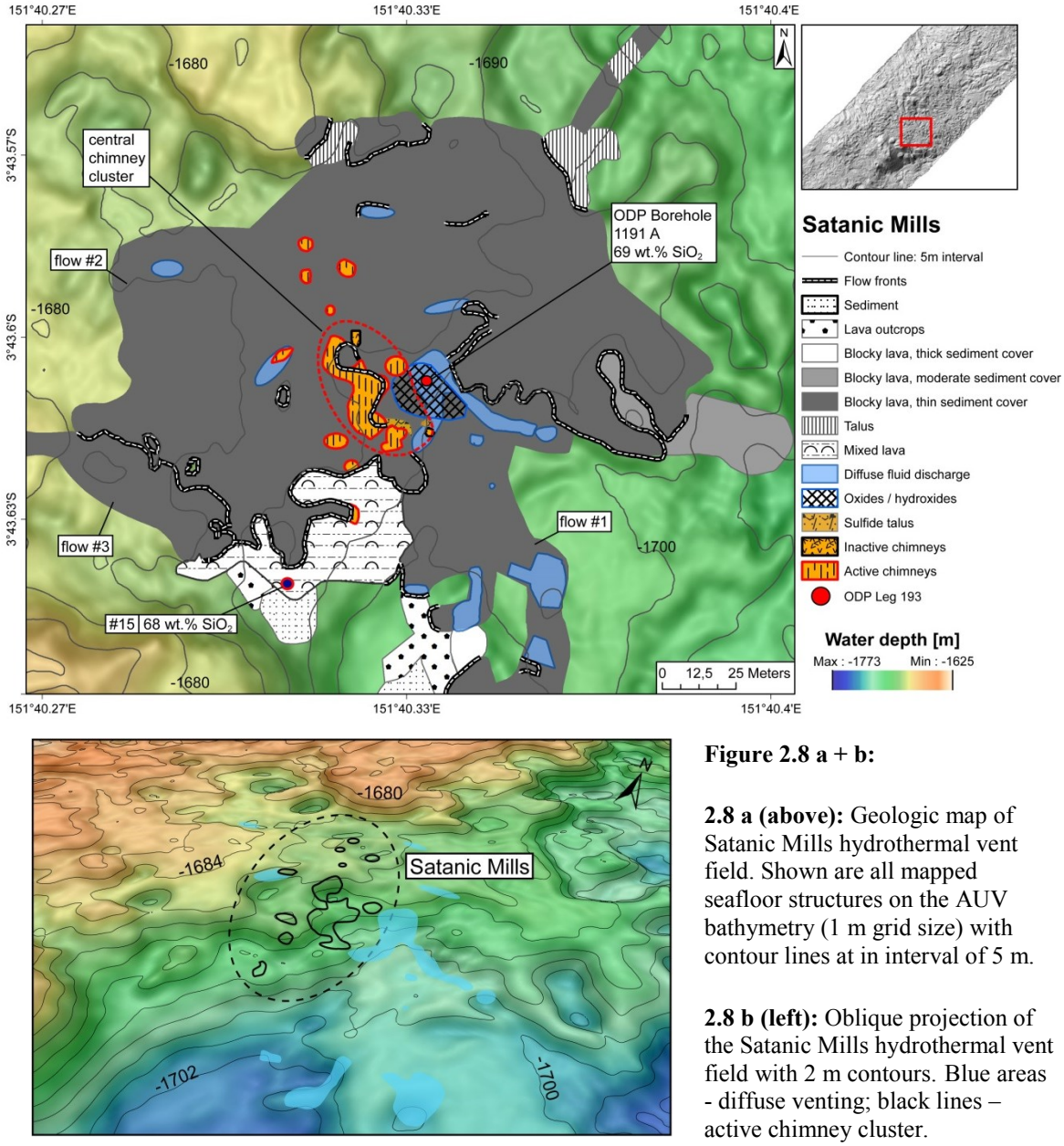

Figure 2.8 a + b:

2.8 a (above): Geologic map of Satanic Mills hydrothermal vent field. Shown are all mapped seafloor structures on the AUV bathymetry (1 m grid size) with contour lines at in interval of 5 m.

2.8 b (left): Oblique projection of the Satanic Mills hydrothermal vent field with 2 m contours. Blue areas - diffuse venting; black lines – active chimney cluster.

In areas of compact flow fronts, the sulphide chimneys have grown directly out of the contact zone between the flow front and the underlying formation. In areas where an apron of talus decorates the flow front, the sulphide chimneys sit on top of the talus pile in discrete clusters. These active vents emit predominantly black smoker fluids from clusters of numerous branched, thin (max. 10 cm) chimneys. Minor chimney clusters and patches of diffuse venting are also found sparsely distributed apparently unrelated to any lava flow fronts. These sites are constrained to small depressions in the lava flow, perhaps related to buried flow fronts or collapse pits.

Blocky lava flows #2 and #3 overlie sediment-covered mixed lava morphologies as can be deduced from seafloor mapping in the southwestern portion of the Satanic Mills

area (Fig. 2.8). In that mixed underlying lava unit, well developed pillow lava tubes are present and disappear towards the west under an increasing thickness of sediment.

In 2011, we measured a T_{max} of 345°C in black smoker fluids venting from chimneys from the central chimney cluster of Satanic Mills. Bubbles of liquid CO_2 could also be observed at this vent site. The distance between the northern and southernmost chimney clusters is ~100 m. The east-west dimension of the field is a maximum width of 40 m. Patches of diffuse venting cover about 690 m² while the active venting chimneys cover an area of ~540 m². ODP hole 1191A attempted to drill into the Satanic Mills field, but got stuck at 20 m and then the hole collapsed ending operations there with no core recovered (Shipboard Scientific Party, 2002a).

2.4.5 North PACManus Vent Area

The prominent SW-NE striking central edifice of the neovolcanic zone of the PACManus Hydrothermal District terminates along strike to the northeast at its deepest point at the location of the Roman Ruins hydrothermal vent field (Fig. 2.4 and 2.9). This is where another separate volcanic center begins just to the northeast of Roman Ruins. Roman Ruins appears to be directly on strike with the central fissure system of the neovolcanic zone. The separate but smaller Roger's Ruins vent field is located ~200 m northwest of Roman Ruins, perpendicular to this neovolcanic trend. Interestingly, further out another 200 m along this perpendicular flowline trend is yet another vent field, Solwara 7 discovered by Nautilus Minerals (Figs. 4 and 9). The slopes around these vent areas are part of a small swale between the two neovolcanic centers and have steep walls (30°) that are covered by talus, blocky lava and sediment (Fig. 2.9). The southwestern wall is less sedimented compared with the northeastern slopes. The slope southeast of Roger's Ruins is dominated by blocky lava, which has, in some areas, blocky as well as clod-like morphologies. A blocky lava knoll with a moderate to thick sediment cover (Fig. 2.9) lies between Roman Ruins and Rogers Ruins and separates the two hydrothermal fields from each other. The region southeast of Roman Ruins is characterised by blocky lava flows without any evidence of hydrothermal activity. Sediment thickness increases markedly with increasing distance from Roman Ruins so that 200 m to the southeast of the vent site, the sediment cover is almost continuous with only sparse outcrops of lava.

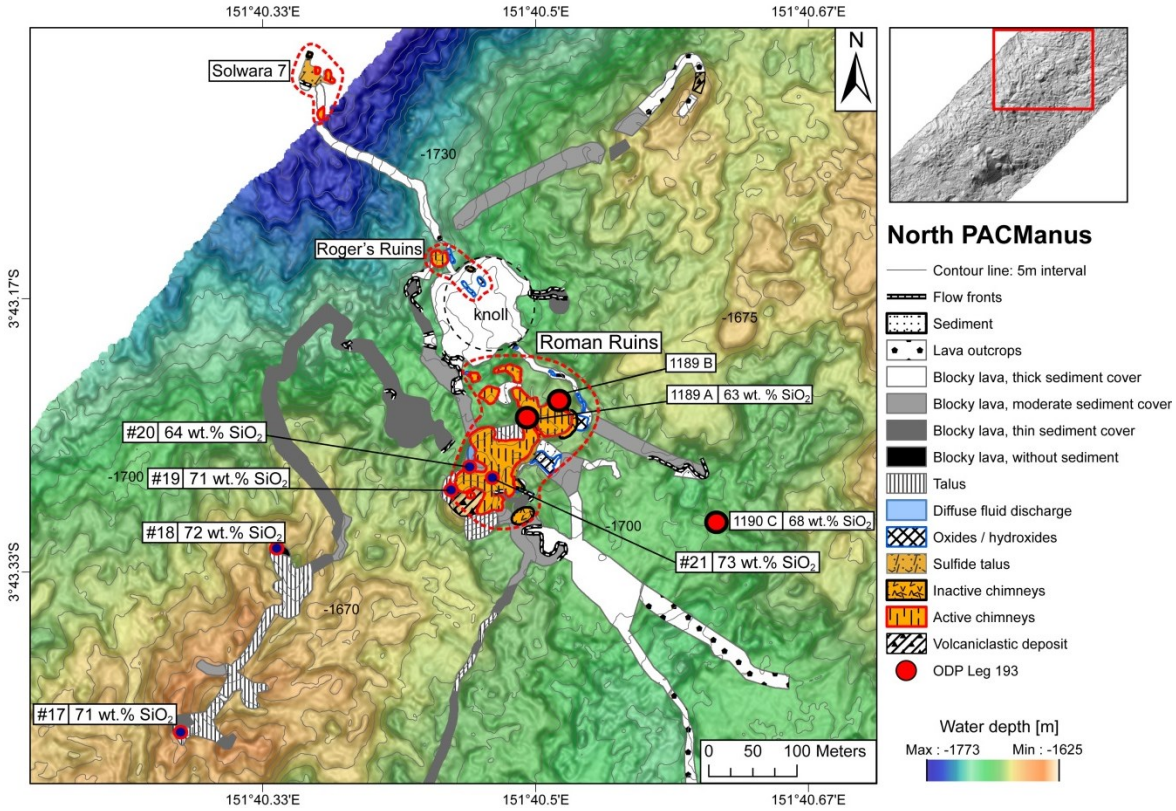

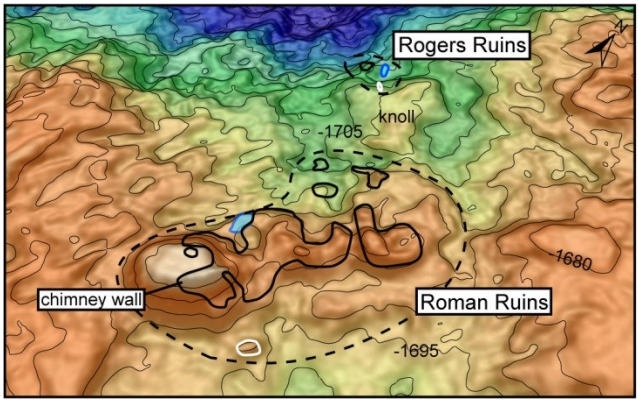

Figure 2.9 a + b:
2.9 a (above): North PACManus. Shown are all mapped seafloor structures including the two hydrothermal fields Rogers Ruins and Roman Ruins on the AUV bathymetry (1 m grid size) with 5 m.

2.9 b (left): Oblique projection of the Roman Ruins and Rogers Ruins hydrothermal area with 5 m contours. Blue areas - diffuse venting; black lines – active chimney cluster; white circles - inactive chimney cluster.

2.4.5.1 Roman Ruins

Roman Ruins, also known as Field F and the Chimney Forest site (Binns and Scott, 1993; Hashimoto et al., 1999), is located at a depth of ~1675 m and is the largest hydrothermal field in the entire PACManus district. It extends approximately 200 m in NE-SW and up to 100 m in NW-SE direction (Fig. 2.9). Active venting chimneys cover an area of ~7000 m² whereas diffuse venting only covers ~135 m². The morphology of the Roman Ruins area is characterised by small mounds, which exhibit countless chimneys. The depressions between the mounds are mainly covered by sulphide talus. A characteristic feature of Roman Ruins are clusters of 0.5 to 7 m high, either columnar, solitary or highly branched smokers with innumerable small columns. Many of the columnar chimneys are topped with white, beehive-like cones that show diffuse venting

through their fragile walls. In many places, an identification of the seafloor was impossible due to limited visibility created by dense black smoke emitted by the vents. Identification of the lava type was often obstructed by piles of sulphide talus. The slopes around the numerous small mounds are littered with sulphide talus. In the gullies between the mounds, clear fluids discharge from cm-wide cracks in the volcanic basement, with temperatures up to 106°C.

The southwestern end of the Roman Ruins hydrothermal field is marked by a circular volcanic cone with a flat plateau and ~35° steep slopes. Sediment and volcaniclastic deposits cover the centre of the plateau, where a solitary branched smoker has grown. At the eastern edge of the plateau, a small lava flow can be traced uphill to the base of a unique feature in the PACManus Hydrothermal District: sulphide chimneys have coalesced into a compact wall issuing black smoker fluids through countless orifices. The wall extends approximately 20 m in SW-NE direction.

ODP boreholes 1189A and 1189B were drilled at the northeastern half of Roman Ruins (Shipboard Scientific Party, 2002c) to a depth of 125.8 and 206 mbsf respectively. We did not find 1189A but visited 1189B, which is in an area surrounded by active chimneys, however, the cased hole showed no signs of hydrothermal discharge either during or after drilling. Although the boreholes are located only ~35 m apart, the drilled lithologies appear to vary substantially between the holes. Intensely altered aphyric dacite dominates core 1189A with fresh dacite limited to the top section (<10 mbsf). And no significant mineralization zones. In contrast, 1189B was cased for the upper 31 m and immediately intersects a hydrothermal stockwork zone (31 - ~85 mbsf). Variably altered dacites with sparsely local stockwork veining dominates the deeper parts of the hole (Shipboard Scientific Party, 2002c; Paulick et al., 2004).

The smokers surrounding borehole 1189B are primarily clusters of branched chimneys with a maximum height of 5-6 meters. Columnar chimneys with beehive-like tops are also present. The vent fluid smoke colour ranges from black to grey for the branched and from light grey to dark grey for the smokers with beehive-like tops. Further to the east, no chimneys are found, but oxide deposits form a small mound with a central depression a few meters in diameter. To the northwest, the topography is characterised by narrow (<10 m) but steep volcanic ridges with crests completely paved with active chimneys. Some of the chimneys are surrounded by oxide mounds that are not included in the map (Fig. 2.9) due to their small lateral extent. A small SW-NE trending trench,

formed by surficial lava morphology, defines the northern edge of the Roman Ruins field. A volcanic rise north of the trench shows thick sediment cover and a few small inactive chimneys and oxide mounds near its top. The Roger's Ruins hydrothermal field lies at the foot of the northwestern slope of that hill (Fig. 2.9).

2.4.5.2 Roger's Ruins

Roger's Ruins is located about 35 m deeper than Roman Ruins on the northern flank of Pual Ridge in 1710 m water depth (Fig. 2.9). The total area covered by chimneys is ~319 m² with a small area of diffuse discharge ~70 m². Roger's Ruins is separated from Roman Ruins by the volcanic hill described above and consists of a main hydrothermal active sulphide chimney complex, a small, inactive chimney group and an area with oxide deposits on a small topographic high. The main field (T_{max}: 320°C in 2006) can be subdivided into one large and one small cluster of smokers. The small cluster is characterised by numerous active chimneys that are highly branched, in contrast to the larger cluster that is composed of mostly inactive, columnar chimneys (max. 9 m high) with diffuse fluid discharge on their base where oxides have accumulated. In addition, diffuse fluid discharge was observed east of the main complex in a small, ~8 m long zone populated with small oxide mounds. The immediate northern and western slope of Rogers Ruins is covered by sulphide and volcanic talus.

2.4.5.3 Solwara 7

Active hydrothermal vent site, Solwara 7, discovered by Nautilus Minerals at a depth of ~1800 m is located just outside the ABE micro-bathymetry map area (Fig. 2.4 and 9). The vent field lies downslope of Roger's Ruins where the seafloor is dominated by blocky lava flows covered by a thick sediment cover with a few mega pillow features that emerge at the base of lava flow lobes. Vigorous fluid flow through a few ~12 m high chimneys were observed in 2011 by ROV MARUM Quest with a T_{max} of 348°C. Several old discharge sites in the closer vicinity to Solwara 7 are marked by collapsed and sediment-covered inactive chimneys.

2.4.6 Vent locations and temporal changes in hydrothermal venting

Several vent areas have been visited repeatedly between 1996 and 2011, so that temporal changes in hydrothermal activity can be documented for this period. Although these recorded changes are mostly gauged by visual appearance, these records still provide insight into the time-scales of changes in venting activity in the PACManus Hydrothermal District.

2.4.6.1 Tsukushi

Active venting of grey to black fluids was observed at Tsukushi during a Shinkai-2000 dive in 1996 with T_{max}. 268°C (Hashimoto et al., 1999). We did not observe any active chimneys in 2006 or 2011. Diffuse venting through the bases of some inactive chimney structures was observed in 2006, and no venting at all in the chimney area in 2011. We conclude that focused hydrothermal venting has been waning since 1996 and ceased altogether between 2006 and 2011. In contrast, diffuse venting through oxide mounds west of the chimney field (Fig. 2.6a) has been continuous between 1996 and 2011, and constant maximum temperatures of venting of around 60°C were measured in 2006 and 2011.

2.4.6.2 Snowcap

Hydrothermal activity of the vent field at the foot of the west slope of Snowcap appears to have decreased in the recent past as patches of dead, unsedimented gastropods occur next to sediment free, small (< 1m), inactive chimneys.

To the southwest, the vent field is bordered by an area characterised by slabs of native sulphur. Sulphur accumulations were seen in other locations in the eastern Manus Basin, such as at Desmos (Gamo et al., 1997; Gena et al., 2001), and North Su (Tivey et al., 2006; Bach et al., 2012). Sulphur vents are also common in hydrothermal systems in submarine island arc volcanoes (Butterfield et al., 2011). These sulphur deposits form from disproportionation of SO_2 delivered to the seafloor by degassing magmatic fluids that mix with seawater-derived fluids (e.g. Gamo et al., 1997). Sulphuric acid-rich vent fluids form in the process. The Snowcap vent fluids in 2006 were not sulphuric acid-type fluids (Reeves et al., 2011), indicating that the sulphur slabs must have formed during an earlier stage, when the magmatic SO_2 flux was higher. Abundant native sulphur as breccia cement in samples collected from the Snowcap dome indicate that discharge of SO_2 must have been pervasive during this earlier stage. This is consistent with the presence of pyrophyllite-rich alteration assemblages in the drill core recovered from Snowcap (Paulick and Bach, 2006; Binns et al., 2007).

2.4.6.3 Fenway

Hashimoto et al. (1999) mentioned the existence of diffuse venting at the location of Fenway but the main chimney sites of Fenway were not discovered until 2006. It is uncertain if the main focused venting through chimneys existed in 1996. In 2006, the hydrothermal activity at Fenway was very intense, with Big Papi being the most active

hydrothermal vent complex of the entire PACManus Hydrothermal District featuring the highest measured fluid temperature of 358°C corresponding to the boiling temperature of seawater at 172 bar (i.e. ~1710 m water depth) (Reeves et al., 2011). In 2011, focused venting of black smoker fluids had decreased dramatically and fewer anhydrite blocks and more sulphide debris was observed. The highest temperature measured in 2011 at Big Papi was 304°C. The bordering parapet did not show any fluid flow in 2006. In 2011, however, vigorous diffuse venting of ~90°C hot fluid was observed in the entire area of the parapet. The activity in the smaller chimney clusters around Big Papi and in the large field of diffuse venting in the north apparently have not changed much between 2006 and 2011.

2.4.6.4 Satanic Mills

The intensity of fluid venting has not changed much at Satanic Mills between 1999 and 2011. Maximum vent temperatures have increased from 280-290°C in 2006 to 335°C in 2011. CO_2 bubbling observed in 2011, indicate that the fluids are at least as rich in CO_2 as they were in 2006 (>200 mM CO_2; Reeves et al., 2011).

2.4.6.5 Roman Ruins

Roman Ruins was discovered by Binns and Scott (1993) and was revisited by (Hashimoto et al., 1999) but detailed information about the fluid composition and temperature were not reported. In 2006 the highest fluid temperature of Roman Ruins (341°C) was measured in the chimney wall area, which was vigorously venting and creating expansive black plumes in the water column. Within the entire PACManus Hydrothermal District, the intensity of hydrothermal activity at Roman Ruins was only surpassed by Big Papi at Fenway in 2006. The orifices of the Roman Ruins sulphide wall were not inspected in 2011, but extensive black smoke constrained ROV work in the immediate environment, so it is likely that the vigour of hydrothermal venting had not subsided much over the period between 2006 and 2011. The activity of small chimneys scattered around the Roman Ruins area does seem to have decreased since 2006 however.

2.3.6.6 Roger's Ruins

Roger's Ruins vents are considered part of the Roman Ruins hydrothermal field despite the ~100 m wide area without hydrothermal activity between them. The fluid compositions of both fields are somewhat similar in that they are thought to have the same source with Roger's Ruins fluids showing a higher amount of seawater mixing (Reeves et al., 2011). Part of the Roman Ruins fluids may be being diverted underground

to Roger's Ruins as it is situated directly at the foot of a volcanic high that is prominent for the area between the two hydrothermal fields. In 2011, hydrothermal activity at Roger's Ruins main cluster had declined and only diffuse venting at the base of the chimneys could be observed. A small cluster of chimneys characterised by highly branched tubes emitting large amounts of black fluids with temperatures up to 320°C was sampled in 2006 (Reeves et al., 2011) and had no discernible change in activity between 2006 und 2011.

2.4.7 Spatial variation in rock compositions

Numerous aphyric, vesicular volcanic rock samples have been collected (Fig. 2.4; Table 2.A1) that show dacitic to rhyolitic compositions, with SiO_2 contents ranging from 63-73 wt.%. Due to the imprecise location of samples dredged during earlier expeditions to PACManus (e.g., Park et al., 2009) we excluded these samples from our analysis and concentrated on non-altered, fresh volcanic rocks from cruises Magellan-06, SO216 and ODP 193 (Table 2.A1).

The most siliceous compositions are found within neovolcanic zone and its NE extension into Roman Ruins. Additional subordinate occurrences of highly siliceous rocks are found at Big Papi and in the crater southwest of Snowcap (Fig. 2.4; Fig. 2.6a and b). Samples with the lowest amount of silica were recovered from outcrop at the bottom of a gully at Roman Ruins and as a loose piece from the bottom of the gully between Big Papi and Fenway dome. Within the Snowcap field and in the surrounding areas, as well as around Satanic Mills, we find the silica composition of samples to be generally of uniform concentrations of 68-69 wt. %.

2.5 Discussion

Since the discovery of PACManus in 1991 it has often been described as one of the largest and most metal-rich marine hydrothermal systems in the ocean (e.g. Binns and Scott, 1993; Auzende et al., 1996; Hashimoto et al., 1999; Petersen et al., 2003; Binns et al., 2007). A first assessment of the distribution and size of the hydrothermal deposits was published by Binns and Scott (1993), but they did not report details about the geological framework of the hydrothermal fields. The ODP Leg 193 drilling program in 2000 provided some insight into the volcanic facies present at these various vent field locations (Shipboard Scientific Party, 2002a; Bartetzko et al., 2003; Paulick et al., 2004) but as mentioned, questions remained as to the geological context of the vent sites (Binns et al.,

2007). Figure 2.10 shows a summary of the dimension and position of the mapped hydrothermal discharge sites based on 20 ROV dives with precise navigation that allows us to update earlier estimates based on photo sled work (Binns and Scott, 1993). In certain cases, the location of some of the vent fields are shifted by up to 140 m (Fig. 2.10), and the overall size of the vent fields is considerably smaller than in the original estimates (Binns and Scott, 1993). In addition, several new vent fields have been added to the inventory of hydrothermal activity within the PACManus Hydrothermal District, i.e. Fenway, Solwara 6, 7 and 8 (Table 2.A2).

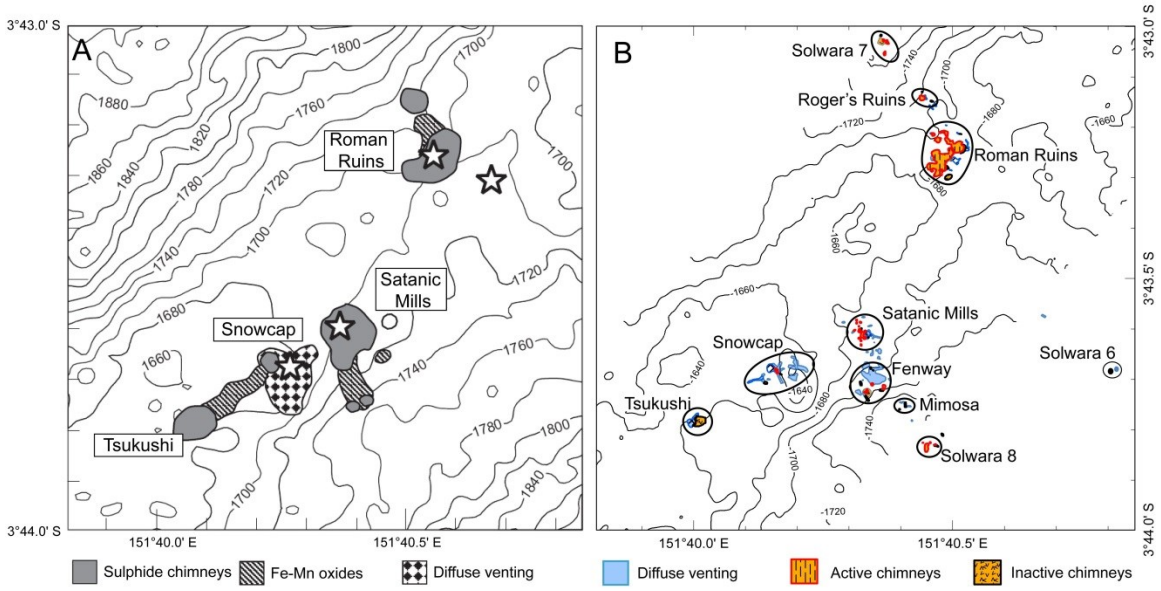

Figure 2.10: Comparison of former mapped hydrothermal fields (Fig. 2.10 A, Binns et al., (2007), modified after Barriga et al. (2000) with the results of this study (Fig. 2.10 B). The black signatures in Figure 10B represent inactive chimney sites whereas the red ones mark active chimney.

The original objective of the 2006 Magellan-06 research cruise was to document the geological context of the ODP drill holes and the relationship between the hydrothermal activity and volcanism within Manus Basin. The PACManus ODP drilling program resulted in holes penetrating between 100 and 380 m deep into the crust of the Snowcap and Roman Ruins areas, but had limited core recovery although logging was more successful (Shipboard Scientific Party, 2002a). The lateral distribution of the recovered volcanic units was unknown at the time of drilling and could only be speculated on as being proximal versus distal based on recovered and borehole imaged volcanic facies (Bartetzko et al., 2003; Paulick et al., 2004). Our results provide a more comprehensive picture of the most recent volcanic phases and their lateral distribution. High-resolution bathymetry maps and rock compositions covering the larger PACManus Hydrothermal District supplement critical information about the most recent volcanic phases that help

provide a framework for understanding the accretion history of Pual Ridge and the relationship to the hydrothermal fields. It is clear from the ROV observations and ABE micro-bathymetry that volcanism dominates over tectonism in this environment. The high-resolution ABE bathymetry maps show a striking morphology with two identifiable types of volcanic terrain: steep-sided lava flows and volcanic domes. In the following sections, we will discuss the first-order differences between the two types of terrain and how these different morphologies may be reconciled in a single volcanic facies model. We will then examine the distribution of hydrothermal vents and how the different types and styles of venting may be controlled by these volcanic features. Lastly, we propose a conceptual model of hydrothermal discharge for this submarine felsic volcanic ridge.

2.5.1 Volcanic Morphology of Pual Ridge

2.5.1.1 Domes

Dome-like structures are found in three locations within the PACManus Hydrothermal District: Snowcap, Fenway and Roman Ruins (sites shown in Fig. 2.3 and 2.9). At Snowcap, ODP Leg 193 drill core had exceedingly low core recovery from the uppermost 40 m of basement and so Bartetzko et al. (2003) used drill hole logging data to interpret Snowcap as being composed of a 35 m thick massive volcanic unit that erupted in place. Paulick et al. (2004) described the recovered rocks as fresh, moderately porphyritic dacite and interpreted this to be the most recent volcanic facies at PACManus. Because of the uncertain nature of the Snowcap dome, we keep this descriptive interpretation for this particular facies and use “dome” as a general term.

Several models for subaqueous silic domes or lava lobe emplacements have been developed from previous observations (e.g. Pichler, 1965; de Rosen-Spence et al., 1980; Yamagishi and Dimroth, 1985; McPhie et al., 1993; Goto and Tsuchiya, 2004). These models propose an endogenous growth with a coherent core that is surrounded by a rim of auto-brecciated and quench-fragmented, in situ and re-sedimented, hyaloclastites. Endogenous growth through syn-eruptive injection of fresh lava into the domes or lava flows can also trigger lava to emerge laterally from the hyaloclastite pile and form lava lobes. Paulick et al. (2004) observed flow banded coherent dacite intruding into a breccia of flow banded clasts in a sample from 157.2 mbsf recovered at Snowcap indicative of this endogenous growth (ODP Site 1188).

Our observations show that Snowcap dome is sediment covered with steeply dipping (~30°) slopes with the uppermost central part of the dome composed of hyaloclastite. In

places the hyaloclastite breccias are monomictic, consisting of massive clasts and could be produced from autobrecciation during dome emplacement. Other areas show volcaniclastic deposits (woody to tube pumice) especially where sediment cover is thin and where small circular depressions are identified in the ROV video. Our observations corroborate the interpretation of Paulick et al. (2004), who considered the Snowcap dome to represent a dacitic volcanic unit with an autobrecciated outer layer and a coherent core. However, our discovery of small volume, unsedimented lava flows on top of the otherwise sedimented dome suggests that there was a more recent volcanic event in the Snowcap area. This event may be related to the extrusion of the lavas building the West Snowcap ridge, which is also largely unsedimented. Distributed around the hyaloclastite-covered dome top are patches of diffuse venting and a varied hydrothermal fauna (Fig. 2.6). Similar, and perhaps related volcaniclastic deposits, can be found on the seafloor west of Snowcap, where they form a circular, cratered feature 35 m in diameter ("crater" in Fig. 2.4; 2.6a,b).

The second dome-like structure identified in our maps is the Fenway dome (Fig. 2.7). The bathymetry shows several mounds in this area but all, except this one, have lava flow features on their top. At Fenway, only the rise to the northeast of Big Papi seems to be a dome or thick lava lobe like the Snowcap dome. Similar to Snowcap, there is widespread diffuse venting in this area. The dome-like feature has abundant uncemented hyaloclastite covering the top with ~30° steep slopes and massive (>1 m) glassy lava outcrops, which resembles the model of a silicic dome after McPhie et al. (1993) with a hyaloclastite rim and emerging lava lobes.

The third dome-like feature is at the southwestern end of the Roman Ruins hydrothermal field (Fig. 2.9). The ~30° steep slopes of this dome are covered by fresh and lightly sedimented volcanic talus and black smoker chimneys. A 20-m long vigorously venting chimney wall forms at the edge of the plateau where a lava flow ~6 m wide and ~35 m long extrudes from the base of the plateau. The Roman Ruins dome lacks the hyaloclastites characteristic of the domes at Snowcap and Fenway. Furthermore, it has a very flat top and a fresh volcanic talus field on its southern slope. This dome may therefore represent a small volcaniclasts-filled volcanic crater rather than a volcanic dome.

2.5.1.2 Volcanic lava facies in the PACManus Hydrothermal District

The majority of the PACManus Hydrothermal District is dominated by volcanic processes with little to no obvious tectonic activity. We can identify individual flow units based on various characteristics that include flow morphology, sediment thickness, and chemical composition. The relatively high sedimentation rate in the Manus Basin allows us to broadly distinguish different volcanic events in the PACManus Hydrothermal District based on sediment thickness. Estimates of sedimentation rate indicate ~15.5 cm/ka in the central Manus Basin over the past 16,000 years (Barash and Kuptsov, 1997), while Hrischeva et al. (2007) calculated an even higher sedimentation rate, not corrected for compaction, of between 26.5 to 33 cm/ka for the eastern Manus Basin.

We define a chronological sequence of lava flows in the area around Snowcap dome based on flow morphology, sediment cover, and variations in the lava SiO_2 concentration. In the earliest stage-1 phase, Snowcap erupted slightly to moderately porphyritic lavas (68 - 69.8 wt. % SiO_2), probably as a dome or cryptodome. Nearby Fenway dome (67.7 - 68.9 wt. % SiO_2) probably also formed during this phase of activity. This period was followed by a second phase of activity (stage-2) with the eruption of aphyric lava with slightly lower SiO_2 concentrations (67.2 – 67.9 wt. % SiO_2). These lavas can be found on the West Snowcap ridge, as well covering the plain between Snowcap and Tsukushi and in the region around Satanic Mills. Flow structures indicate that the West Snowcap ridge was one of the volcanic eruption centres during this period and parts of this ridge stratigraphically overlie the slopes of the Snowcap dome indicating its younger age. Synchronous dykes intruded and emplaced small amounts of lava (66.5 wt. % SiO_2) on top of the northern part of the Snowcap dome.

In the latest phase (stage-3) of activity, massive blocky lava eruptions were emplaced from the neovolcanic zone (Fig. 2.4) with SiO_2 concentrations between 69 and 72.5 wt. %. Flow morphology is rough and several blocky flows overlap each other. One blocky lava flow (69 wt. % SiO_2) can be followed from Satanic Mills, south past the Fenway dome down to the lower terrace below Fenway (Fig. 2.6 + 2.7). The oldest blocky flows of stage 3 are less covered by in situ breccias and show less talus at the flow front. In contrast, the youngest and more siliceous flows in the neovolcanic zone are completely covered by in situ breccias. The volcanic episode that created the crater southwest of Snowcap, the filled crater at Roman Ruins, the tube pumice on top of Snowcap, as well as the feeder dyke underneath Big Papi may all belong to the same

stage because they all have silica contents similar to those of the young blocky lava (70 - 73 wt. % SiO_2).

Three samples with a less siliceous dacitic composition at Roman Ruins and near Big Papi cannot be binned into this same chronologic sequence. The sample near Big Papi (Sample #12, Fig. 2.7a) was a piece of talus (64.1 wt. % SiO_2) that could have originated from the nearby Fenway dacite dome. A small volume melt injection could have triggered a lava lobe to extrude from the dome and the associated hyaloclastite pile to form in situ breccia when quenched by seawater. At Roman Ruins, lavas with similar compositions (62.8 – 64.3 wt. % SiO_2) represent a former sequence of volcanism that might be connected to the event of the Fenway extruded lava lobe. There is a sharp contact between these lavas and the overlying siliceous blocky lava, which probably is associated with the most recent volcanic event from the primary neovolcanic zone to the SW of Roman Ruins (Fig. 2.9).

We know from the work of Bevins and Roach (1979) and De Rosen-Spence et al. (1980) that relating the SiO_2 content of submarine lava and flow morphologies is fraught with difficulties. These authors described rhyodacitic or rhyolitic pillowed or lobate flows, which had previously been assigned to basaltic compositions. In our sample set, there is no obvious correlation between SiO_2 content and flow morphology; although the most rugged blocky lava flows are the most siliceous composition as might be expected from the increased viscosity. Besides lava composition, other factors, such as the pre-flow morphology, the eruption rate, or temperature can affect lava flow type (Bonatti and Harrison, 1988; Gregg and Fink, 1995). It is therefore difficult to establish simple cause-effect relations to account for the different flow types at PACManus. Our observations do show a possible correlation between the SiO_2 content and lava morphologies. But the differences in SiO_2 concentrations are too small to assign these variations solely to the effect of SiO_2 on viscosity. It is likely that magma plumbing dynamics, including recharge and replenishment events caused fluctuations in temperature and eruption rate that led to the varied flow morphologies and rock types.

A striking feature of the Stage 2 volcanic event is the abundance of dacitic pillow and lobate lava flows, which is more common for low-viscosity basaltic lavas. Siliceous lava flows of this morphology have been observed in numerous Archaean and Phanerozoic sequences and have been interpreted to result from high temperatures and high water contents, both of which lower viscosity (Bevins and Roach, 1979; de Rosen-

Spence et al., 1980; Cas, 1992; Gibson et al., 1999; Dinel et al., 2008). These authors suggested that the high water contents indicate deep water environments and incomplete volatile degassing due to the high ambient pressure. Submarine volcanic rift zones also show common multi-stage magmatic evolution paths with repeated events of mingling and mixing between siliceous melts and more primitive melts, which are extracted from the underlying mantle source. These basaltic melts are considerably hotter than more evolved magma and can transfer excess heat to the siliceous magma through the narrow interface between the mingling magma batches. Superheated siliceous magma incurs an increase of the melt fraction and diminishing crystal content, as well as a rise in temperature, which will greatly lower the viscosity. Dinel et al. (2008) proposed that this process is behind the origin of large volumes of pillowed dacitic and aphyric lavas in the Archaean. Indeed, all lava flows sampled in the course of this study from within the PACManus Hydrothermal District have an aphyric texture. In addition, basaltic xenoliths were found within altered dacitic basement from Site 1189 at Romans Ruins (Binns, 2004). These xenoliths may represent parental basaltic magma, which intruded into a fractionating dacitic magma reservoir. Both the aphyric texture and the basaltic xenoliths suggest that superheating could cause low viscosity that might explain the observed variety in lava morphologies at PACManus and the large areal extent of these flows.

Submarine volcanic domes identified within the PACManus Hydrothermal District, are commonly associated with more viscous lava (and/or low extrusion rates) (Pichler, 1965; Yamagishi and Dimroth, 1985; Griffiths and Fink, 1992, 1997; De Rita et al., 2001). The higher apparent viscosity could indicate lower temperatures for the dome-building lava. Shallow drill core from the Snowcap dome reveal moderately porphyritic non-aphyric lava (<5% plagioclase & clinopyroxene; (Shipboard Scientific Party, 2002b). However, this dacite contains xenocrysts of forsteritic olivine (Binns, 2004) and is therefore also affected by interaction with basaltic magma. It appears that there is a range in the extent of superheating from moderate (in the domes) to large (in the flows). The variable lava morphologies may reflect these temperature differences, perhaps in the course of an increasing quantity of heat being transferred in the aftermath of mafic intrusion.

Bartetzko et al. (2003) and Paulick et al. (2004) interpret the different volcanic facies (i.e. lava morphology) from the drill hole data at Snowcap and Roman Ruins based solely on the spatial distance from the volcanic centre, with Snowcap representing a facies

proximal to the main volcanic vent and Roman Ruins representing a medial facies due to the abundance of transported volcaniclastic material. However, our seafloor observations and mapping reveals that these drill locations have a similar distance from the PACManus neovolcanic zone (e.g. 250 – 320 m). Snowcap, Fenway and Roman Ruins all host recently active volcanic vents and no transported volcaniclastic material could be mapped at PACManus.

We conclude, based on the results of seafloor mapping, that the domes and flows represent different stages of magmatic accretion. The transition between these stages may be gradual, as the dome-building event by viscous lava may be followed by a later stage dominated by lava flow. This transition may be related to progressive heating of a silicic magma following a recharge event of hot, mantle-derived melts.

2.5.2 Controls on the distribution and type of hydrothermal venting

The locations of most hydrothermal fields in the PACManus Hydrothermal District follow certain patterns, as does the chimney distribution within these fields. The Tsukushi field is situated adjacent to a blocky lava flow near a volcanic knoll. The Snowcap field lies at the western base of the Snowcap dome and at the contact zone between the dome and the later stage West Snowcap ridge. The Snowcap hydrothermal vent field appears to be unrelated to the latest volcanic deposits on top of the Snowcap dome. Flow structures and morphology imply that the chimneys grew on top or close to the volcanic eruption centre of the West Snowcap ridge lavas. At Satanic Mills, most sulphide chimneys occur along the flow front of the most recent blocky lava flow, except for one small site that is found in a collapse pit within the flow. The chimneys of Fenway field are located directly at the foot of Fenway dome adjacent to the emergent volcanic flows and flow fronts. The Big Papi mound probably developed directly on top of a feeder dyke, which produced a lava lobe. Fresh volcanic and sulphide talus downslope of the lobe indicates recent mass wasting events down the very steep SE slope of Pual Ridge. The three chimney clusters surrounding Big Papi are distributed on flow fronts at the foot of the slopes surrounding Big Papi. At Roman Ruins, most chimneys occur on small mounds (< 5 m) and ridges with volcanic rocks at the base of the chimney complex. This largest smoker field within PACManus developed at the contact between older, relatively Silica-poor (63-64 wt. % SiO_2) lavas and a younger volcanic crater composed of rhyolitic lavas. Based on our observations and interpretations we have conceptualized the relationship between

volcanic architecture and the vent field locations as depicted in Fig. 2.11 in a schematic W-E transect from Snowcap to Fenway to Satanic Mills.

Binns et al. (2007) proposed that fluid flow at PACManus is governed by fractures rather than volcanic facies related porosity distribution. We could not identify any major fractures or faults on the seafloor in 20 ROV dives in the PACManus Hydrothermal District or in the ABE micro-bathymetry. We conclude therefore that the hydrothermal discharge in the shallow subseafloor is controlled by the volcanic permeability structure and not faults. The lava flows, domes and syn-volcanic intrusions have compact, impermeable cores with in-situ brecciated rims surrounded by re-sedimented, volcaniclastic breccias and hyaloclastites (Bartetzko et al., 2003; Paulick et al., 2004). In the absence of tectonic faults and fissuring, buoyancy forces the fluids to migrate through the breccias around the compact cores to reach the seafloor. This type of volcanic permeability control appears to govern hydrothermal discharge at Tsukushi, Satanic Mills, Snowcap and Fenway (except Big Papi). None of the fluid venting temperatures in these locations is close to the boiling curve of seawater. We speculate that hydrothermal fluids likely pool underneath the coherent cores of thick flows and domes and undergo cooling prior to reaching the surface. In places where channelized up-flow from such reservoirs is favoured, e.g. along attached lava lobes (Fig. 2.11, Fenway), chimneys grow. Without channelized flow, the fluids pass through the thick layer of hyaloclastites covering the domes, and disperse laterally to discharge as diffuse venting fields as found at Snowcap dome and Fenway dome (Fig. 2.11).

Other hydrothermal vents at PACManus (Big Papi, Roman Ruins) appear to be related to small volume volcanic bodies that erupted in place and are probably underlain by feeder dykes. The emplacement of feeder dykes may cause a different type of hydrothermal venting, which reflects a shallow but transient heat source. Several features occurring with dyke propagation can enhance fluid flow along their bodies such as: micro-fracturing, cooling and contraction as well as glassy rims that get easily altered. This scenario has been recently described by Stoffers et al. (2006) who observed focused fluid flow with dyke-swarms at the Tonga arc. Circulation caused by feeder dykes intrusion is thought to be the case at the two hottest and most vigorous venting sites inside the PACManus Hydrothermal District: Big Papi and the sulphide wall at Roman Ruins.

The complex and diverse construction of Pual ridge hosts different fluid flow regimes along intrusive bodies and dykes and can explain the varying hydrothermal fluid chemistry (Reeves et al., 2011) even within a few hundred meters of lateral distance.

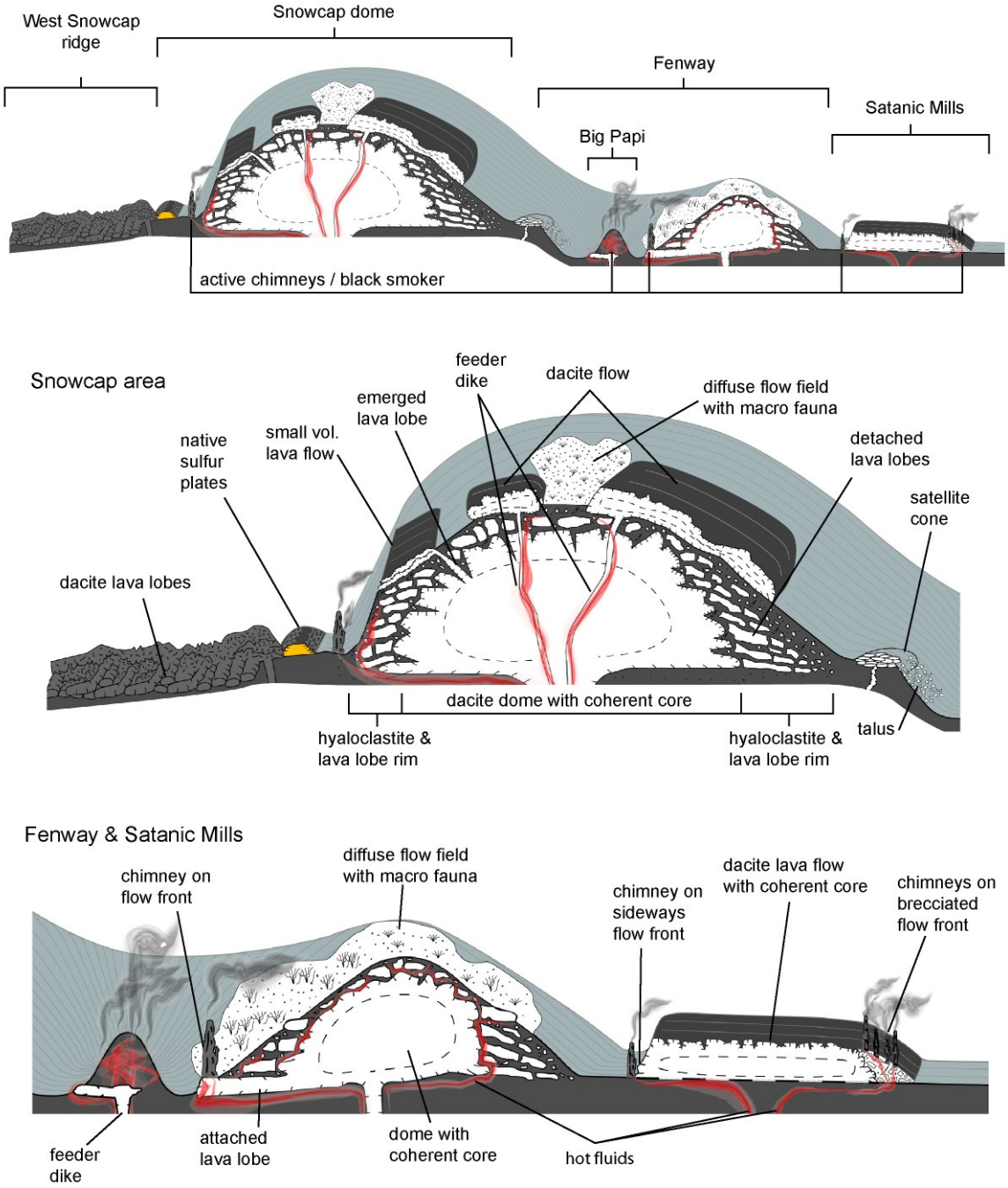

Figure 2.11: Sketch of the volcanic structures at PACManus with suggested fluid pathways. Not for scale.

2.6 Conclusions

ROV observations combined with AUV-based high-resolution bathymetry provide a new perspective on the geological framework of the PACManus Hydrothermal District and its associated hydrothermal fields. Accurate navigation and a quantitative GIS-based analysis revealed a lateral shift of hydrothermal vent site locations of up to 140 m and, in general, a smaller spatial extent of hydrothermal active areas compared with earlier estimates.

The volcanic facies show a wide range of different lava morphologies including pillows, lobate to chaotic jumbled lava flows, massive blocky lava flows and domes. We conclude that these volcanic facies represent different stages of magmatic accretion. In stage-1, slightly to moderately porphyritic lavas (68 - 69.8 wt. % SiO_2) built up domes or cryptodomes. In stage-2, aphyric lava with slightly lower SiO_2 concentrations (67.2 – 67.9 wt. % SiO_2) formed lobate, jumbled and pillowed lava flows. In the most recent stage-3 phase, massive blocky lava with 69 and 72.5 wt. % SiO_2 were emplaced on the seafloor constructing a volcanic ridge identified as the neovolcanic zone of the PACManus Hydrothermal District. The transition between the stages may be gradual and related to progressive heating of a silicic magma following a recharge event of hot, mantle-derived melts.

ROV observations and AUV micro-bathymetry clearly document that volcanic processes dominate over tectonic processes at Pual Ridge. Hydrothermal discharge in the shallow subseafloor at PACManus appears to be controlled by volcanic structures that include domes, dykes and lava flows rather than being governed by tectonic faults and fractures. We recognize two types of volcanic permeability driven hydrothermal circulation: 1) permeability controlled fluid flow through breccias and hyaloclastites associated with domes and 2) channelized fluid flow along dikes and lava lobes.

Finally, our study demonstrates the value of combined high-resolution geophysical mapping with on bottom ROV observations and accurate navigational control within a Geographical Informational System database to resolve the detailed geological setting of the vent sites of the PACManus Hydrothermal District. In particular, the autonomously underwater vehicle ABE collected detailed micro-bathymetry maps that formed a critical template for subsequent ROV dives and bottom exploration and sampling and sets the stage for all future such studies.

2.7 Acknowledgements

We thank the captains and crews of RV Sonne and RV Melville, the ROV teams of Jason-2 and MARUM Quest 4000, the AUV-ABE technical team and the members of the Science Parties for both cruises. Crucial help with bathymetry data processing was provided by Christian dos Santos Ferreira and Paul Wintersteller. The RV Melville work was funded by a combination of the US National Science Foundation grant OCE-0327448 and a collaborative research funding grant from Nautilus Minerals for the ABE surveys. The RV Sonne research cruise was funded through the BMBF (Grant G03216a). Additional funding, including salary support for JT, was provided by the German DFG Research Center/Excellence Cluster "The Ocean in the Earth System". WB acknowledges support from DFG research grant BA1605/4-1.

Finally, we thank Jim Robins and Pat Pepena from Papua New Guinea (PNG) for their help with PNG research permitting.

2.8 Appendix

	Sample	Lat	Lon	Location	SiO_2 (wt. %)	$K_2O + Na_2O$ (wt. %)
1[1]	J2-211-2-R2	-3,72978	151,66654	Tsukushi	67,4	6,2
2[1]	J2-211-3-R1	-3,72793	151,66625	Neovolcanic zone	72,5	6,8
3[1]	J2-214-8-R1	-3,72957	151,66920	Crater (Snowcap)	70,1	6,6
4[1]	J2-214-9-R1	-3,72886	151,66928	W-Snowcap ridge	67,2	6,3
5[1]	J2-211-8-R1	-3,72830	151,66889	W-Snowcap ridge	67,7	6,2
6	SO-216-43-rov-11	-3,72824	151,66931	W-Snowcap ridge	67,9	6,2
7	J2-210-3-r1	-3,72828	151,66990	Snowcap	69,8	7,0
8[2]	ODP 1188A	-3,72827	151,66993	Snowcap	68,3	6,6
9	SO-216-43-rov-10	-3,7272	151,66980	Snowcap	66,6	6,4
10[1]	J2-214-7-R1	-3,72910	151,67062	Snowcap	68,1	6,6
11	J2-212-8-R1	-3,72876	151,67211	Fenway	70,4	6,4
12[1]	J2-216-11-R1	-3,72870	151,67243	Fenway	64,1	6,0
13	J2-210-6-R1	-3,72819	151,67262	Fenway dome	68,9	6,7
14	SO-216-041-rov-1	-3,72825	151,67292	Fenway dome	67,7	6,9
15[1]	J2-209-9-R1	-3,72744	151,67188	Satanic Mills	67,9	6,3
16[2]	ODP 1191A	-3,72680	151,67228	Satanic Mills	69,0	6,6
17[1]	J2-222-12-R1	-3,72385	151,67137	Neovolcanic zone	71,3	6,8
18[1]	J2-222-11-R1	-3,72201	151,67238	Neovolcanic zone	71,8	6,6
19[1]	J2-208-5-R1	-3,72142	151,67412	Roman Ruins	71,4	6,7
20[1]	J2-213-4-R1	-3,72117	151,67434	Roman Ruins	64,4	5,9
21[1]	J2-222-9-R2	-3,72126	151,67457	Roman Ruins	73,3	6,8
22[2]	ODP 1189A	-3,72072	151,67487	Roman Ruins	62,8	5,8
23[2]	ODP 1190C	-3,72172	151,67683	SE of Roman Ruins	67,8	6,7

Table 2.A1:

Rock samples used in this publication.

(W-Snowcap ridge= West Snowcap ridge)

*1. Analyses by Niedermeyer et al. (unpublished)

*2. Analyses by Paulick et al. (2004)

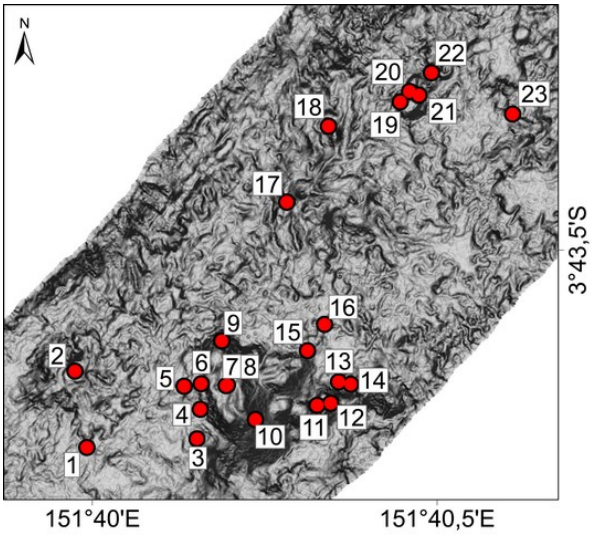

Vent Field Name (Coordinates)	Location	Depth of measurement [m] / Year	Max T [°C] / Year	Areal extent [m²]
Tsukushi	Oxide mounds	1660 / 2006	62 / 2006	Total diffuse: 1792
(151.6667W / 3.7297S)		1665 / 2011	53 / 2011	Total chimneys: 1225
Snowcap	Cluster-1	X (inactive)	X (inactive)	10
(151.6693W / 3.7281S)	Cluster-2	1651 / 2006	63 / 2006	60
	Cluster-3	1639 / 2006	179 / 2006	66
		1644 / 2011	224 / 2011	
	Cluster-4	1643 / 2006	151 / 2006	10
		1647 / 2011	34 / 2011	
				Total chimneys: 146
				Total diffuse: 3680
Fenway	Main field (diffuse)	1701 / 2006	8 / 2006	3300
(151.6723W / 3.7286S)		1709 / 2011	14 / 2011	
	Big Papi	1705 / 2006	353 / 2006	110
		1715 / 2011	304 / 2011	
	Cluster-1	1710 / 2006	330 / 2006	60
		1714 / 2011	313 / 2011	
	Cluster-2	X (partly active)	X (partly active)	247
	Cluster-3	X (inactive)	X (inactive)	16
	Cluster-4	X (inactive)	X (inactive)	71
				Total chimneys: 652
				Total diffuse: 4450

Table 2.A2 : Summary of hydrothermal vent fields within the PACManus Hydrothermal District. Listed are active chimney clusters and diffuse venting fields. Marginal, inactive chimney clusters not mentioned in this publication are included in the total area but not listed separately

Vent Field Name (Coordinates)	Location	Depth of measurement [m] / Year	Max T [°C] / Year	Areal extent [m²]
Satanic Mills (151.672W / 3.7267S)	Central chimney cluster	1685 / 2006 1688 / 2011	295 / 2006 345 / 2011	314 Total chimneys: 564 Total diffuse: 690
Roman Ruins (151.6748W / 3.721S)	Main chimney field marginal active chimney cluster	1666 / 2006 1679 / 2011 X	316 / 2006 334 / 2011 X	6331 678 Total chimneys: 7709 Total diffuse: 135
Rogers Ruins (151.674W / 3.7191S)	Main field	1709 / 2006	320 / 2006	273 Total chimneys: 319 Total diffuse: 70
Solwara-6 (151.6801W / 3.7281S)	x	x	x	Total diffuse: 340
Solwara-7 (151.6728W / 3.7172S)		1774 / 2011	348 / 2011	Total chimneys: 229 Total diffuse: X
Solwara-8 (151.6742W / 3.7305S)	Main field	1740 / 2011	305 / 2011	330 m2 Total chimneys: 501 Total diffuse: X
Mimosa (151.6734W / 3.7293S)	x	x	x	Total chimneys: 120 Total diffuse: 240

Table 2.A2 (continued): Summary of hydrothermal vent fields within the PACManus Hydrothermal District. Listed are active chimney clusters and diffuse venting fields. Marginal, inactive chimney clusters not mentioned in this publication are included in the total area but not listed separately

2.9 References

Auzende, J.-M., Urabe, T., Ruellan, E., Chabroux, D., Charlou, J.-L., Gena, K., Gamo, T., Henry, K., Matsubayashi, O., Matsumoto, T., Naka, J., Nagaya, Y., Okamura, K., 1996. "Shinkai 6500" Dives in the Manus Basin : New STARMER Japanese-French Program. JAMSTEC Journal of Deep Sea Research 12, 323–334.

Bach, W., Cruise Participants, 2011. Report and preliminary results of RV SONNE Cruise SO-216, Townsville (Australia) - Makassar (Indonesia), June 14 – July 23, 2011. BAMBUS, Back-Arc Manus Basin Underwater Solfataras. Berichte, Fachbereich Geowissenschaften, Universität Bremen 280, 87.

Bach, W., Jöns, N., Thal, J., Breuer, C., Shu, L., Dubilier, N., Borowski, C., Meyerdierks, A., Pjevac, P., Brunner, B., Müller, I., Petersen, S., Hourdez, S., Schaen, A., Koloa, K., Jonda, L., MARUM Quest 4000m team, 2012. Interactions between fluids, minerals, and organisms in sulfur-dominated hydrothermal vents in the eastern Manus Basin, Papua New Guinea – A report from RV Sonne Cruise 216. InterRidge News 21, 31–34.

Barash, M.S., Kuptsov, V.M., 1997. Late Quaternary palaeoceanography of the western Woodlark Basin (Solomon Sea) and Manus Basin (Bismarck Sea), Papua New Guinea, from planktic foraminifera and radiocarbon dating. Marine Geology 142, 171–187.

Bartetzko, A., Paulick, H., Iturrino, G., Arnold, J., 2003. Facies reconstruction of a hydrothermally altered dacite extrusive sequence: Evidence from geophysical downhole logging data (ODP Leg 193). Geochemistry Geophysics Geosystems 4, 1087.

Bevins, R.E., Roach, R.A., 1979. Pillow lava and isolated-pillow breccia of rhyodacitic composition from the Fishguard Volcanic Group, Lower Ordovician, SW Wales, United Kingdom. The Journal of Geology 87, 193–201.

Binns, R., Scott, S., 1993. Actively forming polymetallic sulfide deposits associated with felsic volcanic rocks in the eastern Manus back-arc basin, Papua New Guinea. Economic geology 88, 2226–2236.

Binns, R.A., 2004. Data report: spinifex-textured basalt xenoliths at PACMANUS, Papua New Guinea, in: Barriga, F.J.A.S., Binns, R.A., Miller, D.J., Herzig, P.M. (Eds.), Proceedings of the Ocean Drilling Program, Scientific Results. College Station, TX (Ocean Drilling Program), pp. 1–19.

Binns, R.A., Barriga, F.J.A.S., Miller, D.J., 2007. Leg 193 synthesis: Anatomy of an active felsic-hosted hydrothermal system, eastern Manus Basin, Papua New Guinea, in: Barriga, F.J.A.S., Binns, R.A., Miller, D.J., Herzig, P.M. (Eds.), Proceedings of the Ocean Drilling Program, Scientific Results. College Station, TX (Ocean Drilling Program), pp. 1–71.

Bird, P., 2003. An updated digital model of plate boundaries. Geochemistry, Geophysics, Geosystems 4, 1–52.

Bonatti, E., Harrison, C.G. a., 1988. Eruption styles of basalt in oceanic spreading ridges and seamounts: Effect of magma temperature and viscosity. Journal of Geophysical Research 93, 2967.

Butterfield, D. a., Nakamura, K. -i., Takano, B., Lilley, M.D., Lupton, J.E., Resing, J. a., Roe, K.K., 2011. High SO2 flux, sulfur accumulation, and gas fractionation at an erupting submarine volcano. Geology 39, 803–806.

Cas, R., 1992. Submarine volcanism; eruption styles, products, and relevance to understanding the host-rock successions to volcanic-hosted massive sulfide deposits. Economic Geology 87, 511–541.

Craddock, P.R., Bach, W., 2010. Insights to magmatic–hydrothermal processes in the Manus back-arc basin as recorded by anhydrite. Geochimica et Cosmochimica Acta 74, 5514–5536.

De Rosen-Spence, A.F., Provost, G., Dimroth, E., Gochnauer, K., Owen, V., 1980. Archean subaqueous felsic flows, Rouyn-Noranda, Quebec, Canada, and their Quarternary equivalents. Precambrian Research 12, 43–77.

DeRita, D., Giordano, G., Cecili, A., 2001. A model for submarine rhyolite dome growth: Ponza Island (central Italy). Journal of Volcanology and Geothermal Research 107, 221–239.

Dinel, E., Saumur, B.M., Fowler, A.D., 2008. Spherulitic Aphyric Pillow-Lobe Metatholeiitic Dacite Lava of the Timmins Area, Ontario, Canada: A New Archean Facies Formed from Superheated Melts. Economic Geology 103, 1365–1378.

Edmond, J.M., Measures, C., McDuff, R.E., Chan, L.H., Collier, R., Grant, B., Gordon, L.I., Corliss, J.B., 1979. Ridge crest hydrothermal activity and the balances of the major and minor elements in the ocean: The Galapagos data. Earth and Planetary Science Letters 46, 1–18.

Gamo, T., Okamura, K., Charlou, J., Urabe, T., Auzende, J., Ishibashi, J., Shitashima, K., Chiba, H., Shipboard Scientific Party of the ManusFlux Cruise, 1997. Acidic and sulfate-rich hydrothermal fluids from the Manus back-arc basin, Papua New Guinea. Geology 25, 139–142.

Gena, K., Mizuta, T., Ishiyama, D., Urabe, T., 2001. Acid-sulphate Type Alteration and Mineralization in the Desmos Caldera, Manus Back-arc Basin, Papua New Guinea. Resource Geology 51, 31–44.

German, C.R., Lin, J., Parson, L.M., 2004. Mid-Ocean Ridges: Hydrothermal Interactions Between the Lithosphere and Oceans. American Geophysical Union, Washington, D. C.

Gibson, H.L., Morton, R.L., Hudak, G.J., 1999. Submarine volcanic processes, deposits, and environments favourable for the location of volcanic-associated massive sulfide deposits, in: Barrie, C.T., Hannington, M.D. (Eds.), Volcanic-Associated Massive Sulfide Deposits: Processes and Examples in Modern and Ancient Settings. Reviews in Economic Geology 8, pp. 13–51.

Goto, Y., Tsuchiya, N., 2004. Morphology and growth style of a Miocene submarine dacite lava dome at Atsumi, northeast Japan. Journal of Volcanology and Geothermal Research 134, 255–275.

Gregg, T.K.P., Fink, J.H., 1995. Quantification of submarine lava-flow morphology through analog experiments 23–27.

Griffiths, R.W., Fink, J.H., 1992. Solidification and morphology of submarine lavas: a dependence on extrusion rate. Journal of Geophysical Research 97, 19,729–19,737.

Griffiths, R.W., Fink, J.H., 1997. Solidifying Bingham extrusions: a model for the growth of silicic lava domes. Journal of Fluid Mechanics 347, 13–36.

Hannington, M., Jamieson, J., Monecke, T., Petersen, S., Beaulieu, S., 2011. The abundance of seafloor massive sulfide deposits. Geology 39, 1155–1158.

Hannington, M.D., de Ronde, C.E.J., Petersen, S., 2005. Sea-Floor Tectonics and Submarine Hydrothermal Systems. Economic Geology 100th Anni, 111–141.

Hashimoto, J., Ohta, S., Fiala-Médioni, A., Auzende, J., 1999. Hydrothermal vent communities in the Manus Basin, Papua New Guinea: Results of the BIOACCESS cruises' 96 and'98. InterRidge News 8 (2), 12–18.

Herzig, P.M., 1999. Economic potential of sea-floor massive sulphide deposits: ancient and modern. Philosophical Transactions of the Royal Society A: Mathematical, Physical and Engineering Sciences 357, 861–875.

Hrischeva, E., Scott, S., Weston, R., 2007. Metalliferous sediments associated with presently forming volcanogenic massive sulfides: the SuSu Knolls hydrothermal field, eastern Manus Basin, Papua New. Economic Geologyeology 102, 55–73.

Iizasa, K., 1999. Potential Marine Mineral Resources by Hydrothermal Activity. Chemical Industry 50, 379–384.

Lee, S., Ruellan, E., 2006. Tectonic and magmatic evolution of the Bismarck Sea, Papua New Guinea: Review and new synthesis, in: Christie, D.M., Fisher, C.R., Lee, S.-M., Givens, S. (Eds.), Back-Arc Spreading Systems: Geological, Biological, Chemical, and Physical Interactions. Washington, D. C., pp. 263–286.

Martinez, F., Taylor, B., 1996. Backarc spreading, rifting, and microplate rotation, between transform faults in the Manus Basin. Marine Geophysical Research 18, 203–224.

Mcphie, J., Doyle, M., Allen, R., 1993. Volcanic textures: a guide to the interpretation of textures in volcanic rocks. Centre for Ore Deposit and Exploration Studies - University of Tasmania.

Mosier, D.L., Berger, V.I., Singer, D.A., 2009. Volcanogenic massive sulfide deposits of the world; database and grade and tonnage models, U.S. Geological Survey Open-File Report.

Park, S.-H., Lee, S.-M., Kamenov, G.D., Kwon, S.-T., Lee, K.-Y., 2009. Tracing the origin of subduction components beneath the South East rift in the Manus Basin, Papua New Guinea. Chemical Geology 269, 339–349.

Paulick, H., Bach, W., 2006. Phyllosilicate alteration mineral assemblages in the active subsea-floor Pacmanus hydrothermal system, Papua New Guinea, ODP Leg 193. Economic Geology 101, 633–650.

Paulick, H., Vanko, D.., Yeats, C.., 2004. Drill core-based facies reconstruction of a deep-marine felsic volcano hosting an active hydrothermal system (Pual Ridge, Papau New Guinea, ODP Leg 193). Journal of Volcanology and Geothermal Research 130, 31–50.

Petersen, S., Herzig, P., Hannington, M.D., Gemmell, J.B., 2003. Gold-rich massive sulfides from the interior of the felsic-hosted PACMANUS massive sulfide deposit, Eastern Manus Basin (PNG). Mineral Exploration and Sustainable Development 171–174.

Pichler, H., 1965. Acid hyaloclastites. Bulletin Volcanologique 28, 293–310.

Reeves, E.P., Seewald, J.S., Saccocia, P., Bach, W., Craddock, P.R., Shanks, W.C., Sylva, S.P., Walsh, E., Pichler, T., Rosner, M., 2011. Geochemistry of hydrothermal fluids from the PACMANUS, Northeast Pual and Vienna Woods hydrothermal fields, Manus Basin, Papua New Guinea. Geochimica et Cosmochimica Acta 75, 1088–1123.

Sangster, D.F., 1980. Quantitative characteristics of volcanogenic massive sulphide deposits. Bulletin of the Canadian Institute of Mining and Metallurgy 73, 74–81.

Sclater, J.G., Parsons, B., 1981. Oceans and continents: similarities and differences in the mechanisms of heat loss. Journal of Geophysical Research 86, 11535–11552.

Shipboard Scientific Party, 2002a. Leg 193 summary, in: Barriga, F.J.A.S., Binns, R.A., Miller, D.J., Herzig, P.M. (Eds.), Proceedings of the Ocean Drilling Program, Initial Reports. College Station, TX (Ocean Drilling Program), pp. 1–84.

Shipboard Scientific Party, 2002b. Site 1188, in: Binns, R.A., Barriga, F.J.A.S., Miller, D.J., Al., E. (Eds.), Proceedings of the Ocean Drilling Program, Initial Reports. College Station, TX (Ocean Drilling Program), pp. 1–305.

Shipboard Scientific Party, 2002c. Site 1189, in: Binns, R.A., Barriga, F.J.A.S., Miller, D.J., Al., E. (Eds.), Proceedings of the Ocean Drilling Program, Initial Reports. College Station, TX (Ocean Drilling Program), pp. 1–259.

Stoffers, P., Worthington, T.J., Schwarz-Schampera, U., Hannington, M.D., Massoth, G.J., Hekinian, R., Schmidt, M., Lundsten, L.J., Evans, L.J., Vaiomo'unga, R., Kerby, T., 2006. Submarine volcanoes and high-temperature hydrothermal venting on the Tonga arc, southwest Pacific. Geology 34, 453–456.

Taylor, B., 1979. Bismarck Sea: Evolution of a back-arc basin. Geology 7, 171–174.

Taylor, B., Crook, K., Sinton, J., 1994. Extensional transform zones and oblique spreading centers. Journal of geophysical research 99, 19,707–19,718.

Tivey, M., Bach, W., Seewald, J., Tivey, M.K., Vanko, D.A., Shipboard Science Party, 2006. Cruise Report for R/V Melville Cruise MGLN06MV—Hydrothermal Systems in the Eastern Manus Basin: Fluid Chemistry and Magnetic Structure as Guides to Subseafloor Processes.

Van Dover, C.L., Biscotto, M., Gebruk, A., Hashimoto, J., Tunnicliffe, V., Tyler, P., Desbruyeres, D., 2006. Milestones in the discovery of hydrothermal-vent faunas, in: Desbruyeres, D., Segonzac, M., Bright, M. (Eds.), Handbook of Deep-Sea Hydrothermal Vent Fauna. Denisia, pp. 13–25.

Yamagishi, H., Dimroth, E., 1985. A comparison of Miocene and Archean rhyolite hyaloclastites: evidence for a hot and fluid rhyolite lava. Journal of volcanology and geothermal research 23, 337–355.

3. Volcanic and hydrothermal activity of the North Su volcano: New insights from repeated bathymetric surveys and ROV observations

Janis Thal[1*], Maurice Tivey[2], Dana R. Yoerger[2], Dominik Niedermeyer[1], Niels Jöns[1], Wolfgang Bach[1]

[1]MARUM, University of Bremen, 28359 Bremen, Germany

[2]Woods Hole Oceanographic Institution, Woods Hole, MA02543, USA

**corresponding author: Janis Thal*

email: ja_th@uni-bremen.de

Phone: +4942121846405

***Journal of Volcanology and Geothermal Research** - to be submitted*

3.1 Abstract

Comparison of the results from repeated cruises to the North Su volcano in the eastern Manus Basin allowed us to document temporal changes in volcano morphology and hydrothermal activity. Specifically, ship-based multibeam bathymetry data from 2002 and 2011 were merged with micro-bathymetry data recorded by autonomous underwater vehicle (AUV) and by remotely operated vehicle (ROV) and combined with ROV video data from in 2006 and 2011 in a comprehensive geologic mapping study that depicts the volcanic evolution of North Su and analyzes its morphologic expressions.

North Su, part of the SuSu Knolls hydrothermal district, is known as a submarine equivalent to terrestrial high sulfidation Cu-Au mineralization. The complex hydrothermal system hosts acidic white smoker vents less than 100 m asides to black smoker vents. Volcanic rocks of North Su, located in the eastern Manus Basin, Bismarck Sea, are porphyritic andesites with dacitic to rhyolitic glass compositions. We documented that an eruption occurred between 2006 and 2011 where $5.8*10^6$ m^3 of volcanic material has been deposited on an area of $2.1*10^5$ m^2 with a maximum depth change between the surveys of +63 m. This eruption created a new cone, South Peak, that is characterized by a plateau on its summit with localized, small (<10 m diameter) and shallow (<3 m depth) craters that are sign for steam explosion inside the cone. The entire summit area consist of heterolithic clasts (fresh to highly altered clasts with abundant crystal fragments lacking juvenile pyroclastic fragments) that are produced by mixing of in-situ fragmented, high viscous lava that behaves with brittle failure, and by uplifted pre-existing material of previous eruptions. The high-viscous lava produces blocky outcrops, volcanic spines and abundant clastic material.

Volcanic activity at North Su can also be explosive as indicted by an 80 m diameter wide crater observed in the bathymetry prior to the growth of South Peak. Characteristic for North Su is a sand-sized, heterolithic clastic deposit that is locally cemented by hydrothermal precipitates. Hydrothermal cementation clearly increases local slope stability at North Su, due to crystallization of hydrothermal minerals in void spaces, when the fluid discharge occurs through a pile of volcaniclastic sediments. The cemented breccias resist slope collapse events and reside as ridge lines or pillars.

Keywords: Submarine volcano, ROV, AUV, VMS, repeated bathymetry

3.2 Introduction

Terrestrial volcanism has been a focus of natural scientists for centuries but comparably little is known about the submarine counterpart, though three quarters of Earth's volcanic activity takes place in ocean basins. About 32,000 seamounts rising >750 meters above the regional seafloor, most of which are believed to be of volcanic origin, were identified by satellite altimetry and ship-based bathymetry (Wessel, 2001; Hillier and Watts, 2007). While most of these seamounts are intra-plate volcanoes, solitary volcanic edifices also exist in arc settings or along the mid-ocean ridges. The magma compositions vary with tectonic setting, affecting the eruption style, the nature of ejected/deposited material, and the volcanic morphology. Despite of the enormous number of seamounts, only a few have been studied in detail. However, a number of dedicated research cruises in the past decade increased our knowledge of and the perspective on submarine volcanism and the architecture of volcanoes (e.g. Wright et al., 2003; Carey and Sigurdsson, 2007; Chadwick Jr. et al., 2008; Allen and McPhie, 2009; Leat et al., 2010; Schipper et al., 2010; Clague et al., 2011; Deardorff et al., 2011; Resing et al., 2011). For example, subaqueous eruptions along the world-spanning mid-ocean ridges are dominated by effusive eruptions of basaltic, low-viscosity lavas producing pillows and sheet flows (Rubin et al., 2012). Recent discoveries have also indicated that explosive eruptions are not rare (e.g. Sohn et al., 2008; Clague et al., 2009; Helo et al., 2011). In contrast to mid ocean ridges, less-well-characterized volcanic activity in arc settings is highly diverse in space, time and composition; ranging from basalt to rhyolite and featuring variable eruption styles from effusive to explosive to dome emplacement (e.g. Embley et al., 2006; Carey and Sigurdsson, 2007; Allen et al., 2010; Resing et al., 2011).

Hydrothermal activity is commonly observed in relation to volcanic activity. Of special interest are hydrothermal systems associated with felsic volcanism because they are potential analogs for volcanogenic massive sulfide deposits found in continental settings. The felsic host rock combined with degassive volatile loss of magmatic systems facilitate the enrichment of economically important metals such as copper, gold and zinc (e.g. Sangster, 1980; Herzig, 1999; Iizasa, 1999; Hannington et al., 2005, 2011; Mosier et al., 2009).

The SuSu Knolls hydrothermal district in the eastern Manus Basin is a submarine equivalent to terrestrial high sulfidation Cu-Au mineralization (Binns et al., 1997; Moss

and Scott, 2001; Yeats et al., 2008). This is why the Solwara-1 hydrothermal field (also referred to as Suzette) ~3 km northwest of North Su, is a primary prospect site for mineral exploration by Nautilus Minerals Inc (Lipton, 2008). The SuSu Knolls hydrothermal district was first discovered in 1996 during the PACMANUS-III cruise (Binns et al., 1997) and followed by several expeditions of economic interest (Crowhurst and Lowe, 2011) as well as international research cruises that focused on the hydrothermal fluid chemistry, mineral deposition, biology and geology (Auzende et al., 2000; Tivey et al., 2006; Bach et al., 2011).

This study presents a systematic analysis of the central edifice of the SuSu Knolls, the North Su volcano. The active submarine volcano is erupting porphyritic andesite and hosts an associated hydrothermal system. We compared bathymetry from three cruises and combined a Geographical Information Systems (GIS) database of AUV-based micro-bathymetry with video recordings, rock analyses and temperature measurements. Our analysis of the data from three research cruises from 2002, 2006 and 2011 resulted in a comprehensive documentation of the recent volcanic activity and the hydrothermal system.

Data of North Su, collected before the Magellan-06 expedition, were restricted to low resolution photo sled surveys and dredges (Binns et al., 1997). In 2006, the Woods Hole Oceanographic Institution (WHOI), with support from Nautilus Minerals Inc., commenced the Magellan-06 research expedition that provided more detailed information about the geologic setting and hydrothermal system of North Su. High-resolution bathymetry and magnetic data were recorded by autonomous underwater vehicle (AUV) ABE, supplemented by detailed rock and fluid sampling by the remotely-operated vehicle (ROV) Jason-2. In addition, ship-based multibeam bathymetric mapping and CTD casts were conducted over SuSu Knolls. The high-resolution ABE bathymetry from Magellan-06 combined with video recordings from three ROV Jason-2 dives allow us to document the first detailed, georeferenced mapping of the volcanic and hydrothermal structures at North Su. The results led to an increased interest for further surveys at North Su.

In 2011, a follow-up cruise (RV Sonne cruise SO216; Bach et al., 2011), focused on detailed sampling of hydrothermal fluids and biota. An additional twelve ROV dives, using the ROV MARUM Quest4000, were completed in the North Su summit area, allowing us to confirm the meter-scale reliability of the AUV ABE maps generated during the Magellan-06 expedition. The dense data coverage generated during 12 ROV

dives on an area of ~140.000 m² provided important information to expand on the mapping of 2006 and to create a comprehensive dataset of spatial distribution of volcanic and hydrothermal structures on North Su. Additionally, ship-based swath bathymetry from SO-166 cruise (Shipboard Scientific Party, 2002) is used to track further morphologic changes.

3.3 Regional geology

The Manus Basin lies in the eastern Bismarck Sea and is a rapidly opening back-arc basin created by the northward subduction of the Solomon Sea plate at the New Britain Trench (Taylor, 1979; Taylor et al., 1994; Martinez and Taylor, 1996, 2003). The active Bismarck Sea seismic lineation (BSSL) divides the North and South Bismarck Plates. The BSSL is defined by spreading segments and left-lateral transform faults. Rapid clockwise rotation (~ 8° Ma^{-1}) of the South Bismarck Plate (Tregoning et al., 1999) results in an asymmetric spreading of the North and South Bismarck Plate, which causes an eastward propagation of the BSSL.

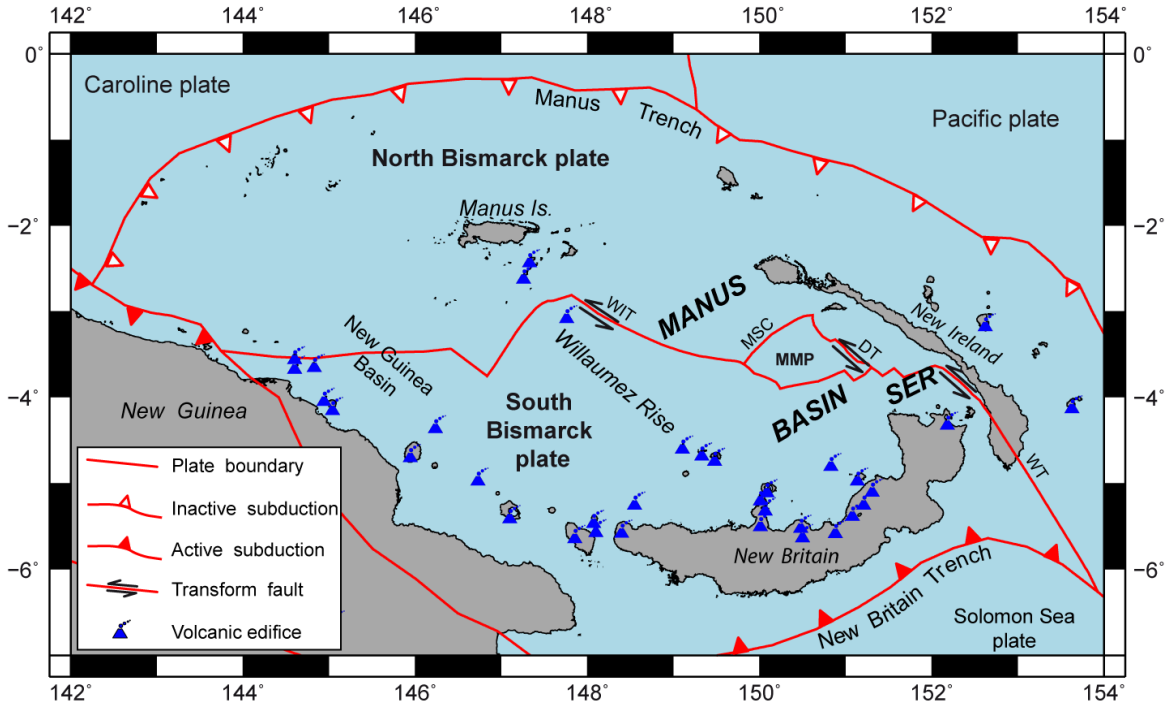

Figure 3.1: Tectonic setting of the Bismarck Sea. Plate boundaries from (Bird, 2003). WIT: Willaumez Transform; MSC: Manus Spreading Center; MMP: Manus Microplate; DT: Djaul Transform; WT: Weitin Transform.

In the central Manus basin, MORB-like lava at the Manus Spreading Center (MSC, Fig. 3.1) indicates true seafloor spreading. In contrast, remnant mid-Cenozoic island arc crust (Coleman and Packham, 1976; Falvey and Pritchard, 1982; Kroenke and Rodda,

1984) is rifted in the eastern part of the basin creating a series of sigmoidal neovolcanic ridges (the South East Ridges; SER) and solitary volcanoes with lava compositions ranging from basalt to rhyodacite (Binns and Scott, 1993). The SER are an E-W oriented ~70km long volcanic zone situated at the easternmost tip of the BSSL and, due to the asymmetric spreading, exhibit the highest spreading rates in the Manus basin (up to 137.5 mm*a-1; (Tregoning et al., 1999; Tregoning, 2002).

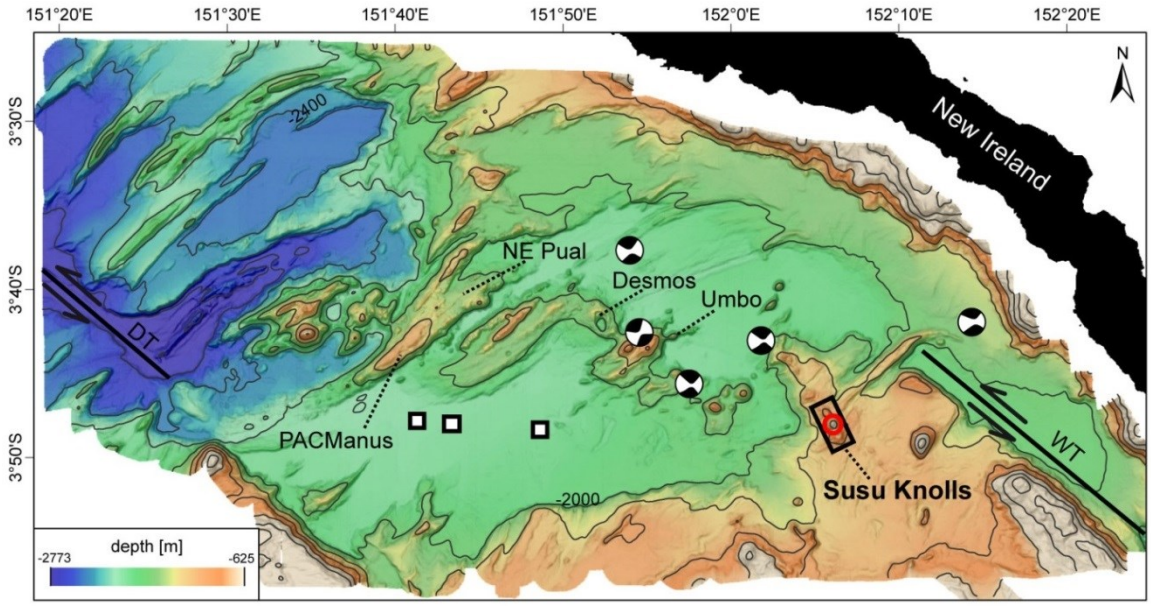

Figure 3.2: Bathymetry of the South East Ridges (SER) in the eastern Manus Basin from research cruise BAMBUS SO-216 (2011) with 200 m contours. Beachballs originate from the global cmt project (Dziewonski et al., 1981; Ekström et al., 2012) and mark the locations of earthquakes between 2006 & 2011 with a magnitude >5. The movement depicted by beachballs represents the stepwise intra-transform, extensional stress regime. Black squares: Bathymetry benchmark tests areas. DT: Djaul Transform; WT: Weitin Transform. Red circle: North Su.

Two left-lateral transform faults (Djaul and Weitin, Fig. 3.1 and 3.2) border the SER (Martinez and Taylor, 1996) and create an intra-transform state that produces the stepwise en-echelon alignment of volcanic ridges and seamounts.

Several hydrothermal vent areas, such as PACManus, Desmos and SuSu Knolls have been discovered at the SER (Binns and Scott, 1993; Auzende et al., 1996, 2000; Gamo et al., 1997; Hashimoto et al., 1999; Tivey et al., 2006; Bach et al., 2011). The accumulation of polymetallic sulfides in these areas has been considered a modern analog of ancient Volcanic Massive Sulfide (VMS) deposits mined on land (e.g. Binns and Scott, 1993; Petersen et al., 2003; Yeats et al., 2008).

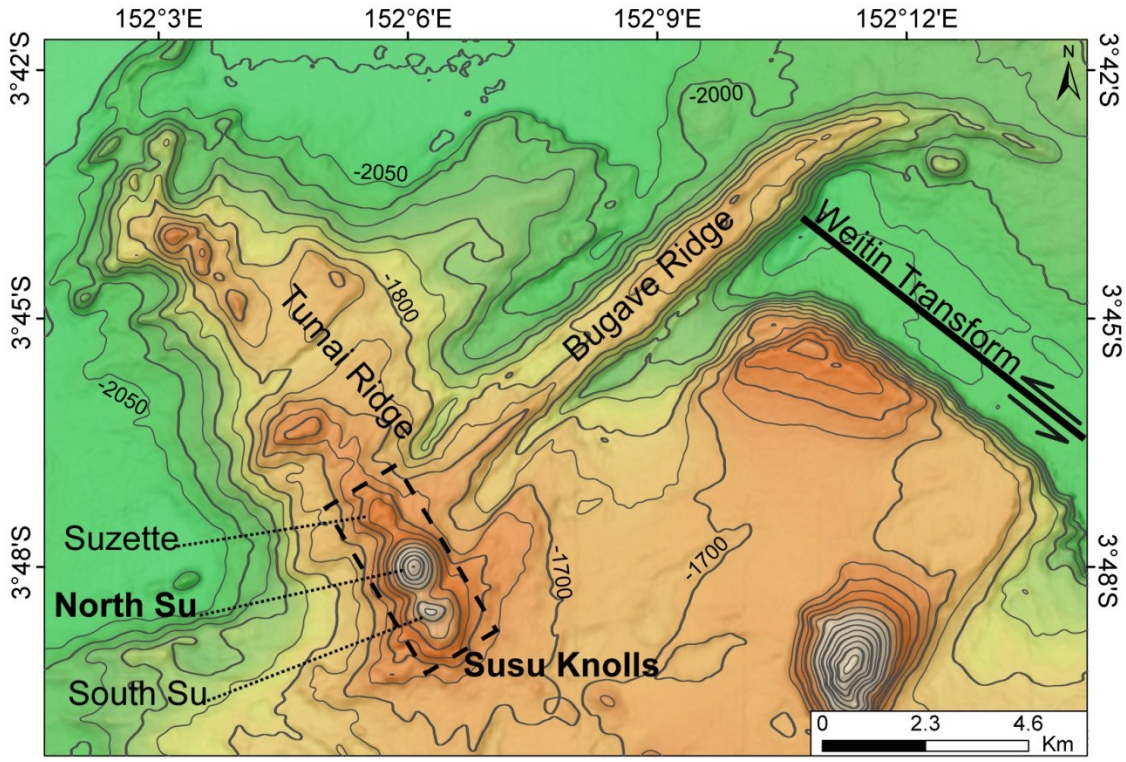

Figure 3.3: Ship-based bathymetry of SuSu Knolls with regional structures. Thick contours: 100 m, thin contours: 50 m. Estimated position of Weitin Transform.

The Susu Knolls area comprises three volcanic edifices (South Su, North Su and Suzette, Fig. 3.3) situated on the NNW striking Tumai Ridge (Moss and Scott, 2001). Hydrothermal venting there was discovered via video sled and dredge surveys during the 1996 PACMANUS III expedition (Binns et al., 1997). Suzette and North Su lie at the intersection of the NE-trending extensional rift structure (Bugave Ridge) that overshoots the Weitin transform. Both ridges comprise lavas with compositions ranging from basaltic to dacitic (Binns and Scott, 1993; Moss, 2000). Suzette is the northernmost edifice of SuSu Knolls and is now subject to commercial interest through Nautilus Minerals Inc. (Solwara-1 prospect). North Su, the central edifice of SuSu Knolls, is a conical-shaped volcanic edifice rising from 1600 m to 1154 m water depth with slopes ranging from 25° to 30° (Fig. 3.6). The seafloor to the NE and SW of North Su is most likely a graben (Fig. 3.3).

3.4 Methods

High-resolution AUV ABE and ROV MARUM Quest bathymetry complemented ship-based multibeam bathymetry along with ROV dives that collected rock as well as fluid samples during two research cruises. A total of three AUV ABE dives (194, 195, 198) and 8 ROV-Jason-2 dives (217, 219, 221, 223-227) focused on the SuSu Knolls area

during RV Melville cruise Magellan-06 in July/August of 2006. Part of ABE dive 194 and three ROV-Jason-2 dives (221, 223, 227) focused on the summit area of North Su.

In June/July of 2011, a follow-up cruise with RV Sonne (SO-216) used the ROV MARUM Quest to record additional seafloor video images and collected samples of fluids, rocks and biota. A total of 12 ROV MARUM Quest dives (296-304, 313, 314, 316) in the summit area of North Su completed the comprehensive dataset. The large number of dives in a fairly small area (~500 m x ~280 m) enabled us to convert regular ROV depth information into a bathymetric map with 10-m grid cell size (Fig. 3.4).

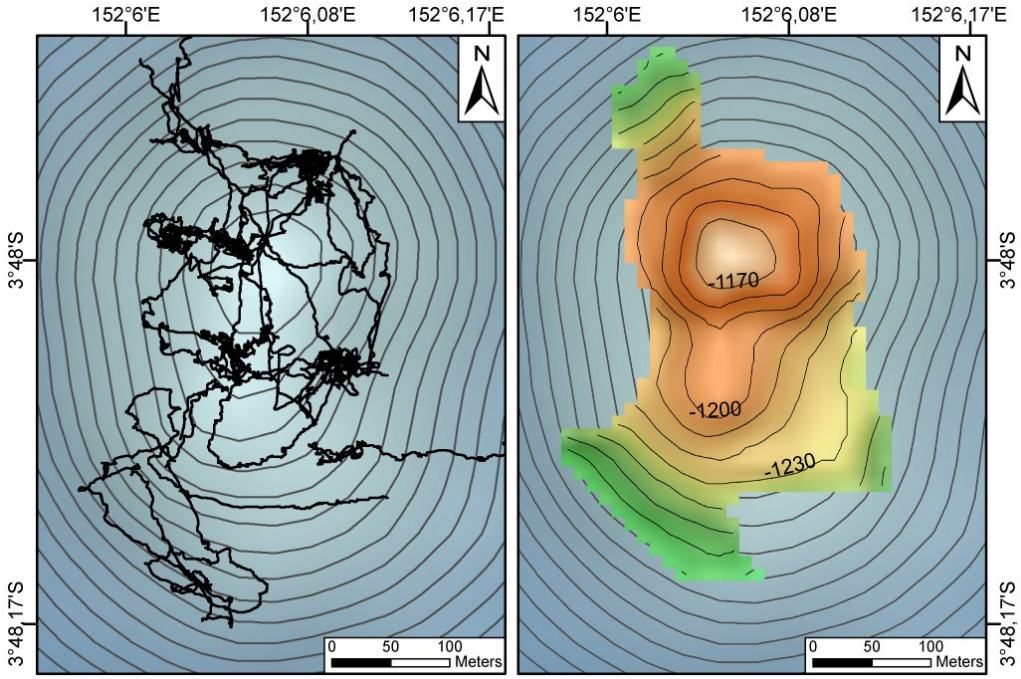

Figure 3.4: ROV Quest track based map and data coverage with SO-216 (2011) ship-based bathymetry background (contours every 10 m). Left: ROV Quest dive tracks; Right: final bathymetric map based on ROV Quest depth data with 10 m grid spacing.

In 2006, AUV ABE carried a 200 kHz Simrad multibeam sonar and typically operated at an altitude of 50 m with a line spacing of 50 m producing a high-resolution bathymetry basemap (Fig. 3.6 and 3.7). A long baseline (LBL) transponder network enabled navigation tracks with <10 m resolution. A 1-meter grid cell map was produced after the raw sonar pings were corrected for the attitude of the vehicle (pitch, roll, and heading) and merged with the navigation. The LBL transponder network also provided a precise navigation for ROV Jason-2 together with a high-data rate (1 Hz) Doppler Velocity Log (DVL) estimate of position. The accuracy of the ROV Jason-2 position is generally <10 m, though the DVL navigation had to be reset during all dives resulting in a few >10 m offsets. Ultra-Short-Baseline Posidonia positioning system, used to navigate

the ROV MARUM Quest during cruise SO-216, had no offsets at all with accuracy of <10 m.

Mineral phases and glass chemistry (appendix, table 3.A2) reported in this paper were determined using a JXA 8900 R Electron Probe Microanalyzer at the Christian-Albrechts-Universität zu Kiel and at the University Bremen using a Cameca SX6000 Electron Probe Microanalyzer. Whole rock powder diffraction analyses (appendix, table 3.A1) were conducted using a PW1800 x-ray diffractometer at the University Bremen.

All ship-based multibeam datasets were cleaned, processed and gridded with the same parameters by the same editor to enhance comparability. We used the workflow suggested in the MB-System man pages (http://www.ldeo.columbia.edu/res/pi/MB-System/html/mbsystem.html). GMT (Generic Mapping Tools, Wessel and Smith, 1991) and ESRI GIS suite were used to manage and visualize the data.

Month/Year	**Cruise ID**	**Sonar System**	**Research Vessel**	**Chief Scientist**
Sept. – October / 2002	So166 – Condrill	EM 120	R/V Sonne	Peter M. Herzig
June – July / 2011	So216 - BAMBUS	EM 120	R/V Sonne	Wolfgang Bach

Table 3.1: Ship-based bathymetry used in this study.

To estimate the volume and extent of morphological changes on North Su due to the eruption, we calculated the depth differences from two ship-based bathymetry surveys with R/V Sonne from 2002 and 2011 (table 3.1). The ship-based bathymetry from 2006 was rejected due to low data quality resulting in depth changes where ROV observations proved that no changes occurred. To assess the noise level of both surveys we chose three benchmark areas (black squares in Fig. 3.2) of flat seafloor away from volcanic ridges or graben structures. We assume that no major topographic changes have occurred between 2002 and 2011 in the benchmark areas. All areas have reasonable data coverage for the bathymetry surveys of both cruises and both datasets have the same lateral extension and resolution as used for the North Su area. The seafloor depth differences for both cruises in all three benchmark areas scatter around +- 5 m with a few outliers that do not exceed values of +-10 m. The typical value used to describe the noise level of comparisons of different aged bathymetry is about +- 10 m (Chadwick Jr. et al., 2008; Clague et al., 2011), which corresponds to our estimated noise level from benchmarks. We used a grid spacing of 20 m, corresponding to the resolution threshold of the sonar system. Together with very steep slopes of North Su we assume that the noise level is even higher as

derived from benchmarks. Therefore, we calculated the area and volume for depth differences in the range of 1) < -10 m and > 10 m (Fig. 3.9a) and in a more conservative approach 2) for values > 20 m (Fig. 3.9b).

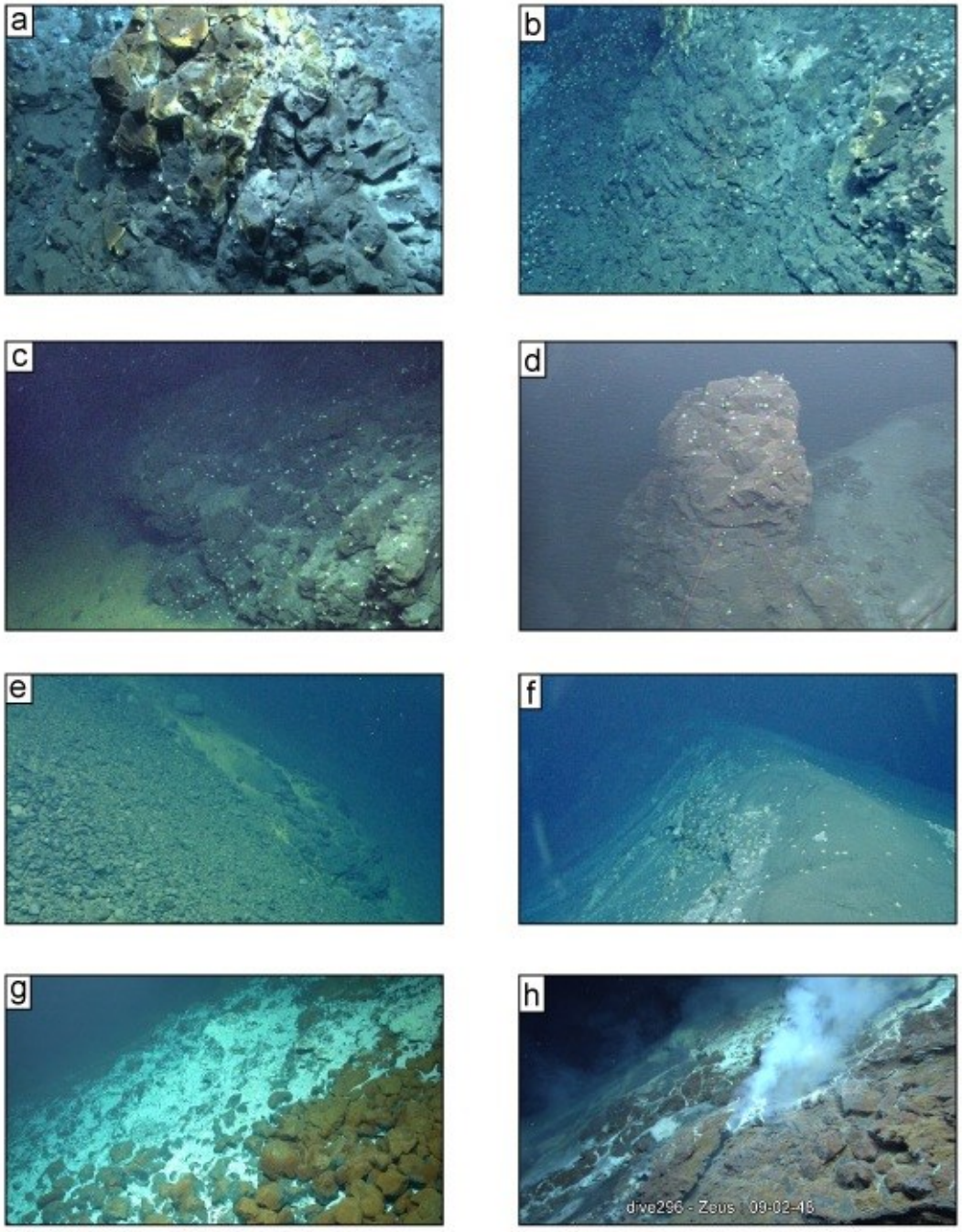

Figure 3.5: Observed volcanic morphologies, lithologies and hydrothermal features. Picture width of structures in the foreground are given in brackets. a) Fissured outcrop. The broken pieces are still in place, NE North Peak (~1 m); b) Downward looking perspective on a vertical lava outcrop, fissured and blocky, NE North Peak (~ 3 m); c) Short (< 5m), columnar, fractured lava flow, SW South Peak (2-3 m); d) Lava spine, North Peak (~2 m); e) Lava lobe breaching through the scree covered slope, SW South Peak (2-3 m); f) View towards NE along the crater rim of South Crater in 2011. The crater center is to the left (~1 m); g) Hydrothermal fluids discharge with abundant native sulfur that starts to bury scree, S South Peak (~1.5 m); h) Hydrothermal cemented crust with hybrid vents, vent#5, NW North Peak (~ 1 m)

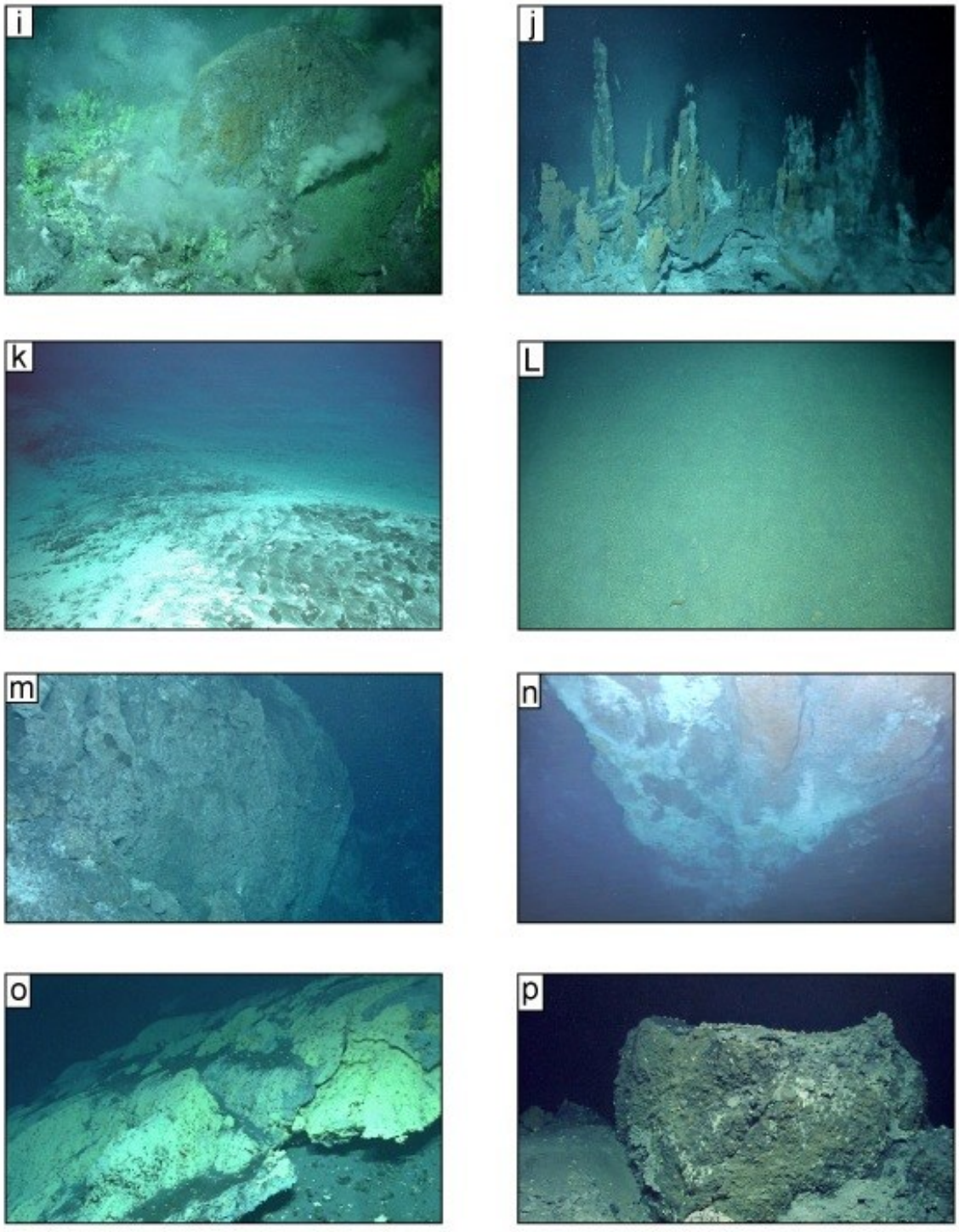

Figure 3.5 (continued): i) Sulfur chimneys and white smoker at Sulfur Candle, vent #7 (~1.5 m); j) Black smoker chimneys, vent #1, North Peak (~2 m); k) Plateau on South Peak with stream ripples (~1.5 m); L) Fine volcaniclastics on South Peak (~1.5 m); m) Cliff of cemented fine volcaniclastics, SW North Peak (~2 m); n) Downward looking perspective of the southern cliff (~14 m high) on North Peak summit (~1.5 m); o) Solidified native sulfur flows, SE of South Crater (~1.5 m); p) Pillar with broken top, built-up by volcaniclastics with native sulfur oozed out of the sites and ontop, next to Sulfur Candle (~ 1.5 m).

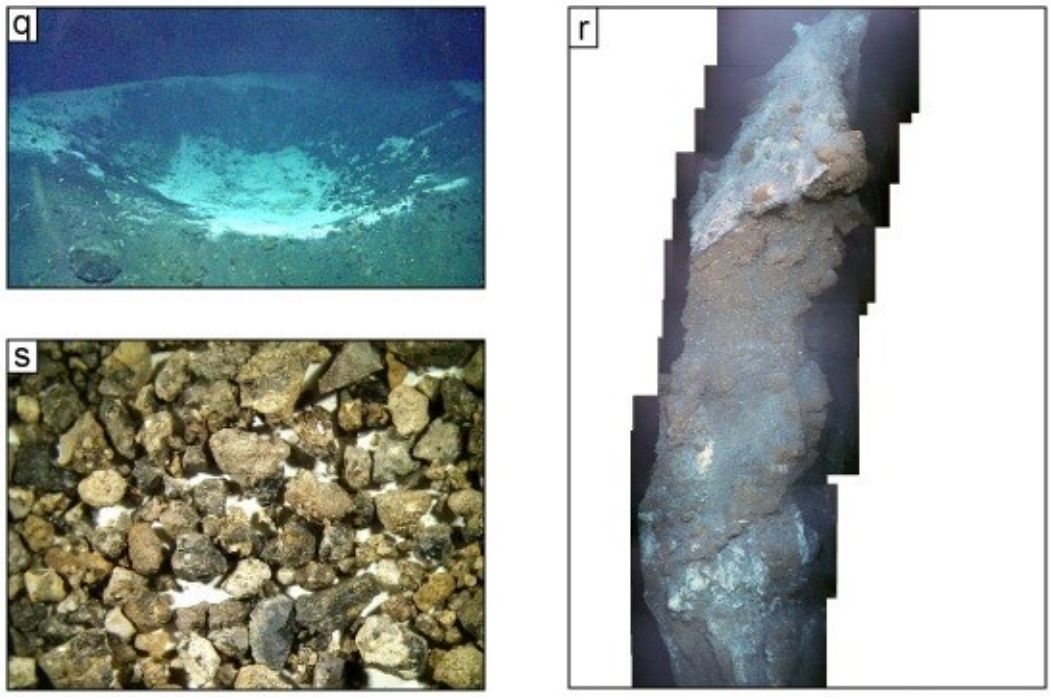

Figure 3.5 (continued): q) A crater of Crater Group on South Peak. The crater diameter is about 4-5 m and <1 m deep; r) 16 m high pillar structure. The lower half is connected to the slope, the top half is free standing, E North Peak; s) Heterolithic clasts that dominate South Peak summit. Sample SO-216-51-ROV-10 (~ 1cm).

Footage from several cameras was used to provide different perspectives of seafloor structures to generate geological maps. ROV Jason-2 carried three video cameras; a pilot camera and a science camera; one fixed camera and two pan and tilt cameras. A similar configuration was set up on ROV MARUM Quest, but with a 14x zoom HD science camera that markedly improved the mapping abilities with the video data. A laser scale device mounted on the ROVs enabled dimensional measurement of seafloor features.

Examples of seafloor structures mapped in this study are portrayed in Figure 3.5. Lithologic terms used in this study are mainly descriptive and we tried to avoid terms with genetic connotations. We refrain from using the term “hyaloclastites” as “hyalo” is Greek for glassy, and clastic material at North Su comprises only minor glass particles. Therefore, we hereinafter use the term “volcaniclastics” to describe fragmental material that appears to have been ejected from the volcano. We mapped all coherent volcanic bodies as volcanic outcrops (e.g. Fig. 3.5 a, b, c, d).

3.5 Results

3.5.1 Volcanic morphology and hydrothermal activity in 2006

North Su volcano rises about 450 m above the surrounding seafloor and its shape in ship-based bathymetry reflects a conical edifice (Fig. 3.6b). AUV micro-bathymetry (Fig. 3.6a) reveals a more complex structure, especially in the summit area as described below.

The mean slope calculated from ship-based bathymetry of the entire volcanic edifice of North Su is between 25° and 30° (Fig. 3.6b). This is consistent with ABE bathymetry below 1350 m. The morphology above 1350 m water depth is more complex and in many places the slope exceeds 30°, including vertical cliffs near the summit. The focus of both research cruises, Magellan-06 and SO-216 was finding and sampling hydrothermal vents, which appear in the topmost ~140 m of the volcano. Therefore, geologic mapping of North Su is limited to the summit area and the uppermost slopes.

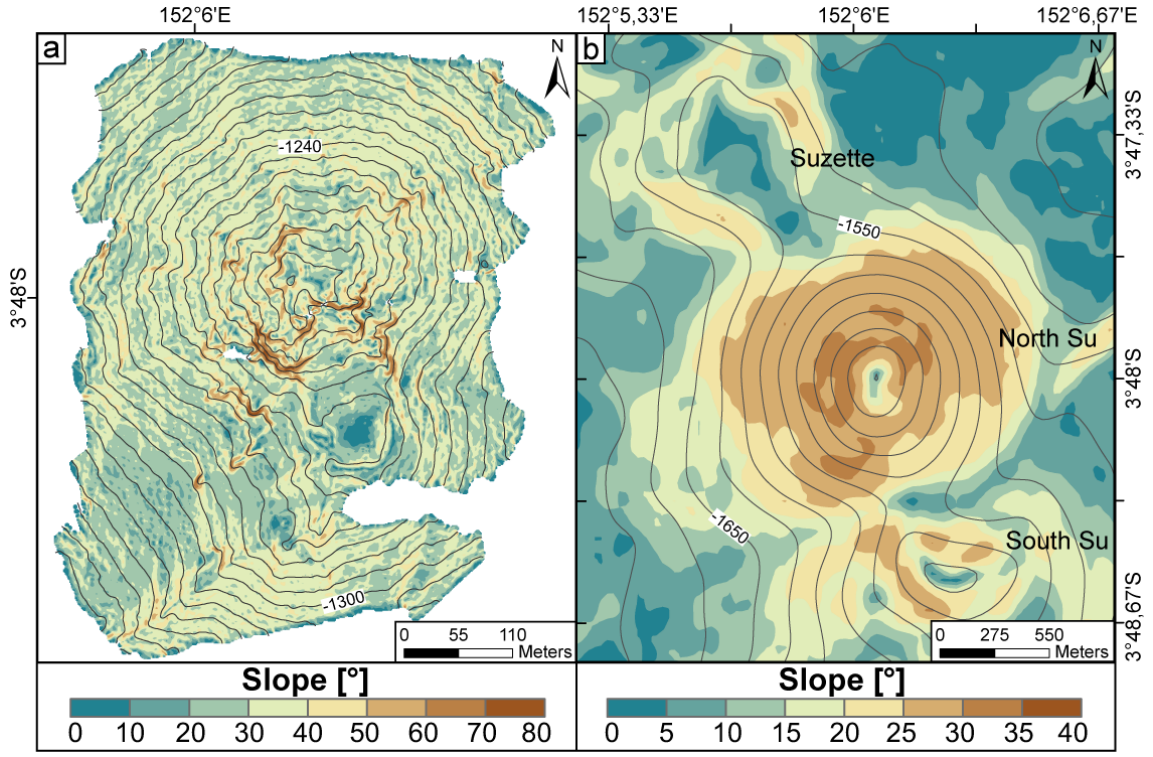

Figure 3.6: SuSu Knolls morphology. a) 2006 – Slopemap of North Su with South Crater. It illustrates the cluster of cliffs on the southern slope of North Peak. AUV ABE 1 m grid; b) 2011 - Slopemap of SuSu Knolls revealing the mean slope on North Su to be 25-30° with steeper slope around the summit areas. Filtered ship-based bathymetry, 32 m grid.

The AUV bathymetry (Fig. 3.6a and 3.7a) revealed that the summit of North Su is double-peaked with a northern peak, reaching 1154 mbsl and representing the main summit, and a southern peak, reaching 1225 mbsl and resembling a crater rim. Therefore, the two structures are herein after referred to as North Peak and South Crater. North peak

has a crescent-shaped crest, which may be a remnant crater rim with a collapsed southern part. The crescent-shaped crest hosts active black smoker vent sites (#1 and #2, Fig. 3.7a) with temperatures up to 302°C. Active chimneys are limited to the N-S trending western site of the crest. At field #1, the chimneys are located on top of a broad convex shield that appears to be a sulfide-cemented flange that has warm fluid (Tmax. 68°C) leaking out from under it. Field #2 is a cluster of chimneys (up to 11 m high) with beehives and multiple orifices. A few inactive chimneys were mapped between fields #1 and #2. Diffuse venting could be observed along the crest indicated by issuing of shimmering water from the seafloor. Besides the sulphide chimneys, the seafloor of North Peak is covered by unconsolidated fine volcaniclastics and scattered >10 cm small clasts, The fine volcaniclastics are a mixture of highly to non-altered volcanic rocks and fractured crystals with a dominant grain size of 1 - 5 mm. In places the volcaniclastics are cemented by hydrothermal barite-sphalerite cement to form slabs. Pyrite and other hydrothermal precipitates occur as well.

No quenched glass shards or pumice fragments were found. No outcrop of effusive volcanic rock exists on the North Peak crest. Below the crest on the western slope at 1220m water depth, vent site #3 is located in a very steep terrain, consisting of volcaniclastic material that forms near-vertical cliffs and pillars. Black-smoker fluids emit through the steep walls with temperatures up to 325°C, and show visual evidence (pulse-like fluid discharge and flashing at the vent orifices) of phase separation. Below the crest to the northeast a vertical volcanic spine (Fig. 3.5 d) breaches through a ridgeline, which is covered by a volcaniclastic deposit.

More volcanic outcrops are present on the ridge-line down from vent site #3, towards vent site #4. These outcrops (e.g. Fig. 3.5 a, b) expose strongly fissured, stubby and blocky lava. The seafloor surrounding the outcrops is covered by sharp-edged, blocky scree. Samples of these outcrops are highly plagioclase-olivine phyric rocks with andesitic bulk composition. At the northeastern slope of North Peak a diffuse vent site (#4, Tmax: 32°C) with macro fauna is developed around the volcanic outcrops with the clear fluids seeping through scree and alongside the more massive outcrops. Some fluids also seem to emit directly from these outcrops, issuing through fissures in the lava. Volcanic outcrops on North Peak are limited to the northeastern slope and one small outcrop at vent site #5. Grey fluids with temperatures <240 °C vented through a

hydrothermal cemented ledge of altered volcanic clasts. The slope between vent site #5 and field #4 is mainly covered by scree and fine volcaniclastics.

Another ridge line stretches north of black smoker field #1 (Fig. 3.7a) downslope towards vent site #5 but does not expose any volcanic rocks. Instead, erosional gullies have excavated the ridge lines interior that is made up of volcaniclastics, similar to the cliffs at vent site #3, but with native sulfur flanges protruding from these walls. This type of lithology of (ridge lines, pillars or cliffs) is typical for the west, south and southeast slopes of North Peak. The seafloor around these protruding structures is covered by loose scree and fine volcaniclastics. The faces of the ridges and cliffs often show signs of hydrothermal activity in the form of white staining, void-fills of native sulfur, and/or bacterial mats. On the eastern slope, another ridgeline is visible on the ABE bathymetry (Fig. 3.7a), with pillars (Fig. 3.5, p and r) that are up to 16 m high and also consist of poorly sorted volcaniclastics.

The southern slope of North Peak, where the crest at vent site #2 terminates into a 14-m high cliff (Fig. 3.5 n) of cemented volcaniclastics is a spectacular example of this type of outcrop. From the base of this cliff the gentlest slope (25°) of North Peak (Fig. 3.7a) extends downslope into South Crater. It is covered with fine volcaniclastics and some lose scree. The slope is bordered to both sides by cliffs or pillars (<1 – 14 m high) of cemented volcaniclastics. On the ridge bordering the gentle slope to the east, white smoker vents have been mapped but not sampled. Another site with white smoker vents (#7) is situated on the slope itself with maximum venting temperature of 71°C.

The east slope is dominated by steep but continuous ridges made up of angular, volcanic blocks (several cm to dm diameter) covered by fine volcaniclastic material. The size and jigsaw fit of blocks indicate an in-situ brecciation of lava flows.

South Crater has a diameter of ~80 m with a max. depth of 13 m and a rim that terminates into the south slope of North Peak. The crater rim was visited only once in 2006 on dive 227, which observed loose, fine volcaniclastics with thin broken crusts and widespread occurrence of white bacterial mats.

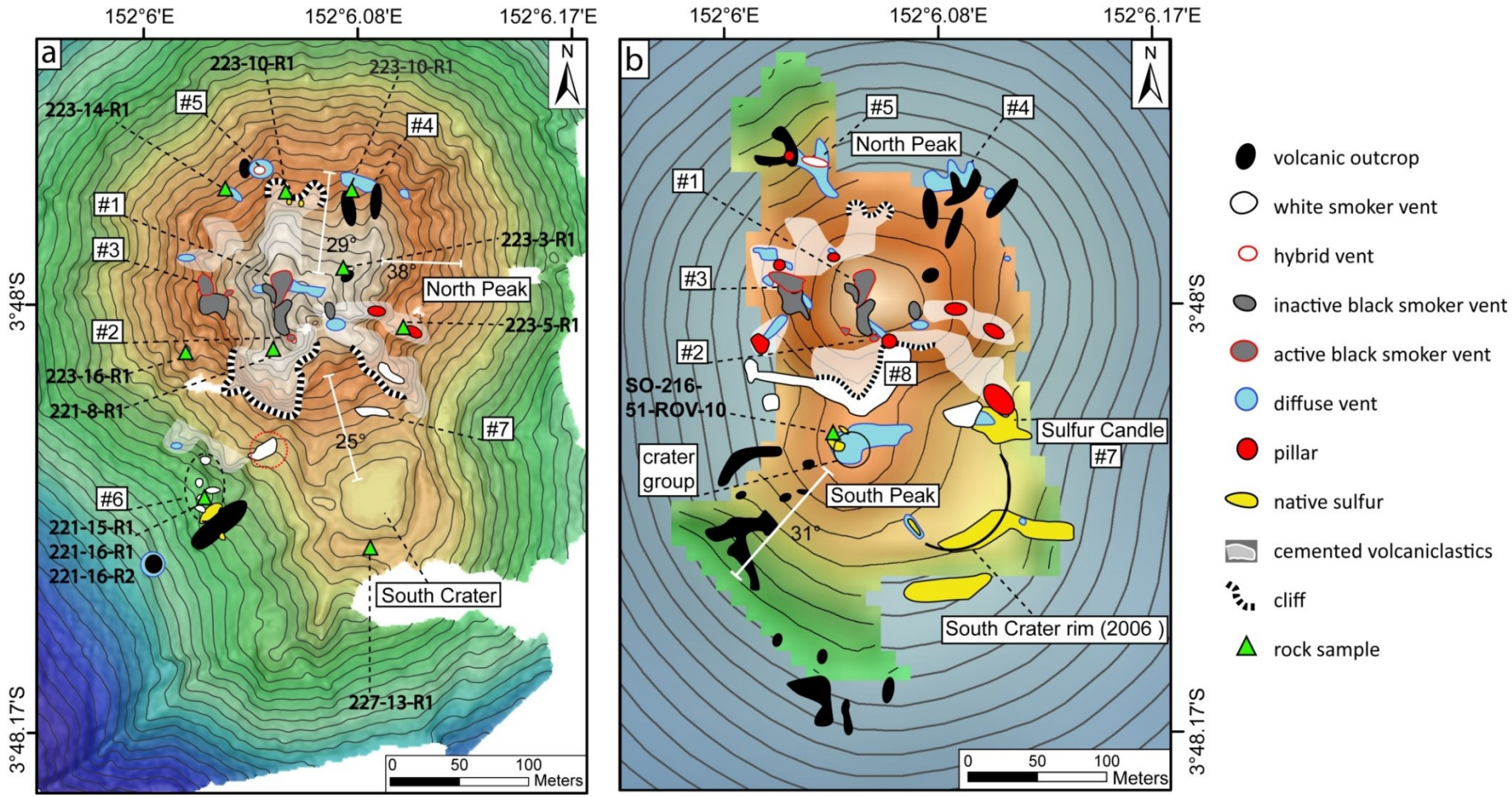

Figure 3.7: a) Geologic map from 2006 on ABE bathymetry (1 m grid spacing) with 5 m contours; dotted red circle indicates the location of the crater group mapped in 2011. b) Geologic map from 2011 on ROV Quest bathymetry (10 m grid spacing) and EM120 bathymetry in the background (32 m grid spacing) with 10 m contours. White bars mark the track for which a mean slope is calculated that is posted next to the bar

Downslope to the west of South Crater several white smoker vents were discovered. A cluster is marked as field #6 where fluids discharge through the scree-covered slope. The fluids were exceptionally acidic, ranging to pH-values as low as 0.87 (Seewald et al., 2014). Fluid temperatures of up to 284°C were measured, but the most acidic fluid was 220°C. When we retracted the T-probe after sticking it into the scree next to the vent site, it was covered with native sulfur, indicating that the scree-covered slope around the vents is saturated with liquid sulfur. A massive NNE-trending volcanic outcrop featured remarkable flanges of native sulfur that appeared to have oozed out of the massive rock. The western slopes of South Crater were generally covered with fine volcaniclastics and littered with clasts up to several 10's of cm in diameter. The south and east slopes of South Crater were not investigated in 2006.

3.5.2 Volcanic morphology and hydrothermal activity in 2011

A new volcanic cone has been emplaced between 2006 and 2011 that covers most of South Crater and its western slope. The eruption buried white smoker vent site #6 but also new white smoker vent sites were discovered. These new vent sites are located along the boundary of North Peak and the new cone (Fig. 3.7b).

Overall, the survey of North Peak its northern, western and eastern slopes in 2011 showed the same lithology and morphology as mapped in 2006. Because high resolution AUV bathymetry was not conducted in 2011, a detailed, area-wide comparison of changes in seafloor morphology was not straightforward. Only areas covered by ROV observation can be compared against the seafloor topography five years earlier.

As shown in the map of 2011 (Fig. 3.7b) the areal extent of some lithologies are better constrained and some new structures were mapped. Slight differences between the contours of mapped lithologies (Fig. 3.7a, b) are also caused by small uncertainties in ROV navigation and the fact that no renewed, up-to-date AUV bathymetry existed for 2011. Additionally, ROV MARUM Quest4000 depth values were consistent with 2006 ROV Jason-2 data as well as with the AUV ABE bathymetry from 2006. The hydrothermal activity in the North Peak summit area apparently had not changed between 2006 and 2011. The location of the chimney fields, the vigor of venting, and the temperature of the black smoker fluids remained constant as did the common occurrence of diffuse venting through sediments around the black smoker chimneys. Likewise venting of boiling fluids on the western slope was observed in both years.

The area of South Crater changed dramatically between 2006 and 2011. A new volcanic cone has built up, consisting of volcaniclastic material and lava (Fig. 3.5 c, e, g, k, l, q, s) with its crest ~50 m west of South Crater center in 2006. We will refer to this structure as South Peak hereinafter. The white smoker vent site #6 of the 2006 survey was buried under > 50 m of volcanic material, as documented by ROV investigations during cruise SO-216 in 2011.

The southern edge of the North Peak crest is defined by a steep wall that was present in 2006. It is marked in Fig. 3.7 as a cliff (Fig. 3.5 n) and 2011 video observations revealed no major morphologic changes, although the abundance of hydrothermal staining and putative microbial mats had increased. No black smoker vents were observed south of that >14 m high structure. The seafloor below this cliff was scattered with scree and fine volcaniclastics, and hosts a huge white smoker vent site (#8) that extends towards west along the boundary of North and South Peak. This extensive white smoker field did not exist in 2006 though scattered white smoker activity was observed in the area (vent #6) in 2006 that are now covered by South Peak volcanics. Very poor visibility inside the white smoker fields limited the video mapping abilities, but zones of extensive altered rocks could be identified.

Another new white smoker field was discovered in 2011 and named Sulfur Candles (#8, Fig. 3.5 i; Fig. 3.7 b). Eponymous are copious amounts of sulfur that formed small chimneys or accumulated in m-sized knolls. Release of bubbles of liquid CO_2 was common and CO_2-clathrate formation could be confirmed visually in an improvised bubble-catching device. The white smoker hydrothermal activity was highly variable within the two weeks of survey work in 2011. For instance, a white smoker chimney situated in between North and South Peak in the easternmost part of white smoker field #8 was nearly inactive during one dive and, 12 days later, vigorous vented white smoker fluids (Fig. 3.8). Similar changes were observed at the Sulfur Candle site, where vigorous boiling sulfur was discharged on the seafloor during dive 302 on 26.06.2011 compared to a much subdued activity 14 days later, when visual observations were made difficult, however, by intense ground-hugging white and yellow turbidity clouds. These fluctuations in activity are not expressed in the entire North Su hydrothermal area. Much rather, they appear to reflect shifts in the locations of vigorous discharge.

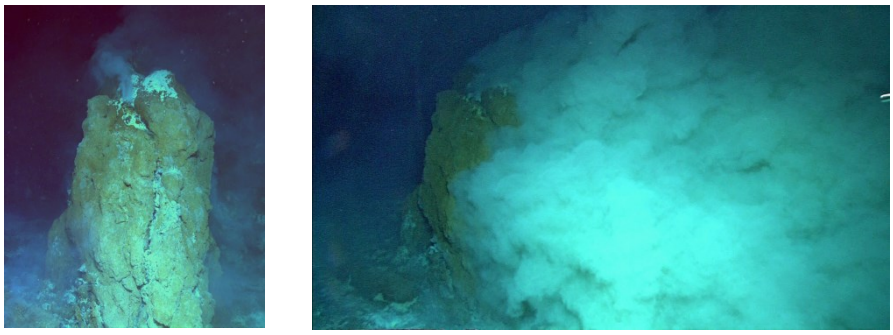

Figure 3.8: Left: White smoker chimney on 27.06.2011; Right: The same chimney 12 days later on 09.07.2011 illustrating the pulsating nature of the white smoker hydrothermal system.

Sulfur Candle is bordered to the east by a ridge line that already existed in 2006. Further inspections in 2011 confirmed a complete buildup of volcaniclastics with pillar structures (Fig. 3.5 p) in absence of coherent volcanic outcrops. The clasts are 1 mm to several cm's in diameter and blocky. Flanges of solidified native sulfur appear to have oozed between the clasts, similar to what was observed on the north slope of North Peak.

At the southern edge of Sulfur Candle, the rim of South Peak crater has the same morphology as was observed in 2006 (Fig. 3.7 b). The rim is covered by fine volcaniclastics, but in some areas the rim is broken and the interior shows abundant native sulfur deposits and volcanic clasts up to several cm in size (Fig. 3.5 f). Following the crater rim to the south, more and more native sulfur flows appear on the outside rim and stick out of the slope (Fig. 3.5 o). In some parts the flow structures of the sulfur flows are still preserved. The eastern and southern slopes below the sulfur flows are littered with scree of broken sulfur slabs as well as fresh and altered volcanic rocks.

South Crater was filled by the eruption of South Peak that emerges to the west. The slopes of South Peak expose predominantly unconsolidated, variably blocky clasts up to several 10's of cm in diameter (Fig. 3.5 e, g). The upper 20 m of the new cone are dominated by sand- and granule-sized volcaniclastics (Fig. 3.5 k, l, q) with less pebbles- and cobble-sized clasts. Only occasional blocky volcanic clasts are up to several tens of centimeters in diameter.

On the west and southwest slopes below the uppermost 20 m of South Peak, fresh volcanic rocks occasionally crop out of the mainly scree-covered slope. Outcrops are blocky, stubby, fissured and (Fig. 3.5 c) similar to outcrops on the northeastern slope of North Peak. Only one lava lobe with a rounded surface was found that slightly breached through the scree covered slope (Fig. 3.5 e). White staining occurs mainly on the southwestern slope, whereas the western slope is almost entirely covered by an

unidentified orange coating, likely Fe oxyhydroxide. Two zones of diffuse fluid discharge, elongated in shape and oriented radial to the center of South Peak crest were observed, and the larger one is included in the map in Figure 3.7 b. The hydrothermal fluids deposit native sulfur and other unidentified phases between the loose rocks that are buried by these precipitates in places.

The morphology of the South Peak crest can be divided into two zones: a plateau (Fig. 3.5 k) and a crater group (Fig. 3.5 q). The location of the crater group on South Peak is also indicated in Figure 3.7a with a red dotted circle. The part of the South Peak crest that is connected to North Peak is a smooth plateau littered with a clasts dominantly <1 cm in diameter (Fig. 3.5 s). The seafloor shows surficial white staining with ripple textures created by currents and occasional native sulfur crusts. Area-wide diffuse seepage of shimmering water was identified.

The area at the edge of the crest features several small (max. 10 m in diameter) and shallow (<3 m) craters (Fig 6 q). The seafloor around the craters is littered with unsorted clasts of variable sizes. The dominant clast size is <10 cm, but outsized blocks in the range of 10's of cm were observed. Diffuse venting of clear fluids was noticeable, with native sulfur crusts at some crater rims.

In the southwestern corner of Figure 3.7a is a NE striking ridge that was not visited in 2006 but clearly imaged by ABE bathymetry. In 2011, the presence of that ridge was visually confirmed by an ROV Quest dive, during which outcrops of massive volcanic rock were observed. The ROV-based bathymetry was identical to the AUV bathymetry from 2006, suggesting that the emplacement of the lava forming this ridge took place before 2006. The area north of the ridge, however, was filled with material from the South Peak eruption.

3.5.3 Morphology changes between 2002 and 2011

We compared ship-based bathymetry datasets from two RV Sonne cruises in 2001 and 2011 (table 3.1) to track the volcanic evolution of North Su and support our ROV observations. Further we used the depth differences between the datasets to measure the volume of erupted material.

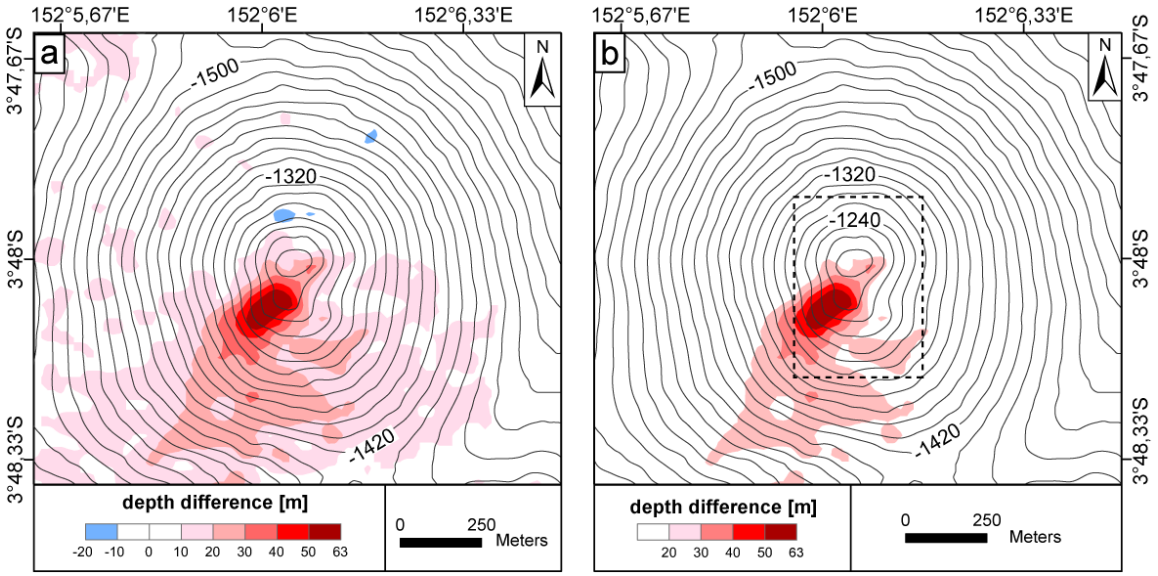

Figure 3.9: Results from SO-166 (2002) and SO-216 (2011) ship-based bathymetry comparison. Contours are from SO-216 bathymetry with interval of 20 m. Red color indicates positive depth changes and blue indicates negative. a) Depth differences > 10 m b) Depth differences >20 m. Dotted rectangle indicates extend of maps in Figure 3.7

The distribution of depth differences at North Su are displayed in Figure 3.9. If we use +/-10 m cut-off (Fig. 3.9 a), the total area of positive changes is $7.2*10^5$ m^2 with a total volume of $12.6*10^6$ m^3. However, this cut-off yields small negative changes on the northern slope of $6*10^3$ m^2 with a volume of $-7.2*10^4$ m^3. ROV depth information from 2006 and 2011 for one area of such with negative changes did not confirm these differences. This and the patchy distribution of values within +/- 20 m substantiate our assumption that only changes computed to be >20 m represent robust results.

Therefore, we use a +/-20 m cut-off that results in positive depth changes only with a calculated volume of $5.8*10^6$ m^3 that cover an area of $2.1*10^5$ m^2. The maximum depth change due to the eruption is +63 m.

The volcanic evolution of North Su with the growth of South Peak is well illustrated by the oblique views in Figure 3.10. Our analyses suggest that the total erupted volume of South Peak is at least $6*10^6$ m^3. The total volume of North Su volcano is $265*10^6$ m^3, assuming the geometry of an ideal cone with a radius of 750 m at its base and a height of 450 m. It would require on the order of 44 South Peak eruptions to build up North Su volcano.

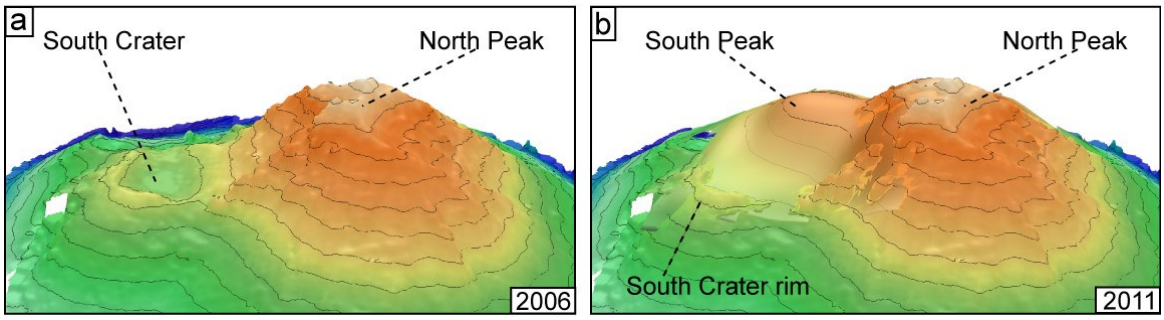

Figure 3.10: Oblique perspectives on North Su from NE. a) AUV ABE bathymetry showing North Peak and South Crater in 2006; b) Same perspective view as (a) with additional ROV Quest bathymetry (2011) depicting the growth of South Peak.

3.5.4 Rock samples

Whole rock analyses by XRF (appendix, Table 3.A1; sample positions in Fig. 3.7) from North Su revealed that rocks plot in the andesite field within the TAS with SiO_2 contents ranging between 59 – 64 wt.%. The texture is porphyritic with phenocrysts of clinopyroxene, orthopyroxene, Ca-rich plagioclase, olivine and Fe-Ti oxides in a dacitic to rhyolitic matrix. The SiO_2 content of glass varies between 68 – 73 wt.% SiO_2.

3.5.5 Products of the South Peak eruption between 2006 and 2011

Sample SO-216-51-ROV-10 (Fig. 3.5 s) originates from the summit area of South Peak and has been taken with a shovel that can be closed after sampling. The sample revealed a heterolithic composition of the fine volcaniclastic material. It consists of clasts that are variably rounded with minor proportions of blocky ones. The clasts are variably altered, ranging from fresh glassy fragments and crystals to advanced argillic alteration and including minor hydrothermal precipitates (gypsum, pyrite, sulfur). Phenocryst fragments comprise clino- and orthopyroxene, plagioclase, olivine, and Fe-Ti oxides. The non-altered volcanic clasts show the same chemical composition as other rock samples from North Su. The majority of clasts are between 0.25 - 5 mm in size. Glass shards with compositions between dacitic to rhyodacitic composition are rare and host abundant plagioclase microlites. We conclude that there was practically no magmatic volatile-driven fragmentation involved in the South Peak eruption because clasts with a fluidal shape like limu o Pele or Pele's hair, indicative for magmatic explosive activity, were not found.

3.5.6 Breccia samples

The summits of North and South Peak consist of volcaniclastics. Whereas the recently formed South Peak does not reveal steep scarps and can therefore be interpreted

only based on its surface structures, the older North Peak allows insights into its interior at the cliff faces and pillars where units of clasts with a thickness up to 16 m are exposed. These exposures indicate that the volcaniclastic cover at the summit region on North Su can be many meters thick. Breccias sampled directly out of cliff faces (Fig. 3.11 a) and picked up from scree at the base of cliffs show a range of clasts that are moderately to highly altered. The clasts represent a mixture of variably rounded fractured bulk rock and phenocryst fragments. Electron Microprobe and x-ray diffraction analyses reveal that the clasts are partly altered to cristobalite and pyrophyllite, with variable alunite. Hydrothermal precipitates comprise alunite and jarosite, as well as cristobalite, pyrite, sulfur, and anhydrite filling void space in between clasts and forming vein networks within the breccias. Raster electron microscopy and element mapping shows compositional variations betwenn clasts and matrix (Figure 3.11 c-e). The element map of Si (Fig. 3.11 d) clearly defines the volcanic clast whereas the element map of S (Fig. 3.11 e) highlights the hydrothermal cement in the void space between clasts.

3.6 Discussion

The knowledge about the geology and volcanology of North Su prior to this publication was based on the results of the first discovery by video sled surveys and dredges (Binns et al., 1997). Based on this data, North Su was interpreted as a dacite dome with a volcanic spine at its crest with adjacent black smoker chimneys. The entire volcanic edifice was supposed to be covered by a thick “tuffite” apron. Our results reveal a different picture of North Su.

3.6.1 Morphological evolution of North Su

The shape of North Su in ship-based bathymetry depicts a conical edifice with smooth slopes in depths greater than 1350 mbsl that we account to abundant clastic debris based on seafloor observations. This interpretation is corroborated by observations on other submarine volcanoes (e.g. West Mata; Clague et al., 2011) where clastic debris forms smooth looking lower slopes in the bathymetry.

Contrary, the upper slopes (above ~1350 m water depth) of North Peak show a highly irregular topography, with oversteepend to near vertical slopes and erosional gullies. Volcanic eruptions at North Su can be explosive and produce craters (e.g. South Crater) or effusive (e.g. South Peak). Effusive eruptions form an edifice with steep and smooth slopes dominantly consisting of volcaniclastics with rare volcanic outcrops. When

the steep slopes of unconsolidated clasts collapse, they leave erosional gullies, ridgelines and pillars that are characteristic for the upper 60 m of North Peak.

A comparison of the ship-based bathymetric maps from 2002 and 2011 (Fig. 3.7, 3.9, 3.10) reveals that North Su volcano has not experienced major morphological changes in that time span, apart for the eruption of South Peak. The combination of ROV video data with AUV bathymetry provides further insights to the evolution of North Su. The following observations are used to develop a sequence of volcanic events: All slopes around North Peak are more or less continuous with steps or ridgelines in the terrain clearly visible in the high-resolution bathymetry of 2006 (Fig. 3.7a). On the southern slope, by contrast, we found very rugged and variably steep terrain in 2006, separated from the more regular other slopes to both sides by near-vertical and up to 14-m high cliffs. These cliffs expose hydrothermally cemented breccia exclusively (Fig. 3.5 m, n), and the seafloor at their base is covered by scree, which is composed of material identical to the breccia visible in the cliff faces. This observation suggests that a minor sector collapse has likely caused the southern slope to break off, create cliffs, and deposit material downslope and into South Crater. The southern slope features a variable steep (25-90°) upper part indicative of collapse and a lower part with a regular slope of 20-25° that transitions into the South crater area (~25°, Fig. 3.7 a). The lower part likely corresponds to the mass-wasted debris that was not transported very far downslope, because South Crater acted as a backstop to gravity flow. The upper part is the headwall of the collapse feature, and is hence autochthonous. The unusual fact that these extremely steep headwall cliffs are made up of breccia is due to the intense hydrothermal cementation and associated mechanical strengthening. This hydrothermal cementation requires a prolonged interaction with hydrothermal fluids at North Peak and contrasts the lose material noticed on the South Crater rim. We therefore hypothesize that South Crater is a younger feature than North Peak. This hypothesis entails that the eruption of South Crater had removed parts of North Peak in a violent eruption. This eruption may or may not have triggered the sector collapse of the south slope of North Peak.

The latest stage of volcanic growth is the emplacement of South Peak, which buried white smoker vent site #6 under a $6*10^6$ m^3 pile of lava and volcaniclastics.

In conclusion, we envisage the following sequence of events in the most recent history of North Su:

1) unspecified eruptions forming North Peak
2) South Crater eruption
3) sector collapse of south slope, perhaps coeval with (2)
4) South Peak eruption

3.6.2 Hydrothermally increased slope stability

The validity of the idea that hydrothermal cementation may increase slope stability is critical for the plausibility of the morphological evolution outlined above. Hydrothermal alteration is often considered a process decreasing slope stability (e.g. Merle and Lénat, 2003), because clay minerals and other alteration phases commonly have lower shear strength than the primary phases they replace. Our observations of steep pillars and cliffs that are exclusively composed of breccia assigns a vital role to cementation, as an unconsolidated pile of volcanic clasts would have low cohesive strength and could not build steep walls.

Petrographic inspection of several breccia samples in thin section and raster electron microscopy, and electron microprobe analyses indicates that hydrothermal scalings commonly glue together volcanic clasts (Fig. 3.11). The bonding between the clasts can be accomplished by coalescence of these coatings, interstitial growth of individual crystals large enough to connect clasts, or complete infill of void space by polycrystalline cements, which often include pyrite. The occurrence of native sulfur in some of these breccias suggests that liquid sulfur impregnated the unconsolidated rubble and led to cementation upon cooling and solidification.

Thin sections of breccia samples (Fig. 3.11 b) show that the clasts and crystal fragments reflect a similar clast composition as observed in sample SO-216-51-ROV-10 (Fig.6 s) which originates from the summit of South Peak. Clasts of such cemented breccia samples are variably altered, but alteration of the breccia is never pervasive. Moreover, clay minerals are minor phases and never form interconnected networks in the rock, which would lower its shear strength. Cristobalite is perhaps the most abundant secondary mineral, partially replacing clasts and filling cracks and void space.

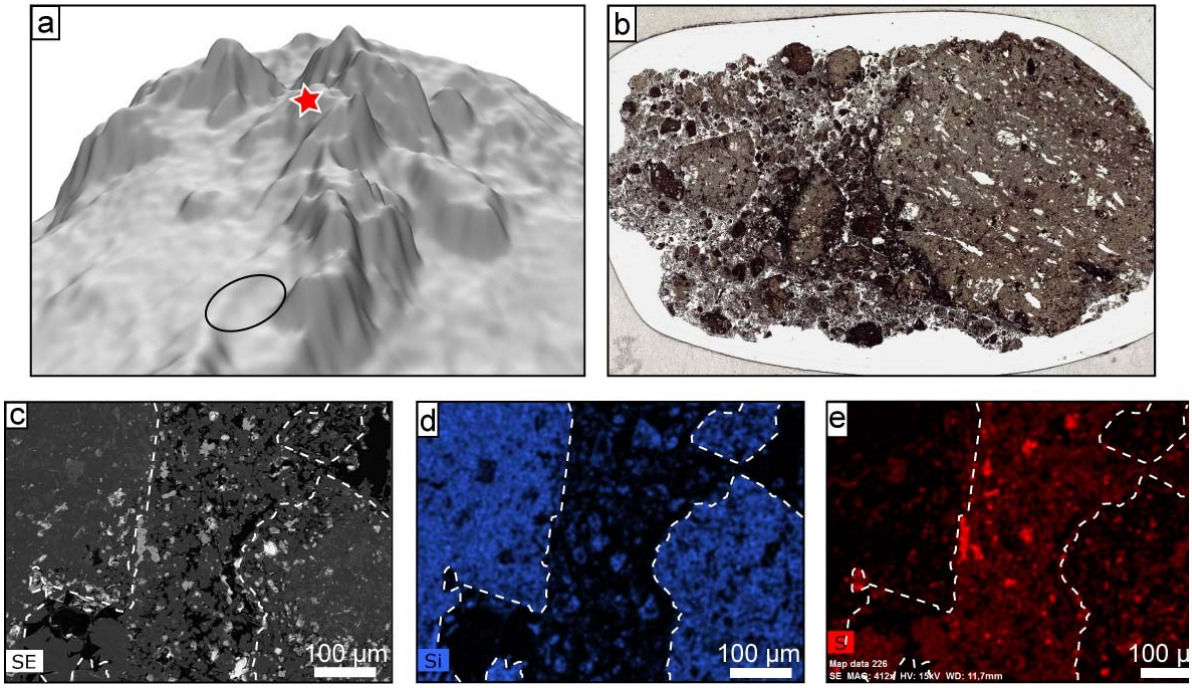

Figure 3.11: Hydrothermally cemented breccias increase the local slope stability. These breccias form pillars, ridgelines and cliffs when the surrounding slope collapses.
a) Oblique perspective from South-East on the southern slope of North Peak. The red star in a indicates sample location for b. Black circle marks the position of Sulfur Candle site.
b) Thinsection of a cemented breccia taken from a cliff. Single clasts are clearly visible within a greyish matrix. Picture width is 3.5 cm. Sample J2-223-6-R1.
c - e) Raster electron microscopy images of the thinsection shown in b. Lithic clasts are highlighted with white outlines. c) Secondary electron image. d) Element map of Si depicting the shape of volcanic clasts. e) Element map of S illustrates the hydrothermal cement filling void space between clasts.

In summary, the non-pervasive nature of alteration, the scarcity of clay minerals, the abundance of cristobalite and the varied styles of cementation all contribute to increase the shear strength relative to the unconsolidated precursor material of the cemented breccias. Essential for this scenario of hydrothermal strengthening of the lithologies observed are: (i) a rubble pile of several meters in thickness, (ii) prolonged discharge of sulfuric acid type fluids, (iii) formation of liquid sulfur by SO_2 disproportionation from these fluids, and (iv) solidification of the sulfur upon cooling.

It is obvious from Figure 3.11 c - e that hydrothermal precipitates crystalize in void space between clasts and thus increase slope stability of the volcaniclastic material due to hydrothermal cementation. The slopes of North Su exceed 30° in some places as shown in the slope map of North Su (Fig. 3.6) and therefore loose material is likely to be re-deposited due to sector collapse events. Sector collapse is a common mechanism on active volcanoes that can be triggered by events such as dike emplacement or intrusion and are widely discussed by Acocella et al. (2005). At the summit of North Peak, sector collapse events transported volcaniclastics downslope but leave the cemented parts as

excavated pillars, cliffs or ridgelines (Fig. 3.5 m, n, p, r) resulting in the observed morphology on North Peak summit.

Another hydrothermal cementation process is presented by a sphalerite-baryt crust (Fig. 3.5 h) which is commonly observed at black smoker hydrothermal fields. This crust occurs on North Peak northwest slope at vent site #5. We assume that this is a result of prolonged discharge of hydrothermal precipitation into the scree covered slope.

The third observation indicating that hydrothermal activity increased slope stability is observed on the ridgeline next to Sulfur Candle. There, rounded pillars up to several meters high and > 1 m in diameter (Fig. 3.5 p) consists of single blocky clast within a fine matrix. Native sulfur was pervasive and solidified tongues of sulfur existed on the vertical pillar surfaces with thicker sulfur deposits on the top. We conclude that the sulfur laden fluids circulated through the clastic deposits prior to a sector collapse and solidified in between the clasts. This process can be observed at the hydrothermal discharge site on South Peak (Fig. 3.5 g) where hydrothermal fluids start to bury loose rocks due to precipitation of native sulfur. Another similarity to the clastic ridgelines on North Peak is the radial orientation to the summit. We assume this to be a cyclic pattern that accompanies volcanic eruptions on North Su as abundant clasts are produced during lava emplacement, followed by hydrothermal discharged through the clastic pile leading to localized cemented structures that stick out the slope when sector collapse events lead to removal of a major part of the slope.

Although hydrothermal activity is considered as a factor of decreasing slope stability, our observations of pillars, cliffs and hydrothermal crust made up of cemented clasts seem to relativize this assumption as the hydrothermal cementation clearly increases local slope stability at North Su when the fluid discharge occurs through a pile of volcaniclastics. The abundance of clasts is related to volcanic eruption when fragmentation processes take place due to interactions of hot lava with cold seawater.

3.6.3 Eruption mechanism

On North Su, we observed several eruption products and volcanic morphologies including different styles of lava flows such as short and thick flows, columnar, blocky flows and spines (Fig. 3.5 a - e). These lava flow morphologies indicate a poor flow behavior and thus a high-viscosity lava. Besides these products of effusive eruptions, explosive eruptions at North Su are indicated by South Crater in 2006 and several intersecting craters on South Peak summit in 2011 (Fig. 3.5 q).

The South Peak summit area, i.e. the craters and the plateau, is the most prominent example of the heterolithic clastic deposits with a dominant grain size between 1 and 5 mm. Below the summit area, widespread autobreccia in the cm-dm size range occur on the slopes of South Su and display a of clast size.

The intersecting craters and the plateau of heterolithic clastic deposits on South Peak indicate that some sort of explosive eruption has occurred that mixed and dispersed the fractured rocks.

Clague et al. (2011) describe a feature on West Mata, NE Lau Basin with morphology similar to the South Peak plateau. The flat-topped plateaus these authors observe are covered entirely by sand-sized clastic deposits. They concluded that this material is most likely deposited from nearby pyroclast-rich eruption plumes. Unfortunately, no detailed description of the sand-sized clastic debris is provided but they mention that the glass chemistry varies and none of the compositions correlate with the ongoing eruptions located just 300-400 m away.

Although the plateaus on both volcanoes are somewhat similar, substantial differences between West Mata and North Su exist. The rock chemistry and lava flow morphologies of West Mata differ from the highly viscous, porphyritic andesites at North Su. West Mata lavas have a boninitic composition and form a variety of typical submarine eruption patterns including pillow lavas and abundant pyroclast formation depending on the type of eruption Resing et al., 2011 (Clague et al., 2009b, 2011).

The model proposed for the West Mata plateau, i.e., a deposit exclusively derived from magmatic eruption plumes, is not applicable to North Su since no volcanic vents exists nearby. Moreover, pyroclasts exhibiting evidence for gas-driven magma fragmentation (bubble walls, pumice, etc.) are not observed in the entire North Su summit area and therefore exclude magmatic explosivity as a possible eruption mechanism. The only vent-like structures near the plateau on South Peak are the adjacent crater group that could act as a source for dispersed clastic deposits.

No formation comparable to the crater group on South Peak is known for the submarine environment. The crater group comprises multiple, small, shallow and intersecting craters with lithic unsorted clasts. Most notably, similar to the adjacent plateau, no pyroclastic deposits were observed.

A morphological analog from land for multiple, shallow and intersecting craters is described by Thorarinsson (1953) for the crater group on Iceland where lava

emplacement onto wet substrate caused rootless explosions that created abundant small craters. We disregard this scenario as lava at North Su is not capable to form widespread lava flows that cover a reasonable area of wet sediment and in addition, these explosions are related to pyroclast-formation.

A perhaps more similar analog are hydrothermal eruptions (Browne and Lawless, 2001) that eject blocky to rounded lithic clasts from predominantly shallow and small craters. Browne and Lawless (2001) consider the injection of magma into a deep hydrothermal aquifer to cause steam explosions besides the classic hydrothermal pressure release theory. The other mechanism known to drive hydrothermal explosions on land is expansion of a low-density phase separated hydrothermal fluid or steam (Browne and Lawless, 2001). In this type of hydrothermal explosion, a crack taps into a subsurface reservoir of such a fluid and the related sudden pressure drop causes catastrophic volume expansion and leading to an explosion. This mechanism is unlikely to cause large explosion in the deep sea, because the ambient pressure at the seafloor (i.e., 115 bar at North Su) would prevent much of the gas expansion one would see at 1 bar.

We therefore favor the hypothesis that the plateau, the crater group and the clastic deposits at South Peak are a product of steam explosions caused by water-magma interactions inside the water saturated clast-dominated volcanic edifice. Also, lava outcrops are clear evidence that the growth of South Peak is related to magmatic activity.

3.6.3.1 Lava emplacement

As none of the mechanisms mentioned above is capable to explain the full spectrum of observed volcanic morphologies and eruption products of North Su, it is essential to consider general magma parameters and linked eruption mechanisms that are related to porphyritic andesites as they occur on North Su.

A subaerial analog of a porphyritic andesite dome emplacement is described by several authors for the 1995 - 1998 eruption at the Soufrière Hills Volcano, Montserrat (Sparks et al., 2000; Melnik and Sparks, 2002; Watts et al., 2002). This episode of volcanic activity comprised a crystal-rich andesite dome growth with short-lived episodic sub-Plinian and Vulcanian explosions. The andesite dome growth was characterized by the extrusion of a hot crystalline solid with minor amounts of residual melt because the magma already began to solidify while rising in the conduit due to decompression, crystallization and degassing (Sparks et al., 2000). The viscous lava was unable to flow and further injection of magma into the dome pushed out lava lobes and spines. A dome

collapse revealed that the interior of the dome was heavily fractured with single fractures up to 50 m long. Sparks (2000) states that this brittle behavior indicates that the crystal-rich lava erupted in a solid state.

Although the Soufrière Hills Volcano is erupting subaerial and therefore not directly comparable with North Su, Sparks et al. (2000) generally discusses in this context the rheology of magma in respect to the crystal content. They note that while most of the crystallization of rhyolitic lava occurs after emplacement due to its behavior as an undercooled melt during extrusion, the timescale for crystallization of gas-rich porphyritic andesite magma is sufficiently fast that an extensive crystallization occurs already within the conduit (Melnik and Sparks, 1999). Thus, gas-rich porphyritic andesite tends to be even more viscous than rhyolite and is the least mobile kind of lava (Sparks et al., 2000).

In general, a highly viscous magma develops strongly non-Newtonian properties and mechanical strength when a percolation threshold is reached as crystals start to form a touching framework (Marsh, 1981). Therefore, highly crystalline magma can deform heterogeneously and fail as a brittle solid (Sparks et al., 2000). Sparks et al. (2000) further notice that the lava morphology of a crystal-rich andesite is strongly dependent on the moment when and where the crystal threshold is reached. The rheological behavior of this type of lava is therefore dependent on internal parameters (e.g. crystal network, vesicles) whereas the flow behavior of dacitic or rhyolitic lava is mainly dependent on external parameters, such as the cooling rate.

The observations from Soufrière Hills Volcano are only partly transferrable to North Su as the eruption style and previous degassing of the magma is strongly dependent on atmospheric pressures. However, the general physical properties of highly crystalline andesitic magma and its behavior observed at Soufrière Hills Volcano are essential. No concept for submarine eruption of crystal rich andesitic magma exists and no active dome emplacement or eruption of viscous lava has yet been witnessed on the seafloor. Therefore, existing eruption models for highly viscous magma are based on laboratory experiments or facies reconstructions of ancient deposits, now exposed on land. Although, these concepts are limited to the emplacement of dacites and rhyolites which are related to the formation of lava domes, abundant pumice or explosive eruptions, they are fundamental to the understanding of North Su eruption mechanisms as they comprise general eruption characteristics. Besides the dominant blocky outcrops that indicate high-

viscosity lava, also lava lobes are observed in a few places. These lobes are formed when the lava flowed over short distance and therefore refers to a lower viscosity. Thus, in the course of an eruption, the viscosity of lava varies.

3.6.3.2 Lava fragmentation, steam explosions and formation of the clastic facies at North Su

Emplacement of viscous lava in a submarine environment is typically envisioned as a thick lobe or dome that is fragmented through quenching, cooling-contraction granulation and autobrecciation upon contact with seawater, resulting in a coherent core that is covered by a monomictic carapace of hyaloclastites and autobreccia (e.g. Pichler, 1965; Yamagishi and Dimroth, 1985; McPhie et al., 1993; Goto and McPhie, 1998; Scutter et al., 1998; Doyle and McPhie, 2000; De Rita et al., 2001; Nemeth et al., 2008). Hyaloclastites in this context describes particles that are disintegrated from the lava through non-explosive quenching whereas clasts produced through non-explosive mechanical disintegration are termed autobreccia.

Several characteristic of South Peak are not consistent with the common models, which are based on crystal poor, dacitic to rhyolitic lava. Firstly, rocks of North Su are crystal-rich andesites with dacitic to rhyodacitic glass. Secondly, on South Peak, we neither observed hyaloclastites nor a monomictic autobreccia deposit.

The clastic deposit on the summit is composed of heterolithic clasts including minor glassy fragments. The latter rather resemble spattered bulk rock than splinters of glass produced through quenching of liquid lava. The lack of hyaloclastites and abundance of blocky, lithic clasts can be explained by the ability of crystal-rich magma to fail as a brittle solid, similar to observation made on Soufrière Hills Volcano (e.g. Sparks et al., 2000; Melnik and Sparks, 2002). Additionally, Yamagishi & Dimroth (1985) assume that a silica-rich magma with porphyritic texture would create blocky, stubby flows or domes that grade into breccia composed predominantly of lithic material. The fact that non-altered clasts are blocky and no fluidal clasts are observed implies a magma fragmentation in the brittle regime. This idea of brittle failure of lava accounts for the abundance of blocky, lithic clasts but cannot explain the crater group or heterolithic composition of the clastic deposit. Therefore, further elaboration of clast formation processes and possible related explosivity is needed.

Theories of clast formation and explosivity due to water-magma interaction include several thermo-hydraulic fracturing mechanisms that account for different clast sizes and

shapes (e.g. Sheridan and Wohletz, 1983; Wohletz, 1983; Kokelaar, 1986; Zimanowski et al., 1991; White, 1996; Skilling et al., 2002; Head and Wilson, 2003; Thiéry and Mercury, 2009).

For a lava that fails by brittle behavior, blocky clasts are mainly produced through quenching (cooling-contraction granulation), mechanical stress (autobrecciation) and hydromagmatic explosions (bulk interaction steam explosivity) (Kokelaar, 1986; Skilling et al., 2002; Head and Wilson, 2003).

Mechanical stress due to lava movement results in autobrecciation which leads to fracturing of lava while it is being emplaced, and produces fissured and blocky outcrops with abundant blocky, clastic material that covers the slopes of North Su.

Cooling-contraction granulation is the process of magma fragmentation due to cooling of magma upon contact with cold sea water. The thermal contraction leads to cracking or granulation, producing sand- and granule-sized clasts (Kokelaar, 1986; Head and Wilson, 2003) as the fine volcaniclastics that are recognized all over North Su. Cooling-contraction granulation is the only fragmentation process that also acts after the emplacement and continues while the lava cools, even if it cools well below the glass-transition temperature (Porreca et al., 2014). This mechanism further explains the large fraction of very small (<4 mm) clasts in between and on top of the larger blocky clasts created by autobrecciation.

Bulk interaction steam explosivity describes the interaction of magmatic heat with water that is either engulfed by magma or trapped close to it. Pressure waves associated with explosions shatter the rigid magma and a tearing apart of the magma occurs (Kokelaar, 1986). This is likely to happen when magma intrudes into wet slurry (e.g. water-saturated sediment) causing local explosions due to steam expansion and disruption of juvenile material and country rock (Zimanowski et al., 1991; Skilling et al., 2002).

If we consider the observation by Sparks (2000) that even on land, where much lower cooling rates occur than in the deep sea, the cracks of a porphyritic andesite dome can extend several ten's of meters, reaching the center of the dome. We argue that such magma emplaced in a submarine environment will also be heavily fractured. If we consider the thermo-hydraulic mechanisms discussed above and the brittle behavior of a crystal-rich magma with its internal heterogeneities, we suggest runaway-fracturing during extrusion.

During extrusion, due to the brittle failure of lava, mechanical stress produces abundant autobreccia and cracks propagate deep into the lava body with simultaneous cooling-contraction granulation causing further fragmentation of clasts and lava. Bulk-interaction steam explosivity occurs upon contact of lava within the water-saturated, clast-dominated slopes of North Su. The trapped seawater inside the cracks and at the lava-water interface below the clastic cover gets flash-heated causing local explosions that further enhance crack-propagation and fragmentation.

This runaway process is believed to occur until the lava has cooled. Several author note that crack propagation can even continue at ambient pressures (Romano et al., 1996; Mungall et al., 1996; Vona et al., 2012 in: (Porreca et al., 2014).

Although it is most plausible that bulk-interaction steam explosivity causes the formation of the crater group, we cannot exclude that syn- or even post-eruptive magmatic degassing can also produce gas jets that form craters when discharged at the seafloor and deposit heterolithic clasts as argued with steam explosivity.

We propose that following eruption mechanisms, illustrated in Figure 3.12, created South Peak and generally occur on North Su:

Highly viscous, crystal-rich felsic magma erupts slowly into the water-saturated slope of North Su. The slope consists of coherent lava and abundant clastic material which is variably altered. Additional altered and lithic material might be contributed by upward transportation of vent wall-rocks with the rising magma. The lava fails with brittle behavior upon contact with cold seawater due to dynamic stress induced autobrecciation, cooling-contraction granulation and bulk-interaction steam explosivity creating a self-amplifying fragmentation process. Additional uprising magma occasionally pushes a fraction of magma through the pile of syn-eruptive and pre-existing clasts onto the seafloor in the form of lobes (Fig. 3.12). Dependent on the rheology of each lobe during emplacement, they form either short and rugged flows or heavily ragged outcrops without surficial signs of lava flow.

In the course of the eruption, local steam explosions cause a turbulent mixing of blocky juvenile fragments (i.e., fragmented intruding magma) and variably altered lithologies. This cover of heterolithic clasts will also be uplifted in the course of further injection of magma and mechanic and steam-propelled turbulent reworking cause clasts to develop variably rounded shapes.

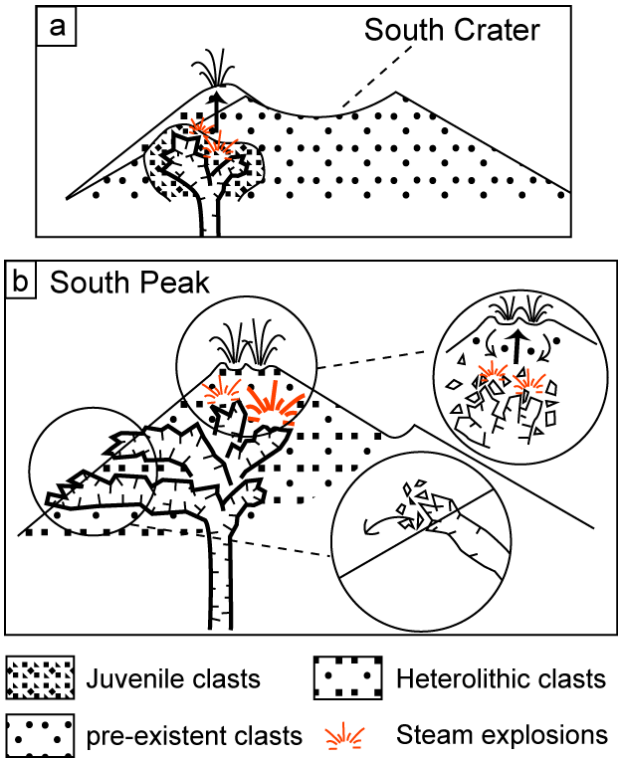

Figure 3.12: Simplified sketch explaining the observed morphologic and volcanic features at the South Peak eruption.
a) High viscous magma intrudes into the water-saturated volcaniclastic governed slope of North Su. Non-explosive fragmentation and steam explosivity disrupts the pre-existent material with the erupting lava that fails in brittle behavior due to its high crystal content and semi-solid state, causing dominantly lithic clasts that mix with the pre-existing material of North Su.
b) The magma erupts as single lobes that occasionally breach through that clastic cover which than suffer from further fragmentation resulting in blocky outcrops. Steam explosions accompany the fragmenting magma producing clast-laden steam jets that thrust through the clastic cover and emit heterolithic material onto the seafloor. This process creates a group of small, randomly scattered, shallow craters. Due to uplift during the ongoing eruption and enhanced by several explosion, clasts are reworked which is expressed by a rounded shape.

The numerous small intersecting craters are caused by jets of steam that transport clasts of variable origin, shape, and size to the seafloor where they form a lithology that mimics products of hydrothermal eruptions. Strong currents transported parts of the ejected material a few meters towards North Peak where they deposited to build up a plateau with dominantly sand-sized clasts. Larger clasts remained closer to the crater center.

These proximal volcanic lithologies share characteristics (i.e. rounded grains, fine clast size, heterolithic composition) of deposits that would traditionally be interpreted in facies reconstructions as distal or as reworked volcaniclastic sediments. Our results indicate that heterolithic breccias with variably rounded clasts may also form in the course of the complex porphyritic magma-water interactions associated with a volcanic event near the summit of a felsic volcano.

3.6.3.3 Evidence of larger explosive eruptions

A crater, 80 m wide and 13 meter deep, was observed in 2006 (Fig. 3.7 a) on the southern flank of North Su. It resembles the type tuff ring or tuff cone that is typically associated to phreatomagmatic eruptions. Very limited ROV observation from 2006 restricted a detailed analysis but remnants of the rim were observed in 2011 (Fig. 3.5 f) and revealed a mixture of lithic clasts with abundant fine volcaniclastics and native sulfur.

In 2011 magmatic degassing was present at North Su which is common for felsic arc-related magma systems. Therefore, a plumbed conduit is likely to result in a violent explosion. Due to the limited sample set of fine volcaniclastics on North Su we cannot completely exclude the existence of minor pyroclastic deposits. However, if we consider the same crystal-rich magma to be involved in the eruption as for the South Peak eruption, the juvenile material would consist of blocky bulk rock clasts and crystal fragments, and lack typical pyroclasts.

Based on dredge samples and photo-sled surveys during PACMANUS-III expedition in 1996 Binns et al., 1997 and Moss and Scott, (2001) interpreted North and South Su as porphyritic dacite domes. Binns (2004) and Hrischeva (2007) describe a widespread "tuffite" apron, up to several meters thick and covering the entire SuSu Knolls area. This apron was sampled with sediment cores only at Suzette revealing a layered (cm scale), dark sand-sized sediment that is locally sulfidic (Hrischeva (2007). The sandy deposits contain phenocrysts of plagioclase, pyroxene and magnetite as well as fragments of dacite glass with and without microlites and altered dacite. The glass fragments show blocky to platy and even elongated vesicular shapes (Hrischeva et al., 2007). These authors argue that the sandy deposits are fed by material derived from the North Su and South Su porphyritic lavas. Thin veneers of sandy deposits occur in even more distal areas (i.e., around 5 km W of North Su) where Hrischeva et al. (2007) found fractured volcanic material similar to what was described at Suzette. Especially the microlite-rich dacite fragments, believed to be derived from flow interiors, and the altered dacite clasts are interpreted by Binns (2004) and Hrischeva et al. (2007) as products of violent hydrothermal eruptions that occurred from deep seated hydrothermal reservoirs below North and South Su.

Hydrothermal eruptions are fueled by steam expansion due to a sudden pressure drop (Browne and Lawless, 2001). At North Su this large extent of steam expansion is unlikely to occur, given a hydrostatic pressure of >115 bar (e.g. 1150m water depth) and an additional unknown lithostatic pressure. Although it is not impossible to create a gas phase in an aquifer at a high pressure regime (Thiéry and Mercury, 2009; Buttinelli et al., 2011), this mechanism requires particular circumstances (i.e. assimilation of carbonates) and has never been described or observed in a deep sea environment.

Moreover, explosive behavior is a common feature on arc-related volcanoes with felsic, porphyritic and volatile-rich magmas (e.g. Carey and Sigurdsson, 2007). Finally,

no petrologic analyses have ever been published or mentioned that would verify that deposits on Suzette are actually related to rocks originating from North Su. Therefore we exclude the hydrothermal eruption theory of Binns (2004) from our consideration here.

3.7 Summary and Conclusion

Our analyses show that North Su is a double peaked active volcano with a divers hydrothermal system. Black and white smoker fluids emit with less than 100 m lateral distance to each other. CO_2-release is ubiquitous at pulsating white smoker vents from which activity varies significantly within a two-week observation time. A new vent site "Sulfur Candle" has been documented where chimneys of native sulfur exist.

Repeated bathymetric surveys revealed that a new cone, South Peak, was emplaced between 2006 and 2011 on the south western slope of North Su. Volcanic material with an estimated volume of $5.8*10^6$ m^3 has been deposited on an area of $2.1*10^5$ m^2 with a maximum depth change between the surveys of +63 m. The slopes of South Peak are dominated by clastic material that show an upward-fining trend towards its summit where a plateau developed next to a group of several small (max. 10 m diameter) and shallow (<3 m) craters. The fine volcaniclastic material covering the South Peak summit consists of heterolithic clasts that lack signs for pyroclastic fragmentation. Intense thermo-hydraulic fracturing of the magma upon contact with seawater and water-saturated volcaniclastic deposits produced abundant clastic material and syn-eruptive steam explosivity caused clastic-laden jets to thrust through the clastic pile and erupt onto the seafloor creating a crater group similar to craters produced by hydrothermal eruptions on land. The lack of pyroclasts is interpreted to result from a high-viscosity, crystal-rich magma that fails as a brittle solid upon stress. The high viscosity allowed the lava to form dominantly blocky and short lava outcrops.

Outcrops on North Su North Peak suggest that magma erupted previously in a similar pattern that created blocky outcrops and volcanic spines as observed at the Soufrière Hills Volcano where porphyritic andesitic lava erupted in a semi-solid state (Sparks et al., 2000; Watts et al., 2002). Short (<10 m) lava lobes show that magma is also erupted in a less viscous state.

A relative chronologic sequence of the most recent volcanic events of North Su was developed:

1) unspecified eruptions forming North Peak
2) South Crater eruption
3) sector collapse of south slope, perhaps coeval with (2)
4) South Peak eruption

The 80 m-wide South Crater is obvious on the AUV bathymetry from 2006 that indicates volcanic eruptions at North Su can be explosive as well. This eruption probably caused a sector collapse on the older North Peak of North Su but clastic material resisted the collapse in many places near the summit of North Peak due to hydrothermal cementation of clastic deposits. Despite the common opinion that hydrothermal activity triggers slope collapses, hydrothermal activity has increased local slope stability where hydrothermal precipitates crystalized in-between the clasts and cemented them. The southern and western slope below the summit of North Peak, cliffs and pillars expose up to 16 m thick units of hydrothermally cemented heterolithic clast breccias.

Our observations give further insights into the volcanologic frame of a developing Cu-Au ore deposit and can help geologists with facies interpretation. Proximal volcanic lithologies on North Su share characteristics (i.e. rounded grains, fine clast size, heterolithic composition) of deposits that would traditionally be interpreted in facies reconstructions as distal or as redeposited lithologies. Our results indicate that heterolithic breccias with variably rounded clasts may also form in the course of the complex porphyritic magma-water interactions associated with a volcanic event near the summit of a felsic volcano.

3.8 Acknowledgments

We thank the captains and crews of RV Sonne and RV Melville, the ROV teams of Jason-2 and MARUM Quest 4000, the AUV-ABE technical team and the members of the Science Parties for both cruises. The RV Melville work was funded by a combination of the US National Science Foundation grant OCE-0327448 and a collaborative research funding grant from Nautilus Minerals for the ABE surveys. The RV Sonne research cruise was funded through the BMBF (Grant G03216a). Additional funding, including salary support for JT, was provided by the German DFG Research Center/Excellence

Cluster “The Ocean in the Earth System”. WB acknowledges support from DFG research grant BA1605/4-1.

Crucial help with volcanic clast analyses was provided by Adam Soule and a considerate review of Timothy Schroeder helped to improve the manuscript.

Finally, we thank Jim Robins and Pat Pepena from Papua New Guinea (PNG) for their help with PNG research permitting.

3.9 Appendix

	Sample # J2-221-				Sample # J2-223-						J2-227-
wt.%	**8-R1**	**15-R1**	**16-R1**	**16-R2**	**3-R1**	**5-R1**	**9-R2**	**10-R1**	**14-R1**	**16-R1**	**13-R1**
SiO2	59.59	60.46	61.39	60.07	61.21	61.34	60.86	61.54	62.16	62.52	63.73
TiO2	0.54	0.56	0.56	0.55	0.57	0.57	0.56	0.58	0.58	0.57	0.56
Al_2O_3	13.95	14.69	14.69	14.36	14.90	14.69	14.83	14.78	14.97	14.85	14.76
Fe_2O_3	6.94	6.60	5.85	7.17	7.34	6.29	7.06	7.15	6.59	6.36	4.39
MnO	0.130	0.127	0.120	0.138	0.152	0.120	0.131	0.132	0.128	0.122	0.086
MgO	4.09	2.81	2.61	4.20	3.08	2.25	3.08	2.60	2.75	2.32	2.16
CaO	6.48	5.96	5.81	7.05	6.44	5.78	6.43	5.90	6.12	5.50	5.21
Na_2O	2.94	3.60	2.69	3.40	3.73	4.41	3.65	3.82	3.77	3.90	3.95
K_2O	0.78	0.98	0.80	0.87	0.98	1.12	0.97	1.03	1.01	1.08	0.88
P_2O_5	0.17	0.15	0.13	0.17	0.21	0.19	0.19	0.20	0.19	0.19	0.09
H_2O	2.65	1.55	3.33	1.17	0.97	1.41	1.28	1.02	1.06	1.26	1.41
CO_2	0.02	0.03	0.04	0.02	0.03	0.04	0.06	0.06	0.03	0.03	0.03
Total	98.35	97.60	98.10	99.17	99.62	98.20	99.10	98.80	99.35	98.70	97.33

Table 3.A1: Results of whole rock XRF analyses. All iron measured as Fe_2O_3.

	Sample # J2-221-		Sample # J2-223-			
wt. %	**8-r1**	**16-r1**	**5-R1**	**9-r2**	**10-R1**	**14-r1**
SiO_2	66,87	68,18	74,11	72,90	74,45	73,51
TiO_2	0,61	0,62	0,56	0,49	0,49	0,56
Al_2O_3	13,40	13,28	12,60	12,75	12,39	12,64
Cr_2O_3	0,000	0,000	0,010	0,000	0,017	0,017
FeO	5,67	5,54	3,48	2,76	3,48	3,09
MnO	0,12	0,13	0,09	0,10	0,08	0,06
MgO	1,32	1,18	0,38	0,23	0,43	0,24
CaO	3,99	3,85	2,06	2,13	2,02	2,04
Na_2O	3,53	3,65	4,35	3,64	4,41	4,43
K_2O	1,42	1,50	1,92	1,71	1,95	1,85
P_2O_5	0,29	0,30	0,13	0,10	0,21	0,12
SO_3	0,02	0,01	0,00	0,00	0,00	0,00
BaO	0,00	0,00	0,08	0,00	0,07	0,00
Cl	0,22	0,22	0,26	0,26	0,26	0,27
Total	97,46	98,46	99,93	97,06	100,17	98,82

Table 3.A2: Glass analyses measured with EPMA.

3.10 References

Allen, S.R., Fiske, R.S., Tamura, Y., 2010. Effects of water depth on pumice formation in submarine domes at Sumisu, Izu-Bonin arc, western Pacific. Geology 38, 391–394.

Allen, S.R., McPhie, J., 2009. Products of neptunian eruptions. Geology 37, 639–642.

Auzende, J.-M., Ishibashi, J.-I., Beaudoin, Y.C., Charlou, J.-L., Delteil, J., Donval, J.-P., Fouquet, Y., Ildefonse, B., Kimura, H., Nishio, Y., Radford-Knoery, J., Ruøllan, E., 2000. Extensive magmatic and hydrothermal activity documented in Manus Basin. Eos, Trans. Am. Geophys. Union 81, 449–453.

Auzende, J.-M., Urabe, T., Party, S., 1996. Cruise explores hydrothermal vents of the Manus Basin. Eos (Transactions, Am. Geophys. Union) 77, 244.

Bach, W., Jöns, N., Thal, J., Breuer, C., Shu, L., Dubilier, N., Borowski, C., Meyerdierks, A., Pjevac, P., Brunner, B., Müller, I., Petersen, S., Hourdez, S., Schaen, A., Koloa, K., Jonda, L., Team, M.Q. 4000m, 2011. Report and preliminary results of RV SONNE Cruise SO-216, Townsville (Australia) - Makassar (Indonesia), June 14 – July 23, 2011. BAMBUS, Back-Arc Manus Basin Underwater Solfataras. Berichte, Fachbereich Geowissenschaften, Univ. Bremen 280, 87.

Binns, R.A., 2004. Eastern Manus basin, Papua New Guinea: Guides for volcanogenic massive sulphide exploration from a modern seafloor analogue, in: McConachy, T., McInnes, B. (Eds.), Copper-Zinc Massive Sulphide Deposits in Western Australia. CSIRO Explores, pp. 59–80.

Binns, R.A., Scott, S., 1993. Actively forming polymetallic sulfide deposits associated with felsic volcanic rocks in the eastern Manus back-arc basin, Papua New Guinea. Econ. Geol. 88, 2226–2236.

Binns, R.A., Scott, S.D., Gemmell, J.B., Crook, K.A.W., Party, S., 1997. The SuSu Knolls Hydrothermal Field, Eastern Manus Basin, Papua New Guinea. Eos Trans. AGU Fall Meet. Suppl. 78, #V22E–02 (abstr.).

Browne, P., Lawless, J., 2001. Characteristics of hydrothermal eruptions, with examples from New Zealand and elsewhere. Earth-Science Rev. 52, 299–331.

Buttinelli, M., De Rita, D., Cremisini, C., Cimarelli, C., 2011. Deep explosive focal depths during maar forming magmatic-hydrothermal eruption: Baccano Crater, Central Italy. Bull. Volcanol. 73, 899–915.

Carey, S., Sigurdsson, H., 2007. Exploring Submarine Arc Volcanoes. Oceanography 20, 80–89.

Chadwick Jr., W.W., Wright, I.C., Schwarz-Schampera, U., Hyvernaud, O., Reymond, D., de Ronde, C.E.J., 2008. Cyclic eruptions and sector collapses at Monowai submarine volcano, Kermadec arc: 1998-2007. Geochemistry, Geophys. Geosystems 9, 1–17.

Clague, D.A., Paduan, J.B., Caress, D.W., Thomas, H., Chadwick Jr., W.W., Merle, S.G., 2011. Volcanic morphology of West Mata Volcano, NE Lau Basin, based on high-resolution bathymetry and depth changes. Geochemistry, Geophys. Geosystems 12, 1–21.

Clague, D.A., Paduan, J.B., Davis, A.S., 2009a. Widespread strombolian eruptions of mid-ocean ridge basalt. J. Volcanol. Geotherm. Res. 180, 171–188.

Clague, D.A., Rubin, K., Keller, N., 2009b. Products of submarine fountains and bubble-burst eruptive activity at 1200 m on West Mata Volcano, Lau Basin. AGU Fall Meet. Suppl. 90, Abstract V43I – 02.

Coleman, P.J., Packham, G.H., 1976. The Melanesian Borderlands and India — Pacific plates' boundary. Earth-Science Rev. 12, 197–233.

Crowhurst, P., Lowe, J., 2011. Exploration and resource drilling of seafloor massive sulfide (SMS) deposits in the Bismarck Sea, Papua New Guinea. Ocean. 2011 1–6.

De Rita, D., Giordano, G., Cecili, A., 2001. A model for submarine rhyolite dome growth: Ponza Island (central Italy). J. Volcanol. Geotherm. Res. 107, 221–239.

Deardorff, N.D., Cashman, K. V., Chadwick Jr., W.W., 2011. Observations of eruptive plume dynamics and pyroclastic deposits from submarine explosive eruptions at NW Rota-1, Mariana arc. J. Volcanol. Geotherm. Res. 202, 47–59.

Doyle, M.G., McPhie, J., 2000. Facies architecture of a silicic intrusion-dominated volcanic centre at Highway–Reward, Queensland, Australia. J. Volcanol. Geotherm. Res. 99, 79–96.

Dziewoński, A.M., Chou, T.-A., Woodhouse, J.H., 1981. Determination of earthquake source parameters from waveform data for studies of global and regional seismicity. J. Geophys. Res. 86, 2825.

Ekström, G., Nettles, M., Dziewoński, A.M., 2012. The global CMT project 2004–2010: Centroid-moment tensors for 13,017 earthquakes. Phys. Earth Planet. Inter. 200-201, 1–9.

Embley, R.W., Chadwick Jr., W.W., Baker, E.T., Butterfield, D.A., Resing, J.A., de Ronde, C.E.J., Tunnicliffe, V., Lupton, J.E., Juniper, S.K., Rubin, K.H., Stern, R.J., Lebon, G.T., Nakamura, K., Merle, S.G., Hein, J.R., Wiens, D.A., Tamura, Y., 2006. Long-term eruptive activity at a submarine arc volcano. Nature 441, 494–7.

Falvey, D.A., Pritchard, T., 1982. Preliminary Paleomagnetic Results from Northern Papua New Guinea : Evidence for Large Microplate Rotations, in: Watson, S.T. (Ed.), Transactions of the Third Circum-Pacific Energy and Mineral Resources Conference. American Association of Petrolium Geologists, Tulsa, Oklahoma, pp. 593–600.

Gamo, T., Okamura, K., Charlou, J., Urabe, T., Auzende, J., Ishibashi, J., Shitashima, K., Chiba, H., Shipboard Scientific Party of the ManusFlux Cruise, 1997. Acidic and

sulfate-rich hydrothermal fluids from the Manus back-arc basin, Papua New Guinea. Geology 25, 139–142.

Goto, Y., McPhie, J., 1998. Endogenous growth of a Miocene submarine dacite cryptodome, Rebun Island, Hokkaido, Japan. J. Volcanol. Geotherm. Res. 84, 273–286.

Hannington, M.D., de Ronde, C.E.J., Petersen, S., 2005. Sea-Floor Tectonics and Submarine Hydrothermal Systems. Econ. Geol. 100th Anni, 111–141.

Hannington, M.D., Jamieson, J., Monecke, T., Petersen, S., Beaulieu, S., 2011. The abundance of seafloor massive sulfide deposits. Geology 39, 1155–1158.

Hashimoto, J., Ohta, S., Fiala-Médioni, A., Auzende, J., 1999. Hydrothermal vent communities in the Manus Basin, Papua New Guinea: Results of the BIOACCESS cruises' 96 and'98. InterRidge News 8 (2), 12–18.

Head, J.W., Wilson, L., 2003. Deep submarine pyroclastic eruptions: theory and predicted landforms and deposits. J. Volcanol. Geotherm. Res. 121, 155–193.

Helo, C., Longpré, M.-A., Shimizu, N., Clague, D.A., Stix, J., 2011. Explosive eruptions at mid-ocean ridges driven by CO2-rich magmas. Nat. Geosci. 4, 260–263.

Herzig, P.M., 1999. Economic potential of sea-floor massive sulphide deposits: ancient and modern. Philos. Trans. R. Soc. A Math. Phys. Eng. Sci. 357, 861–875.

Hillier, J.K., Watts, A.B., 2007. Global distribution of seamounts from ship-track bathymetry data. Geophys. Res. Lett. 34, L13304.

Hrischeva, E., Scott, S.D., Weston, R., 2007. Metalliferous sediments associated with presently forming volcanogenic massive sulfides: the SuSu Knolls hydrothermal field, eastern Manus Basin, Papua New. Econ. Geol. 102, 55–73.

Iizasa, K., 1999. Potential Marine Mineral Resources by Hydrothermal Activity. Chem. Ind. 50, 379–384.

Kokelaar, P., 1986. Magma-water interactions in subaqueous and emergent basaltic. Bull. Volcanol. 48, 275–289.

Kroenke, L., Rodda, P., 1984. Cenozoic tectonic development of the Southwest Pacific. U.N. ESCAP, CCOP/SOPAC Tech. Bull. 6.

Leat, P.T., Tate, A.J., Tappin, D.R., Day, S.J., Owen, M.J., 2010. Growth and mass wasting of volcanic centers in the northern South Sandwich arc, South Atlantic, revealed by new multibeam mapping. Mar. Geol. 275, 110–126.

Lipton, I., 2008. Mineral resource estimate, Solwara 1 project, Bismarck Sea, Papua New Guinea: NI43-101 Technical Report for Nautilus Minerals Inc.

Marsh, B.D., 1981. On the crystallinity, probability of occurrence, and rheology of lava and magma. Contrib. to Mineral. Petrol. 78, 85–98.

Martinez, F., Taylor, B., 1996. Backarc spreading, rifting, and microplate rotation, between transform faults in the Manus Basin. Mar. Geophys. Res. 18, 203–224.

Martinez, F., Taylor, B., 2003. Controls on back-arc crustal accretion: insights from the Lau, Manus and Mariana basins. Geol. Soc. London, Spec. Publ. 219, 19–54.

McPhie, J., Doyle, M.G., Allen, S.R., 1993. Volcanic textures: a guide to the interpretation of textures in volcanic rocks. Centre for Ore Deposit and Exploration Studies - University of Tasmania.

Melnik, O., Sparks, R.S.J., 1999. Nonlinear dynamics of lava dome extrusion. Nature 402, 37–41.

Melnik, O., Sparks, R.S.J., 2002. Dynamics of magma ascent and lava extrusion at Soufriere Hills Volcano, Montserrat. Geol. Soc. London, Mem. 21, 153–171.

Merle, O., Lénat, J.-F., 2003. Hybrid collapse mechanism at Piton de la Fournaise volcano, Reunion Island, Indian Ocean. J. Geophys. Res. 108, 2166.

Mosier, D.L., Berger, V.I., Singer, D.A., 2009. Volcanogenic massive sulfide deposits of the world; database and grade and tonnage models, U.S. Geological Survey Open-File Report.

Moss, R., 2000. Geochemistry and mineralogy of gold in the PACMANUS and Susu knolls hydrothermal systems, eastern Manus basin, Papua New Guinea. University of Toronto.

Moss, R., Scott, S.D., 2001. Geochemistry and Mineralogy of Gold-Rich Hydrothermal Precipitates From the Eastern Manus Basin, Papua New Guinea. Can. Mineral. 39, 957–978.

Nemeth, K., Pecskay, Z., Martin, U., Gmeling, K., Molnar, F., Cronin, S.J., 2008. Hyaloclastites, peperites and soft-sediment deformation textures of a shallow subaqueous Miocene rhyolitic dome-cryptodome complex, Palhaza, Hungary. Geol. Soc. London, Spec. Publ. 302, 63–86.

Petersen, S., Herzig, P., Hannington, M.D., Gemmell, J.B., 2003. Gold-rich massive sulfides from the interior of the felsic-hosted PACMANUS massive sulfide deposit, Eastern Manus Basin (PNG), in: Eliopoulos et al. (Ed.), Mineral Exploration and Sustainable Development. Millpress, Rotterdam, pp. 171–174.

Pichler, H., 1965. Acid hyaloclastites. Bull. Volcanol. 28, 293–310.

Porreca, M., Cifelli, F., Soriano, C., Giordano, G., Romano, C., Conticelli, S., Mattei, M., 2014. Hyaloclastite fragmentation below the glass transition: An example from El Barronal submarine volcanic complex (Spain). Geology 42, 87–90.

Resing, J.A., Rubin, K.H., Embley, R.W., Lupton, J.E., Baker, E.T., Dziak, R.P., Baumberger, T., Lilley, M.D., Huber, J.A., Shank, T.M., Butterfield, D.A., Clague, D.A., Keller, N.S., Merle, S.G., Buck, N.J., Michael, P.J., Soule, A., Caress, D.W., Walker, S.L., Davis, R., Cowen, J.P., Reysenbach, A.-L., Thomas, H., 2011. Active submarine eruption of boninite in the northeastern Lau Basin. Nat. Geosci. 4, 799–806.

Rubin, K.H., Soule, S.A., Chadwick Jr., W.W., Fornari, D.. J., Clague, D.A., Embley, R.W., Baker, E.T., Perfit, M.R., Caress, D.W., Dziak, R.P., 2012. Volcanic eruptions in the deep sea. Oceanography 25, 142–157.

Sangster, D.F., 1980. Quantitative characteristics of volcanogenic massive sulphide deposits. Bull. Can. Inst. Min. Metall. 73, 74–81.

Schipper, C.I., White, J.D.L., Houghton, B.F., Shimizu, N., Stewart, R.B., 2010. Explosive submarine eruptions driven by volatile-coupled degassing at Lō`ihi Seamount, Hawai`i. Earth Planet. Sci. Lett. 295, 497–510.

Scutter, C., Cas, R.A.F., Moore, C., De Rita, D., 1998. Facies architecture and origin of a submarine rhyolitic lava flow-dome complex, Ponza, Italy. J. Geophys. … 103, 27,551–27,566.

Seewald, J., Reeves, E.P, Bach, W., Saccocia, P.J., Craddock, P.R., Shanks III, W.C., Sylva, S.P., Pichler, T., Rosner, M., Walsh, E., 2014. Submarine Venting of Magmatic Volatiles in the Eastern Manus Basin, Papua New Guinea. Geochim. Cosmochim. Acta XX.

Sheridan, M.F., Wohletz, K.H., 1983. Hydrovolcanism: Basic considerations and review. J. Volcanol. Geotherm. Res. 17, 1–29.

Shipboard Scientific Party, 2002. SO-166 CONDRILL.

Skilling, I.P., White, J.D.L., McPhie, J., 2002. Peperite: a review of magma–sediment mingling. J. Volcanol. Geotherm. Res. 114, 1–17.

Sohn, R. a, Willis, C., Humphris, S.E., Shank, T.M., Singh, H., Edmonds, H.N., Kunz, C., Hedman, U., Helmke, E., Jakuba, M., Liljebladh, B., Linder, J., Murphy, C., Nakamura, K.-I., Sato, T., Schlindwein, V., Stranne, C., Tausenfreund, M., Upchurch, L., Winsor, P., Jakobsson, M., Soule, A., 2008. Explosive volcanism on the ultraslow-spreading Gakkel ridge, Arctic Ocean. Nature 453, 1236–8.

Sparks, R.S.J., Murphy, M.D., Lejeune, A.M., Watts, R.B., Barclay, J., Young, S.R., 2000. Control on the emplacement of the andesite lava dome of the Soufriere Hills volcano, Montserrat by degassing-induced crystallization. Terra Nov. 12, 14–20.

Taylor, B., 1979. Bismarck Sea: Evolution of a back-arc basin. Geology 7, 171–174.

Taylor, B., Crook, K., Sinton, J., 1994. Extensional transform zones and oblique spreading centers. J. Geophys. Res. 99, 19,707–19,718.

Thiéry, R., Mercury, L., 2009. Explosive properties of water in volcanic and hydrothermal systems. J. Geophys. Res. 114, B05205.

Thorarinsson, S., 1953. The crater groups in Iceland. Bull. Volcanol. 14, 3–44.

Tivey, M.A., Bach, W., Seewald, J., Tivey, M.K., Vanko, D.A., Party, S.S., 2006. Cruise Report for R/V Melville Cruise MGLN06MV—Hydrothermal Systems in the Eastern Manus Basin: Fluid Chemistry and Magnetic Structure as Guides to Subseafloor Processes.

Tregoning, P., 2002. Plate kinematics in the western Pacific derived from geodetic observations. J. Geophys. Res. 107, 1–8.

Tregoning, P., Jackson, R.J., Mcqueen, H., Larnbeck, K., Stevens, C., Little, R.P., Curley, R., Rosa, R., 1999. Motion of the South Bismarck Plate, Papua New Guinea. Geophys. … 26, 3517–3520.

Watts, R.B., Herd, R. a., Sparks, R.S.J., Young, S.R., 2002. Growth patterns and emplacement of the andesitic lava dome at Soufriere Hills Volcano, Montserrat. Geol. Soc. London, Mem. 21, 115–152.

Wessel, P., 2001. Global distribution of seamounts inferred from gridded Geosat/ERS-1 altimetry. J. Geophys. Res. 106, 19,431–19,441.

Wessel, P., Smith, W.H.F., 1991. Free software helps map and display data. Eos, Trans. Am. Geophys. Union 72, 441–441.

White, J.D.L., 1996. Impure coolants and interaction dynamics of phreatomagmatic eruptions. J. Volcanol. Geotherm. Res. 74, 155–170.

Wohletz, K.H., 1983. Mechanisms of hydrovolcanic pyroclast formation: Grain-size, scanning electron microscopy, and experimental studies. J. Volcanol. Geotherm. Res. 17, 31–63.

Wright, I.C., Gamble, J.A., Shane, P.A.R., 2003. Submarine silicic volcanism of the Healy caldera, southern Kermadec arc (SW Pacific): I-volcanology and eruption mechanisms. Bull. Volcanol. 65, 15–29.

Yamagishi, H., Dimroth, E., 1985. A comparison of Miocene and Archean rhyolite hyaloclastites: evidence for a hot and fluid rhyolite lava. J. Volcanol. Geotherm. Res. 23, 337–355.

Yeats, C.J., Binns, R.A., Parr, J., 2008. The SuSu Knolls hydrothermal field, Eastern Manus Basin, Papua New Guinea: An actively forming submarine high sulfidation copper-gold system, in: International Geological Congress. Oslo, p. MRD–03.

Zimanowski, B., Fröhlich, G., Lorenz, V., 1991. Quantitative experiments on phreatomagmatic explosions. J. Volcanol. Geotherm. Res. 48, 341–358.

4. Conclusion and outlook

Of cornerstone importance for the geologic mapping studies in the eastern Manus Basin are 1-m resolution AUV bathymetric maps that were combined with rock samples, fluid measurement and, in particular, ROV video recordings. The vast majority of ROV dives were conducted for the purpose of collecting biota, fluid and rock samples and only a few dives were dedicated to mapping and exploration of unknown terrain. Therefore, most videos were recorded while the ROV was serving the interests of various scientists that were focused on sampling and not mapping. This thesis demonstrates that these videos nonetheless bear high potential for yielding insightful geological maps. The comprehensive mapping projects have advanced and renewed the knowledge of the PACManus Hydrothermal District and the North Su volcano. They set the foundation for any further scientific research in these areas and enable other scientist to place their findings into the local geologic framework.

The advantage of ROV-based seafloor mapping is that the ROV can operate as usual and scientists can still follow interesting observations spontaneously. Usually, when ROV work is conducted on the seafloor, scientist are often interested in point source data as biological, fluid or rock samples or they use the ROV for the search of such sampling sites. While working on the seafloor, several video cameras constantly record the environment in which the research is accomplished. Extensive databases are constructed to store the vast amount of video data but the interest in these visual informations of the seafloor decreases dramatically after the expedition is accomplished. Therefore, in most cases, these videos are primarily produced for orientation and immediate use while being on sea. Only in rare cases, a systematic post-cruise analysis is conducted and thus most of the information stored in the videos are never extracted. Although, the usual ROV videos include already sufficient information for geologic mapping, some aspects with only minor impact on the ROV operation can enhance the usability of such data for mapping purposes. One aspect regards the transfer between sampling sites. When points of interest of a research project are dislocated for several tens of meters or more, it is common that the ROV moves with an altitude from which seafloor structures are not identifiable anymore. This is due to the tight operation schedule on marine research expeditions and ROVs can maneuver faster when a secure distance to the seafloor is kept. However, the vast amount of visual informations that these transects can produce outweigh the extra time consumed by the slower ROV speed when operating closer to the seafloor. For

geologically varied terrains such as the eastern Manus Basin with its poorly understood felsic volcanic processes, it is worthwhile to keep bottom view while transiting between the study sites. Additionally, when the same route is used several times during one expedition a lateral shift of only several meters between the routes can further increase the knowledge of the local seafloor structures. This approach was considered on the BAMBUS cruise in 2011 and it significantly improved the outcome of each dive. As this thesis has shown, regular ROV videos recorded as mentioned above bear a high potential for comprehensive geologic mapping projects if high-resolution bathymetry is available. For such mapping purposes, a precise bathymetric map is of cornerstone importance as the ROV position in the deep sea is biased by navigation uncertainty. The detailed topography allows the mapping scientist to rectify the position of the ROV and to correctly address visually obtained informations onto morphologic structure in the bathymetry.

On the Magellan-06 cruise, local transponder networks were deployed on the seafloor in which the ROV and AUV navigated. This technology enables precise (< 10m) navigation in general, but in the rough terrain of PACManus and North Su, volcanic structures caused occasional signal shadows which resulted in significant local navigation errors. In 2011, a ship-based navigation system was used which did not suffer from signal shadows but the overall uncertainty was around 10 m. Without the complex morphology at both study areas that was used to correct these uncertainties when possible, a high resolution mapping on the level of details provided by the AUV bathymetry would not be possible. Therefore, an increased precision in ROV navigation is essential for areas without such pronounced morphology.

For such areas, another mapping technique might be more appropriate which is photo-mosaicking, where a vehicle moves in an organized grid to cover the entire area of interest. The mosaicking technique allows a rectification of ROV positions due to the identification of the same seafloor structure in different overlapping images. Thus, this method produces coherent precise maps with a resolution below the navigation uncertainty of ROVs even without operating on a high-resolution bathymetry with pronounced morphology. This is not applicable in our case since the ROV tracks are wide spread and disorganized and nearly no overlapping footage exists at all.

The recent advances in seafloor mapping techniques (Roman et al., 2012) develop into subcentimeter resolutions with ROVs. But the high time consumption of ROV

operations will still limit its application. With the technical progress in these years, especially in the field of robotics and autonomous systems, I anticipate that future AUVs will be more powerful tools for mapping. These AUVs will be equipped with stereographic cameras recording 3D pictures, laser scanning systems for fluid emission detection, downward and forward looking sonars for bathymetry and flare detection and a sub bottom profiling chirp sensor that completes the ultimate mapping tool. For such system, the time consumption would not be problematic anymore, as in the meantime, scientist can do sample work with ROVs. Until then, varied approaches such as demonstrated in this thesis work, may be combined to assess the local geologic framework with a m-scale resolution. Complementary photo-mosaicking is the best method for submeter resolution mapping of areas with limited extend. Finally, vast amounts of video data are already recorded and stored in research centers around the world and bear important informations that could be analyzed to produce high-resolution geologic maps of the seafloor without even going on another expedition.

Besides the comprehensive data sets that will support future research at PACManus and North Su, our results show that these two areas and the Manus Basin in general, can play a key role in the further understanding of back-arc basin magmatic systems, related hydrothermal circulation and submarine volcanism in general.

The scientific community had their focus regarding submarine volcanism on MOR basaltic systems for a long time. Therefore, low-viscous basaltic submarine volcanism is well understood compared to intermediate and high-silica volcanism at oceanic island arc related settings. These volcanic systems include a wide range of magma compositions and eruption styles. Their systematic exploration has just begun in the last decade (Carey and Sigurdsson, 2007). As the Manus Basin hosts a seafloor spreading center, volcanic ridges, seamounts and rifts, it is a perfect area to determine governing mechanisms in back-arc and island arc volcanism.

Besides studies of volcanism, the Manus Basin is also predestined for studies on the generation of VMS deposits. In the eastern Manus Basin, Nautilus Minerals already holds exploration licenses for deep sea mining of hydrothermal sulfide deposits that are rich in Cu and Au. Extended research of the local geologic setting with its manifold rock and related hydrothermal fluid compositions contributes important knowledge to the understanding of ore forming processes. Analyses of facies distribution at these hydrothermal fields also help exploration geologist with facies reconstructions on land.

At PACManus, on an area of only a few hundred meters, various lava flow morphologies including pillows, block lavas and lobate flows appear next to each other. Also, lava domes and craters exist and therefore nearly the entire suite of possible lava flow morphologies is present. Further sampling, mapping and a focus on volcanic structures during ROV dives would help to identify the dipping points at which it is determined what eruption styles and products occur. It is still unclear, how the silica, crystal and volatile contents influence submarine volcanism that is also governed by the water depth, lava viscosity and lava temperature. A systematic analysis could help to discriminate between certain parameters and examine their influence on eruption style.

North Su also has a high potential for future scientific work, especially due to the fact that the emplacement of South Peak reset the development of hydrothermal discharge sites. On one hand, this eruption buried hydrothermal fields but on the other hand we observed first hydrothermal deposits emerge the clastic pile of South Peak. Therefore, South Peak offers scientist of various disciplines to discover the development of hydrothermal fields from their birth on. At other hydrothermal fields, it is commonly unknown, how old these systems are. Emerging domes may be a common signature of growing arc volcanoes and solitary volcanic centers in back-arcs. Many of the volcanoes of the Kermadec arc, for instance, feature these domes and some, e.g., the Brothers Volcano, show breccia cliffs, sulfur chimneys, and plateaus covered by sand-sized clastic deposits (de Ronde et al., 2011) very similar to what I observed at North Su. The formation mechanisms proposed for North Su in this thesis may hence have much wider implications.

Another point of interest for future expeditions could be the clastic deposits that are related to dome emplacements at PACManus and North Su. Especially, the high viscous magma at North Su produced huge amounts of fine clasts. Sulfide deposits at both hydrothermal systems are rich in metals of economic interests. So far, the majority of analyses of metal concentration focused on sulfide precipitates as black smoker chimneys. But at North Su and PACManus the fluid discharge occurred also through the clastic deposits. These clastic piles could act as magnificent substrates in which hydrothermal precipitates can fall out and crystallize, as observed on North Su, were hydrothermal deposits already cemented the clasts. In the course of this dissertation, I did not focus on metal deposits and therefore did not measure their concentration in the clastic deposits.

However, these cemented clastic horizons might be of economic interest if a significant amount of metal-rich fluids precipitate.

Additionally, a renewed AUV survey at North Su would be of significant benefit as it would depict the detailed morphologic changes that the South Peak eruption has caused. Our ROV based observations are spatially limited although they are sufficient to identify the nature of the new cone. However, AUV bathymetry would allow an area wide comparison of the changes that occurred with a more accurate estimation of depth changes and erupted volume.

In general, the petrology of North Su and PACManus rocks are typical for opening back-arc basins and oceanic island arcs as well as their hydrothermal fluids. Therefore, it is likely that the findings from both case studies can be applied to similar volcanic and tectonic settings. As more than 7,000 km of oceanic island arc exist on earth (de Ronde et al., 2003), this research has a global implication.

4.1 References

Carey, S., Sigurdsson, H., 2007. Exploring Submarine Arc Volcanoes. Oceanography 20, 80–89.

De Ronde, C.E.J., Massoth, G.J., Baker, E.T., Lupton, J.E., 2003. Submarine hydrothermal venting related to volcanic arcs, Giggenbach Memorial Volume, in: Simmons, S.F., Graham, I.J. (Eds.), Volcanic, Geothermal and Ore-Forming Fluids: Rulers and Witnesses of Processes within the Earth. Society of Economic Geologists, pp. 91–110.

De Ronde, C.E.J., Massoth, G.J., Butterfield, D. a., Christenson, B.W., Ishibashi, J., Ditchburn, R.G., Hannington, M.D., Brathwaite, R.L., Lupton, J.E., Kamenetsky, V.S., Graham, I.J., Zellmer, G.F., Dziak, R.P., Embley, R.W., Dekov, V.M., Munnik, F., Lahr, J., Evans, L.J., Takai, K., 2011. Submarine hydrothermal activity and gold-rich mineralization at Brothers Volcano, Kermadec Arc, New Zealand. Miner. Depos. 46, 541–584.

Roman, C., Inglis, G., Vaughn, J.I., Smart, C., Douillard, B., Williams, S., 2012. The development of high-resolution seafloor mapping techniques, in: Bell, K.L.C., Elliot, K., Martinez, C., Fuller, S.A. (Eds.), New Frontiers in Ocean Exploration: The E/V Nautilus and NOAA Ship Okeanos Explorer 2011 Field Season. Oceanography 25(1), pp. 42–45.

Acknowledgements

First of all I like to thank Prof. Dr. Wolfgang Bach for giving me the opportunity to conduct this thesis work. Over the last three years, he provided continuous support and feedback and enabled me to present my work on international conferences, to visit other scientists in Japan and the United States, and to participate in international research expeditions where I could gain important experiences, not only of scientific benefit.

I am also most grateful to Maurice Tivey for supporting my work with essential data, without it, this thesis would not have been possible. He significantly improved the first manuscript and provided important help for the second manuscript when he received me at the Woods Hole Oceanographic Institution and at his home.

I like to thank Gerhard Bohrmann for being the second supervisor and reviewing this thesis.

Niels Jöns was of great help for EPMA measurements and data interpretation. Further I like to thank him for critical reviewing various texts, for taking care of the bathymetry surveys on So-216 and for a pleasant work alongside him in the last three years.

Crucial help with bathymetry data processing was provided by Paul Wintersteller and Christian dos Santos Ferreira.

Many thanks also go to Christian Hansen for last-minute help with this thesis, for enriching discussions on world politics and being a perfect office-roommate.

I am grateful to Adam Soule for important help with the identification and classification of the heterolithic clastic deposits of North Su and sharing his knowledge of vocanology.

Also thanks to Yann Marcon and Jan-Hendrik Körber for pleasant and beneficial conversation and discussions on seafloor mapping, GIS and other stuff.

Special thanks go to Dominik Niedermeyer for providing me with extensive rock analyses from the Manus Basin.

I also like to thank Andreas Klügel for beneficial discussions on volcanology.

Michael Hentscher was a great office-roommate and always of great help for chemical questions and for great cakes.

Further, I like to thank all my colleagues, Svenja, Nikki, Basti, Andreas, Elliot, Stefan, Wolf-Achim and Patrick for the pleasant time.

Special thanks also go to Jutta Aid Majdari for administrative help and especially for delightful conversations.

Important for my work-life balance are my friends, which is why I like thank all of them to spent their time with me.

I am thankful to be a part of a wonderful family and like to address special thanks to my parents and sisters for continuous support and to believe in me.

Finally I like to express my gratitude to Catharina. She always supported me and helped me to stay focused, especially in the final phase when she also supervised my physical and mental health. I am deeply grateful to share my life with her.

Janis Thal

Vahrer Straße 170

28309 Bremen

Erklärung

Gemäß § 6 Abs. 5 der Promotionsordnung der Universität Bremen für die mathematischen, natur- und ingenieurswissenschaftlichen Fachbereiche versichere ich hiermit, dass ich

1. die Arbeit ohne unerlaubte fremde Hilfe angefertigt habe,

2. keine anderen als die von mir angegebenen Quellen und Hilfsmittel benutzt habe und

3. die den benutzten Werken wörtlich oder inhaltlich entnommenen Stellen als solche kenntlich gemacht habe.

Bremen, den 27.02.2014

Janis Thal